AGING INVESTIGATION OF A CAST-CURE POLYMER BONDED EXPLOSIVE IN TERMS OF CHEMICAL AND PHYSICAL PROPERTIES

A THESIS SUBMITTED TO
THE GRADUATE SCHOOL OF NATURAL AND APPLIED SCIENCES
OF
MIDDLE EAST TECHNICAL UNIVERSITY

BY

TARIK YÜCEL

IN PARTIAL FULFILLMENT OF THE REQUIREMENTS
FOR
THE DEGREE OF DOCTOR OF PHILOSOPHY
IN
POLYMER SCIENCE AND TECHNOLOGY

JULY 2025

Approval of the thesis:

AGING INVESTIGATION OF A CAST-CURE POLYMER BONDED EXPLOSIVE IN TERMS OF CHEMICAL AND PHYSICAL PROPERTIES

submitted by **TARIK YÜCEL** in partial fulfillment of the requirements for the degree of **Doctor of Philosophy in Polymer Science and Technology, Middle East Technical University** by,

Prof. Dr. Naci Emre Altun
Dean, **Graduate School of Natural and Applied Sciences** _____

Prof. Dr. Necati Özkan
Head of the Department, **Polymer Science and Technology** _____

Prof. Dr. Necati Özkan
Supervisor, **Polymer Science and Technology, METU** _____

Assoc. Prof. Dr. Taner Atalar
Co-Supervisor, **TÜBİTAK SAGE** _____

Examining Committee Members:

Prof. Dr. Cevdet Kaynak
Metallurgical and Materials Eng., METU _____

Prof. Dr. Necati Özkan
Polymer Science and Technology, METU _____

Prof. Dr. Göknur Bayram
Chemical Engineering, METU _____

Asst. Prof. Dr. Cemal Merih Şengönül
Manufacturing Engineering, Atılım Uni. _____

Asst. Prof. Dr. Cengiz Uzun
Chemistry, Hacettepe Uni. _____

Date: 02.07.2025

I hereby declare that all information in this document has been obtained and presented in accordance with academic rules and ethical conduct. I also declare that, as required by these rules and conduct, I have fully cited and referenced all material and results that are not original to this work.

Name Last name : Tarık Yücel

Signature :

ABSTRACT

AGING INVESTIGATION OF A CAST-CURE POLYMER BONDED EXPLOSIVE IN TERMS OF CHEMICAL AND PHYSICAL PROPERTIES

Yücel, Tarık
Doctor of Philosophy, Polimer Science and Technology
Supervisor: Prof. Dr. Necati ÖZKAN
Co-Supervisor: Doç. Dr. Taner ATALAR

July 2025, 120 pages

In this study, the physical and chemical effects of aging on castable plastic bonded explosive (PBXN-109), in which the antioxidant content was changed by subjecting it to accelerated aging, were examined and for this purpose, Shore A hardness, crosslink density, antioxidant content, tension test, fourier transform infrared spectroscopy (FTIR), dynamic mechanical analysis (DMA) and scanning electron microscope (SEM) anayzes were performed. The accelerated aging temperature was chosen between 30°C and 80°C. Aging times have been determined to correspond to approximately 10 year thermal equivalent load for aging temperatures of 60°C and above. As a result of the study, it was understood that crosslinking and chain scission are two competing processes and chain scission is more dominant at high temperatures. It has been observed that stress-strain properties reflect the physical effects of aging more clearly than chemical effects. On the other hand, it has been shown that high AO content has a slowing effect on the chemical effects of aging. In addition, it has been understood that the bonding agent has an important function in this type of polymer compositions and its deficiency has an accelerating effect on aging. Finally, the shelf life of the explosive was calculated to be approximately 10 years using the Arrhenius and Berthelot approaches.

Keywords: PBXN-109, Aging, Cast-cure explosives, Crosslinking, Antioxidants.

ÖZ

DÖKÜLEBİLİR PLASTİK BAĞLI BİR PATLAYICININ YAŞLANMASININ KİMYASAL VE FİZİKSEL ÖZELLİKLER AÇISINDAN İNCELENMESİ

Yücel, Tarık
Doktora, Polimer Bilim ve Teknolojisi
Tez Yöneticisi: Prof. Dr. Necati ÖZKAN
Ortak Tez Yöneticisi: Doç. Dr. Taner ATALAR

Temmuz 2025, 120 sayfa

Bu çalışmada, hızlandırılmış yaşlandırmaya tabi tutularak antioksidan içeriğinin de değiştirildiği dökülebilir bir plastik bağlı patlayıcı (PBXN-109) üzerinde yaşlanmanın fiziksel ve kimyasal etkileri incelenmiş ve bu amaçla Shore A sertlik, çapraz bağlanma yoğunluğu, antioksidan içeriği, çekme testi, fourier dönüşümlü kızılötesi spektroskopisi (FTIR), dinamik mekanik analiz (DMA) ve taramalı elektron mikroskobu (SEM) analizleri gerçekleştirilmiştir. Hızlandırılmış yaşlandırma sıcaklıkları 30°C ile 80°C aralığında seçilmiştir. Yaşlandırma süreleri 60°C ve üzeri yaşlandırma sıcaklıkları için yaklaşık 10 yıllık termal eşdeğer yüke karşılık gelecek biçimde belirlenmiştir. Çalışma sonucunda çapraz bağlanma ve bağ kopmalarının birbiriyle yarışan iki süreç olduğu ve yüksek sıcaklıklarda bağ kopmalarının daha baskın olduğu anlaşılmıştır. Gerilim-gerinim özelliklerinin yaşlanmanın fiziksel etkilerini kimyasal etkilerden daha net yansıttığı görülmüştür. Öte yandan yüksek AO içeriğinin yaşlanmanın kimyasal etkilerini yavaşlatıcı bir etkiye sahip olduğu da gösterilmiştir. Bunlara ek olarak bağlanma maddesinin bu tip polimer bileşimlerinde önemli bir işleve sahip olduğu ve eksikliğinin yaşlanmayı

hızlandırıcı bir etki yarattığı anlaşılmıştır. Son olarak patlayıcının raf ömrü Arrhenius ve Berthelot yaklaşımları kullanılarak yaklaşık 10 yıl olarak hesaplanmıştır.

Anahtar Kelimeler: PBXN-109, Yaşlanma, Dökülerek kürleşebilen patlayıcı, Çapraz bağlanma, Antioksidan.

To My Family

ACKNOWLEDGMENTS

I would like to express my deepest gratitude to my thesis supervisor, Prof. Dr. Necati ÖZKAN, for his invaluable guidance, support, and insights throughout every stage of this thesis. I also extend my sincere thanks to my co-supervisor, Assoc. Prof. Dr. Taner ATALAR, for his invaluable contributions and guidance.

I would like to thank the members of my thesis examining committee, Prof. Dr. Cevdet KAYNAK and Dr. Cemal Merih ŞENGÖNÜL, for their valuable feedback and constructive suggestions.

I am especially grateful to my dear friend, Assoc. Prof. Dr. Güler Bengüsu TEZEL TANRISEVER, for her unwavering support, insightful advice, and sincere encouragement throughout this journey.

I would also like to thank my institution, Defence Industries Research and Development Institute (TUBITAK SAGE) , for providing the necessary laboratory facilities and technical resources that greatly contributed to the success of this work. The support and opportunities offered have played a vital role in completing this thesis. In particular, I would like to extend my deepest gratitude to my colleague Anıl TATLIDİLLİ whose support during the experimental phase of this study was gratefully acknowledged.

Finally, I extend my heartfelt thanks to my family, my son Toprak YÜCEL and my dear wife Dr. Burcu OPAK YÜCEL, who have always been by my side and whose love and support have illuminated my path.

TABLE OF CONTENTS

ABSTRACT v

ÖZ vii

ACKNOWLEDGMENTS x

TABLE OF CONTENTS xi

LIST OF TABLES xiii

LIST OF FIGURES xiv

LIST OF ABBREVIATIONS xx

ABBREVIATIONS xx

LIST OF SYMBOLS xxii

SYMBOLS xxii

1 INTRODUCTION 1

1.1 Polymer Bonded Explosives 1

1.2 Aging of Energetic Materials 6

1.2.1 Crosslinking 7

1.2.2 Chain Scission 9

1.2.3 Migration of Low Molecular Weight Components 10

1.2.4 Dewetting 11

1.3 Scope of the Study 11

2 LITERATURE REVIEW 13

3 EXPERIMENTAL 21

3.1 Explosives Production 22

3.2 Explosives Sample Preparation 23

3.3 Aging Procedure 25

3.4 Test Methods 29
3.4.1 Hardness Measurement 29
3.4.2 Crosslink Density Measurement 31
3.4.3 Antioxidant Measurement 34
3.4.4 Tension Test 35
3.4.5 Fourier Transform Infrared Spectroscopy (FTIR) Measurements 36
3.4.6 Dynamic Mechanical Analysis (DMA) Tests 36
3.4.7 Scanning Electron Microscopy (SEM) Analysis 37
4 RESULTS AND DISCUSSION 39
4.1 Shore A Hardness 39
4.2 Crosslink Density 43
4.3 Antioxidant Content 50
4.4 Tensile Properties 54
4.5 FTIR Analysis 64
4.6 Dynamic Mechanical Analysis 71
4.7 SEM Analysis 85
4.8 Comparison of Crosslink Density, Tension, FTIR and DMA Test Results 94
4.9 Shelf Life Prediction 99
5 CONCLUSION AND FUTURE WORKS 105
REFERENCES 109
CURRICULUM VITAE 119

LIST OF TABLES

TABLES

Table 3.1 Aged explosive formulations 21
Table 3.2 Aging temperatures and test intervals for the R1, R2 and R3 formulations (60˚C only for R2 and R3)..... 26
Table 3.3 Equivalent isothermal aging durations at elevated temperatures for predicting long-term behavior at 25˚C 28
Table 3.4 Conducted tests and schedule for each aging temperatures for all temparatures (60˚C only for R2 and R3) 29
Table 4.1 The deconvoluted carbonyl spectrum area ratios (interacted/non-interacted) of the aged R1 formulation at different aging times 69
Table 4.2 The deconvoluted carbonyl spectrum area ratios (interacted/non-interacted) of the aged R2 and R3 formulations at different aging times at 60˚C.. 70
Table 4.3 Predicted life-time based on Arrhenius at different aging temperatures 102
Table 4.4 Data for Berthelot calculations 103
Table 4.5 Predicted Shelf Life Comparison of Arrhenius and Berthelot Approaches 104

LIST OF FIGURES

FIGURES

Figure 1.1. RDX structure (Daniel, 2006) 2
Figure 1.2. HTPB structure (Daniel, 2006) 3
Figure 1.3. Generic polyurethane reaction between HTPB and IPDI (Lucio & De La Fuente, 2014) 3
Figure 1.4. DHE structure (Daniel, 2006) 4
Figure 1.5. AO2246 structure (Eslam, Sherif, Ahmed, & Hosam, 2020) 5
Figure 1.6. TPB structure (Ou & Yapeng, 2018) 5
Figure 1.7. DOA structure (Jaidan, Abou-Rachid, Lafleur-Lambert, & Brisson, 2011) 6
Figure 1.8. Oxidative degradation reactions of HTPB (Eslam, Sherif, Ahmed, & Hosam, 2020) 8
Figure 1.9. Chain scission mechanism of HTPB-IPDI based polyurethane (PU) ... 10
Figure 1.10. Diffusion of plasticizer through polymer (Khanlari, Bayat, & Bayat, 2022) 11
Figure 3.1. Explosive production in a planetary mixer 22
Figure 3.2. Explosive block sample in plastic package and its dimensions 24
Figure 3.3. Dog-bone shaped tensile test specimens prepared from sliced explosive composite layers 25
Figure 3.4. Shore A hardness measurement and illustriation of indenter through material 30
Figure 3.5. Shore A hardness measurment locations on sample 31
Figure 3.6. Crosslink density measurement test set-up and its components 32
Figure 3.7. A representative load-displacement curve for a tested sample, used to ascertain the compression modulus necessary for crosslink density measurement 33
Figure 3.8. Standard dimensions for uniaxial tensile specimen (Adel & Liang, 2019) 35
Figure 3.9. Instron universal testing machine 36

Figure 3.10. Sample in tension clamp at DMA 37
Figure 4.1. Shore A hardness change as a function of the aging time at all aging temperatures for the R1 formulation 40
Figure 4.2. Shore A hardness change as a function of the aging time at 60°C for R2 formulation 41
Figure 4.3. Shore A hardness change as a function of the aging time at 60°C for R3 formulation 41
Figure 4.4. Crosslink density change as a function of the aging time at 80°C for the R1 formulation 45
Figure 4.5. Crosslink density change as a function of the aging time at 70°C for the R1 formulation 46
Figure 4.6. Crosslink density change as a function of the aging time at 60°C for the R1 formulation 46
Figure 4.7. Crosslink density change as a function of the aging time at 50°C for the R1 formulation 47
Figure 4.8. Crosslink density change as a function of the aging time at 30°C for the R1 formulation 47
Figure 4.9. Crosslink density change as a function of the aging time at 60°C for the R2 formulation 48
Figure 4.10. Crosslink density change as a function of the aging time at 60°C for the R3 formulation 49
Figure 4.11. Radical Attack Prevention of Antioxidant at HTPB-IPDI Polyurethane Structure (Wang, Zhang, Liu, & Hao, 2015) 50
Figure 4.12. Antioxidant content change of the R1 formulation as a function of aging time at different temperatures 51
Figure 4.13. AO depletion rate of the R1, R2 and R3 formulation at aging temperature of 60ºC 53
Figure 4.14. The strain at maximum load as a function of the aging time at 80°C for the R1 formulation 55

Figure 4.15. The strain at maximum load as a function of the aging time at 70°C for the R1 formulation 56
Figure 4.16. The strain at maximum load as a function of the aging time at 60°C for the R1 formulation 56
Figure 4.17. The strain at maximum load as a function of the aging time at 50°C for the R1 formulation 57
Figure 4.18. The strain at maximum load as a function of the aging time at 30°C for the R1 formulation 57
Figure 4.19. Time-rate of change of strain for the R1 formulation at different aging temperatures for the R1 formulation 59
Figure 4.20. Time-rate of change of strain for the R1 and R2 formulations at 60°C aging temperature 60
Figure 4.21. The strain at maximum load as a function of the aging time at 60°C for the R3 formulation 61
Figure 4.22. The maximum tensile stress as a function of the aging time at 80°C for the R1 formulation 62
Figure 4.23. The maximum tensile stress as a function of the aging time at 70°C for the R1 formulation 62
Figure 4.24. The maximum tensile stress as a function of the aging time at 60°C for the R1 formulation 63
Figure 4.25. The maximum tensile stress as a function of the aging time at 50°C for the R1 formulation 63
Figure 4.26. The maximum tensile stress as a function of the aging time at 30°C for the R1 formulation 64
Figure 4.27. FTIR Spectrum of a Typical Polyurethane (Tcharkhtchi et al., 2014) 65
Figure 4.28. FTIR spectrum of the R1, R2 and R3 formulations at t_0 65
Figure 4.29. Schematic represantation of hydrogen bond interaction between crosslinked HTPB-IPDI polymer chains 66
Figure 4.30. Carbonyl region spectrum change of the R1 formulation with aging at 60°C 67

Figure 4.31. Peak analysis example plot of the R1 at time t_0 68
Figure 4.32. Hard and soft segment regions at IPDI-HTPB polyurethane chain structure..... 72
Figure 4.33. Tan (δ) change of the R1 formulation at 80°C aging temperature as a function of temperature sweep at different aging times..... 73
Figure 4.34. Change of $T_{g,unrest}$ as a function of aging time for the R1 formulation aged at 80°C..... 73
Figure 4.35. Storage modulus (E') as a function of temperature for the R1 formulation aged at 80°C..... 74
Figure 4.36. Storage Modulus (E', at 40°C) as a function of aging time for the R1 formulation aged at 80°C..... 74
Figure 4.37. Tan (δ) change of the R1 formulation at 60°C aging temperature as a function of temperature sweep at different aging times..... 75
Figure 4.38. Change of $T_{g,unrest}$ as a function of aging time for the R1 formulation aged at 60°C..... 76
Figure 4.39. Storage modulus (E') as a function of temperature for the R1 formulation aged at 60°C..... 76
Figure 4.40. Storage Modulus (E', at 40°C) as a function of aging time for the R1 formulation aged at 60°C..... 77
Figure 4.41. Tan (δ) change of the R1 formulation at 30°C aging temperature as a function of temperature sweep at different aging times..... 78
Figure 4.42. Change of $T_{g,unrest}$ as a function of aging time for the R1 formulation aged at 30°C..... 78
Figure 4.43. Storage modulus (E') as a function of temperature for the R1 formulation aged at 30°C..... 79
Figure 4.44. Storage Modulus (E', at 40°C) as a function of aging time for the R1 formulation aged at 30°C..... 79
Figure 4.45. Tan (δ) change of the R2 formulation at 60°C aging temperature as a function of temperature sweep at different aging times..... 80

Figure 4.46. Change of $T_{g,unrest}$ as a function of aging time for the R2 formulation aged at 60°C 80
Figure 4.47. Storage modulus (E') as a function of temperature for the R2 formulation aged at 60°C..... 81
Figure 4.48. Storage Modulus (E', at 40°C) as a function of aging time for the R2 formulation aged at 60°C..... 81
Figure 4.49. Tan (δ) change of the R3 formulation at 60°C aging temperature as a function of temperature sweep at different aging times 82
Figure 4.50. Change of $T_{g,unrest}$ as a function of aging time for the R3 formulation aged at 60°C 83
Figure 4.51. Storage modulus (E') as a function of temperature for the R3 formulation aged at 60°C..... 84
Figure 4.52. Storage Modulus (E', at 40°C) as a function of aging time for the R3 formulation aged at 60°C..... 84
Figure 4.53. SEM images of the time-dependent fracture surfaces of the dog-bone specimens remained after tensile testing of the R1 formulation, aged at 30°C..... 87
Figure 4.54. SEM images of the time-dependent fracture surfaces of the dog-bone specimens remained after tensile testing of the R1 formulation, aged at 80°C..... 89
Figure 4.55. SEM images of the time-dependent fracture surfaces of the dog-bone specimens remained after tensile testing of the R1 formulation, aged at 60°C..... 91
Figure 4.56. SEM images of the time-dependent fracture surfaces of the dog-bone specimens remained after tensile testing of the R2 formulation, aged at 60°C..... 92
Figure 4.57. SEM images of the time-dependent fracture surfaces of the dog-bone specimens remained after tensile testing of the R3 formulation, aged at 60°C..... 93
Figure 4.58. Property change of the R1 formulation as a function of time at 80°C 95
Figure 4.59. Property change of the R1 formulation as a function of time at 60°C 96
Figure 4.60. Property change of the R1 formulation as a function of time at 30°C 97

Figure 4.61. Property change of the R2 formulation as a function of time at 60°C 98
Figure 4.62. Property change of the R3 formulation as a function of time at 60°C 99
Figure 4.63. The determination of the slopes of the strain against time curves for the R1 formulation at different aging temperatures 100
Figure 4.64. ln k vs. 1/T plot to determine Arrhenius parameters for the R1 formulation 101
Figure 4.65. T vs. log (t) plot to determine shelf life from Berthelot 103

LIST OF ABBREVIATIONS

ABBREVIATIONS

Al	:	Aluminum
AO	:	Antioxidant
AO2246	:	2,2-methylene-bis (4-methyl-6-tert-butyl-phenol)
AP	:	Ammonium Perchlorate
ATR	:	Attenuated Total Reflectance
CXM-7	:	Coated Explosive Material (DOA coated RDX)
DBTL	:	Dibutyltin Dilaurate
DHE	:	N,N-di(2-hydroxyethyl) dimethyl hydantoin (Dentacol)
DINA	:	Diisononyl Adipate
DMA	:	Dynamic Mechanical Analysis
DOA	:	Dioctyl Adipate
DOP	:	Dioctyl Phthalate
DSC	:	Differential Scanning Calorimetry
FTIR	:	Fourier Transform Infrared Spectroscopy
HMDI	:	Hexamethylene Diisocyanate
HMX	:	High Melting Explosive (Octogen)
HTPB	:	Hydroxyterminated Polybutadiene
IDP	:	Isodecyl Pellargonate
IPDI	:	Isophorone Diisocyanate
LIBS	:	Laser-Induced Breakdown Spectroscopy

PBX	:	Polymer Bonded Explosive
PBXN-109	:	Plastic (Polymer) Bonded Explosives Navy
PU	:	Polyurethane
RDX	:	Royal Demolition Explosive (Hexogen)
SCP	:	Solid Composite Propellant
SEM	:	Scanning Electron Microscopy
SRP	:	Solid Rocket Propellant
STANAG	:	Standardization Agreement
TDI	:	Toluene Diisocyanate
TPB	:	Triphenylbismuth
UV	:	Ultraviolet
WLF	:	Williams Landell Ferry

LIST OF SYMBOLS

SYMBOLS

A	:	Pre-Exponential Factor
A_o	:	Area of the cross section (i.e. circular face)
C	:	Crosslink density
E’	:	Storage Modulus
E_a	:	Activation Energy
F	:	Acceleration or deceleration factor per 10°C temperature change
G	:	Gram
H	:	Pre-factor
h_o	:	Height of the sample
mg	:	Miligram
ml	:	Milliliter
mm	:	Millimeters
R	:	Gas constant (8.315 J/mole.K)
S	:	Slope of the weight vs. displacement curve at crosslink density measurement x 9.807 m/s^2
T	:	Temperature
T_g	:	Glass Transition Temperature
$T_{g\text{-}rest}$	:	Restricted Region Glass Transition Temperature
$T_{g\text{-}unest}$	:	Restricted Region Glass Transition Temperature
t_E	:	In-use time at temperature T_E

t_T : Test time at test or aging temperature T_T

T_T : Test or aging temperature

T_E : In-use temperature

ml : Microliter

ΔT_F : Temperature interval assigned to actual value of factor F, mostly 10ºC

CHAPTER 1

INTRODUCTION

Energetic materials constitute fundamental ingredients in the formulation of explosive and solid propellant compositions. An explosive is defined as a substance comprising energetic materials capable of undergoing a rapid decomposition reaction, yielding a swift volumetric expansion of gas that can perform mechanical work on the surrounding environment. Explosives represent a significant category of energetic materials, manufactured globally in substantial volumes for both military and mining applications. While generally exhibiting a tolerable degree of initiation sensitivity, the crystalline structures of explosives in their final state are frequently coated with polymeric materials to mitigate sensitivity or to augment mechanical characteristics. The designation "PBX," an acronym for polymer bonded or plastic bonded explosives, encompasses a broad spectrum of explosive formulations that integrate polymer binders. This nomenclature includes compositions fabricated through pressing or solid, chemically crosslinked matrices (Szala, 2021). The specific explosive under investigation in this study is a cast-cure polymer (polyurethane-based crosslinked elastomer) bonded explosive. Unless explicitly stated otherwise, the terms "PBX" or "Polymer Bonded Explosives" as employed herein will specifically denote cast-cure polymer bonded explosives.

1.1 Polymer Bonded Explosives

Polymer bonded explosives (PBXs) primarily comprise energetic fillers, a polymeric binder, and plasticizing agents. Certain formulations may also incorporate antioxidants, crosslinking agents, bonding agents, catalysts, and metallic additives. Fundamentally, PBXs consist of crystalline organic filler particles dispersed within a compliant polymer matrix. The energetic filler materials are the constituents

responsible for the principal energy release of an explosive upon initiation. The most prevalent energetic fillers include cyclotetramethylene tetranitramine (HMX) and cyclotrimethylene trinitramine (RDX). The filler material employed in this investigation is RDX as a form of coated with plasticizer (CXM-7), the chemical structure of which is illustrated in Figure 1.1. The reason of the usage of coated material is safety consideration during handling and transportation.

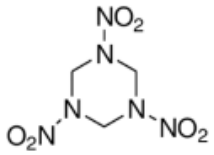


Figure 1.1. RDX structure (Daniel, 2006)

The use of metal additives in explosive formulations is common. Among metal additives, aluminum is mostly preferred one due to its high energetic content, ease of availability and relatively affordable cost. Application of aluminum powder in plastic bonded explosives was reviewed, highlighting its effectiveness as an overall energy enhancer (Joseph, 1993). The reactions between aluminum and the primary detonation products of high explosives release a significant amount of energy, resulting in prolonged high pressure effects (Vadhe, Pawar, & Sinha, 2008).

Hydroxy-terminated polybutadiene (HTPB) is a prevalent binder material employed in the formulation of solid composite propellants (SCPs) and polymer bonded explosives (Daniel, 2006). Due to its ability to cure at low temperatures and allowing high solid filler loading while retaining the desired mechanical properties and ease of processing , it is favorable over other binders (Hasırcı, Akbaş, & Aksoy, 1994); (Kumar, Kumaraswamy, Jain, & Murthy, 2022). At thermoset compositions, HTPB reacts with curing agent which is a kind of diisocyanate resulting polyurethane structure. Structure of HTPB is shown in Figure 1.2.

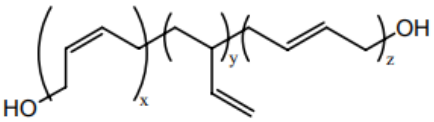


Figure 1.2. HTPB structure (Daniel, 2006)

Isocyanate based curing agents are commonly applied in systems that use HTPB binder, resulting in the formation of a polyurethane structure at the end of the reaction (Ma et al. 2022). Isocyanates are critical in the development of the hard segments within polyurethanes during the curing process, thereby influencing the mechanical properties of the final material by modulating the curing kinetics. Different isocyanate groups exhibit varying cure rates and reaction tendencies, which influence the pot life of the mixture, this is the period during which the polyurethane remains workable before crosslink increases viscosity and initiates curing (Ganivada, Dhara, Jana, & Jana, 2022); (Lucio & De La Fuente, 2014). The isocyanates mostly used in polyurethane based composite systems are isophorone diisocyanate (IPDI), toluene diisocyanate (TDI) and hexamethylene diisocyanate (HMDI). The curing agent specifically employed in this investigation is IPDI. A generalized schematic of the polyurethane formation reaction involving HTPB and IPDI is presented in Figure 1.3.

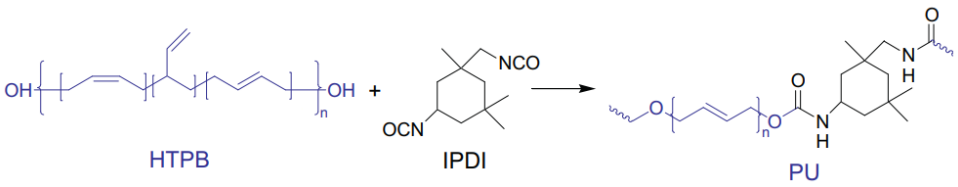


Figure 1.3. Generic polyurethane reaction between HTPB and IPDI (Lucio & De La Fuente, 2014)

The incorporation of a bonding agent into PBX formulations serves to augment the interfacial interaction between the solid particulate phase and the continuous polymer matrix, consequently enhancing the mechanical integrity of the explosive material (Sciamareli, Takahashi, Marta, & Koshun, 2002; Ali & Zhang, 2008). These bonding agents, like Dentacol (DHE), possess functional groups capable of

interacting with the solid filler materials and reacting with the polymer system, thereby facilitating a more robust integration between the solid fillers and the polymer matrix within the PBX (Zhang, Zhao, & Tan, 2005). The principal constituent of DHE, N,N-di(2-hydroxyethyl) dimethyl hydantoin, forms chemical bonds with isocyanates via its hydroxyl functionalities and engages in interactions with nitramine explosives, such as RDX and HMX, through its amide groups (Yadav, Pant, & Das, 2020; Daniel, 2006). The chemical structure of DHE is shown in Figure 1.4.

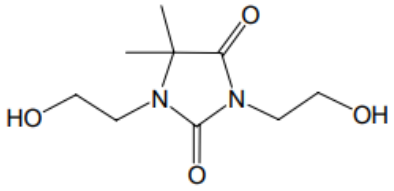


Figure 1.4. DHE structure (Daniel, 2006)

Oxidative reactions negatively impact the viscoelastic properties of PBXs and can degrade the mechanical integrity of it by spreading throughout the entire grain, potentially leading to system failure. Antioxidant materials help to stabilize the binder and protect it from these oxidative effects (Celina, J.M., Winters, Assink, & Minier, 2006). These antioxidants prevent the continuation of the degradation chain by donating hydrogen atoms to the radicals formed in the structure. They generally consist of phenol or aromatic amines. The depletion of antioxidants is closely linked to the oxidative crosslinking process; once antioxidants are exhausted, thermal oxidative degradation accelerates significantly (Eslam, Sherif, Ahmed, & Hosam, 2020). Antioxidant used in this study is 2,2-methylene-bis (4-methyl-6-tert-butyl-phenol) (AO2246) which is a phenolic antioxidant and its structure is illustrated in Figure 1.5.

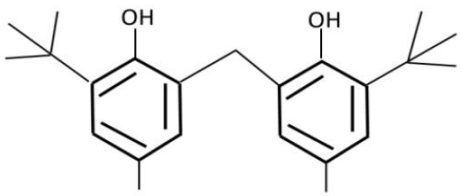


Figure 1.5. AO2246 structure (Eslam, Sherif, Ahmed, & Hosam, 2020)

Catalysts like dibutyltin dilaurate (DBTL) and triphenylbismuth (TPB) are used in HTPB-based polyurethanes to effectively lower curing temperatures (Ou, Chang, & Zhang, 2015). Their catalytic activity and mechanisms have been studied through various techniques (Hailu, Guthausen, Becker, Konig, & Geissler, 2010). Previous researches have demonstrated that these catalysts speed up the crosslinking process between HTPB and the curing agent by forming complexes with reactive groups, which reduces the activation energy of the reaction (Bina, Kannan, & Ninan, 2004); (Catherine, Krishnan, & Ninan, 2000). Catalyst used in this study is TPB and its structure is shown in Figure 1.6.

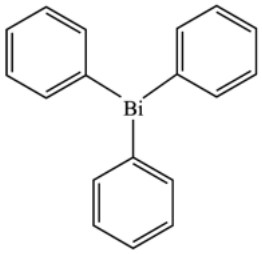


Figure 1.6. TPB structure (Ou & Yapeng, 2018)

A plasticizer is a low molecular weight additive that facilitates the manufacturing of PBXs that are otherwise challenging to process on their own. Adding a plasticizer offers several advantages, such as enhancing flow and flexibility, lowering the glass transition temperature, improving mechanical properties, and enabling usage in low-temperature conditions. Phthalates and adipates are the primary plasticizers commonly used in PBXs and solid composite propellants. Among the most widely used are dioctyl phthalate (DOP), isodecyl pellargonate (IDP), diisononyl phthalate

(DINP), dioctyl adipate (DOA), and diisononyl adipate (DINA) (Yılmaz, Şen, & Kaya, 2014). DOA plasticizer was used in this study. The chemical structure of DOA is shown in Figure 1.7.

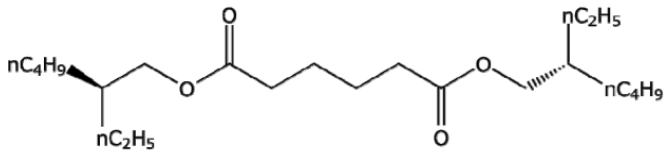


Figure 1.7. DOA structure (Jaidan, Abou-Rachid, Lafleur-Lambert, & Brisson, 2011)

Due to exposure to natural elements or specific work environments, energetic materials are easily influenced by factors such as vibration, heat, oxygen, light or some other environmental effects during processing, storage, or use. These influences can lead to physical or chemical changes, causing the materials to degrade and potentially become unusable (Pan, Nan, & Chen, 2022). Aging of energetic materials is a complex process that may involve many factors and interactions. Before reviewing studies in the literature, it is necessary to understand the aging mechanisms in energetic materials.

1.2 Aging of Energetic Materials

Aging of energetic materials (SCPs and PBXs) refers to the decline in physical, ballistic, and mechanical properties over time, caused by changes in physical characteristics or chemical composition as a result of the material's interaction with its environment (Van Breugel, 2018); (Gates, 2008). The observed changes can appear in various forms, including softening, hardening, swelling, discoloration or gas release. Different components may react with one another or with the surrounding environment, leading to permanent changes that can significantly impact both ballistic and physical characteristics (de la Fuente, 2009).

Munitions are produced in large quantities, stored for extended periods, and often transported to various harsh and remote launch sites prior to their intended use. Generally, the minimum service life requirement for any energetic material is 10 years following the casting of the propellant or explosive to the rocket motors or warheads. Although these munitions are stored under controlled conditions before actual deployment in a missile, the energetic material is subjected to mechanical, thermal, and vibratory loads, and its chemically active components interact with environmental factors such as temperature, humidity and oxygen (Naseem, Yerra, Murthy, & Ramakrishna, 2021).

Crosslinkage or oxidation of the polymeric binder, chain scission, migration of the low molecular weight additives (i.e. Plasticizer) and dewetting are some main possible aging mechanisms which can be categorized as physical and chemical effects of aging (Hasırcı, Akbaş, & Aksoy, 1994); (Kishore, Verneker, & Prasad, 1979); (Cerri S. , Bohn, Menke, & Galfetti, 2013).

The term **"**physical effects/mechanisms of aging**"** which will be frequently emphasized in this thesis, should not be confused with "physical aging" terminology which is the process by which polymer molecules slowly adapt their conformations to a new temperature below the glass transition temperature. Physical effects/mechanisms of aging refer to the possible physical changes and mechanisms (i.e. dewetting, thermal stress, plasticizer diffusion) that may occur in a material due to aging.

1.2.1 Crosslinking

HTPB is a prepolymer that gives the material its viscoelastic properties and flexibility. However, the double bonds it contains are prone to oxidation (Bunyan, Cunliffe, Davis, & Kirby, 1993); (Sbegue & Villar, 2016). It is generally recognized that the primary aging process involves an oxidative crosslinking reaction of the π bonds in the HTPB pre-polymer backbone (Coquillat, Verdu, Colin, Audounin, & Nevie, 2007) (Celina, J.M., Winters, Assink, & Minier, 2006). These π bonds are

susceptible to attack by oxygen in the air and various free radicals (Eslam, Sherif, Ahmed, & Hosam, 2020).

The unsaturated double bonds present in hydroxy-terminated polybutadiene (HTPB), as depicted in Figure 1.8, render it susceptible to various oxidation reactions, including peroxidation, hydroperoxidation, and crosslinking. These oxidative processes can lead to a deterioration of the material's viscoelastic characteristics and potentially induce malfunctions in the systems where HTPB is employed.

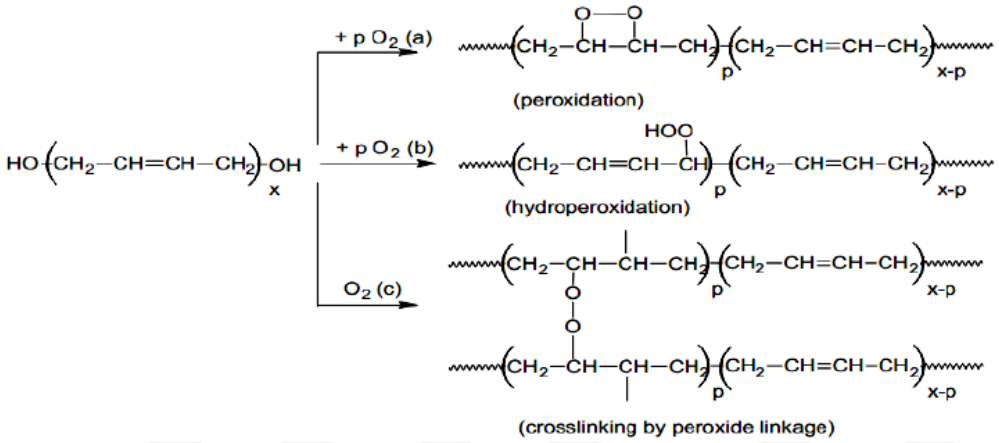


Figure 1.8. Oxidative degradation reactions of HTPB (Eslam, Sherif, Ahmed, & Hosam, 2020)

An increase in crosslink density within the polymer network results in a more branched macromolecular architecture. This augmentation of average molecular weight is inversely correlated with material flexibility (Adel & Liang, 2019). The inclusion of antioxidants serves to mitigate these oxidative degradation pathways to a specific degree (Celina, J.M., Winters, Assink, & Minier, 2006). Their mechanism of action involves the donation of hydrogen atoms to free radicals, thereby inhibiting the formation of further radical species and consequently preventing their interaction with the unsaturated double bonds present in the polymer.

1.2.2 Chain Scission

In hydroxy-terminated polybutadiene (HTPB) and isophorone diisocyanate (IPDI) based polyurethane systems, two primary radicalic reactions are observed. One of these is the oxidative crosslink process as previously discussed. The second involves the degradation and scission of macromolecular chains, which becomes more pronounced with increasing thermal and mechanical stress subsequent to the crosslinking. Elevated temperatures associated with thermal aging induce alterations in the material's microstructure. Thermal energy can initiate chain scission processes, resulting in a heterogeneous morphology characterized by a distribution of soft and hard segments within the polyurethane matrix. However, the rate at which this microstructural evolution occurs is depend on the specific compositional formulation of the polyurethane material (Tcharkhtchi et al., 2014). The processes of crosslink and chain scission represent two concurrently occurring and counteracting phenomena within the material (Cerri S. , Bohn, Menke, & Galfetti, 2009); (Adel & Liang, 2019). Consequently, a rigorous approach is necessary when characterizing the aging behavior of the material to account for the dynamic interplay between these competing mechanisms. In hydroxy-terminated polybutadiene (HTPB) and isophorone diisocyanate (IPDI) based polyurethane systems, generic illustration of chain scission reaction is shown in Figure 1.9.

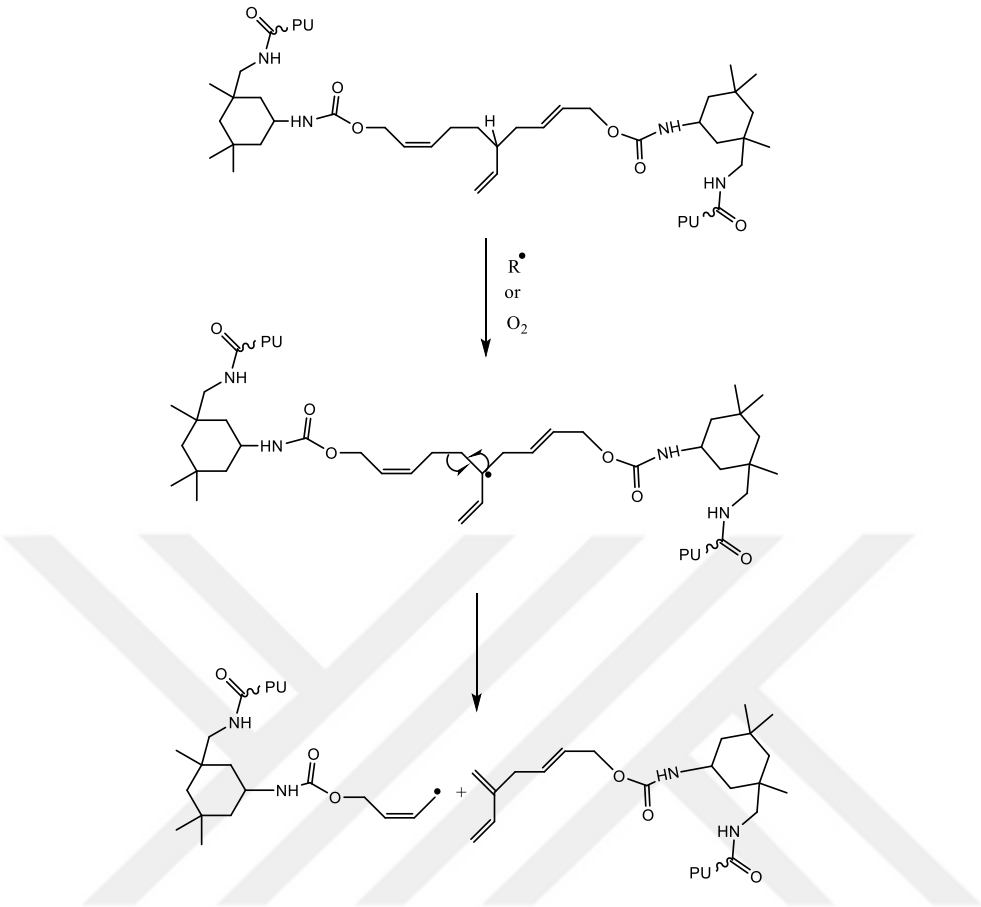


Figure 1.9. Chain scission mechanism of HTPB-IPDI based polyurethane (PU)

1.2.3 Migration of Low Molecular Weight Components

Migration of non-chemically bonding additives is an important aging mechanism. Plasticizer migration represents a significant challenge in the application of plasticizers within polymeric matrices. Plasticizers are additives used to improve processability, flowability and workability of polymer bonded explosives by elongating the polymer chain structure. They are inert components with low molecular weight. A substantial body of research has established that plasticizer migration is critical behavior, with significant implications for the homogeneity of propellant compositions (Yaacob et al., 2023). This phenomenon entails the diffusion of plasticizer molecules within the polymer bulk, leading to their subsequent exudation onto the material surface, a process observed even under non-

aggressive storage environments. Due to this migration, it is possible to observe composition changes in energetic materials, mechanical and performance property changes such as dewetting and related structural integration and ballistic problems (Khan, 1993); (Bennet & Carpenter, 1983); (Gottlieb & Bar, 2003). Figure 1.10 illustrate the diffusion of plasticizer through polymer structure.

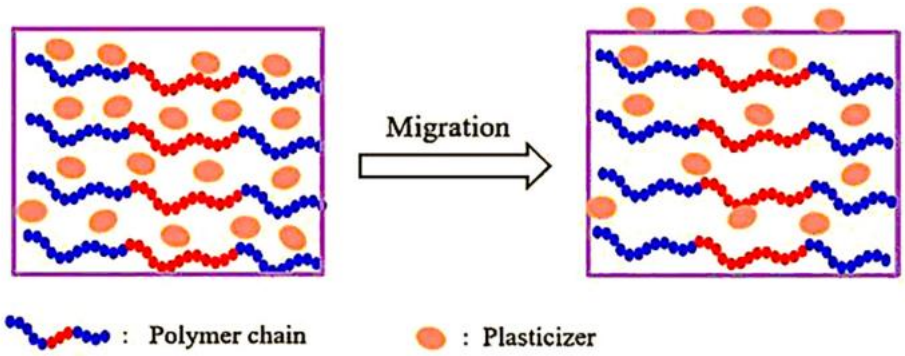


Figure 1.10. Diffusion of plasticizer through polymer (Khanlari, Bayat, & Bayat, 2022)

1.2.4 Dewetting

The separation of particles from the matrix due to interface failure is known as dewetting, a common form of damage that has a significant impact on the mechanical properties of the polymer bonded explosives and solid composite propellant (Zou & Zi-Jie, 2023). External forces or aging can lead to de-bonding or cracking in the cured PBXs if the interactions between the polymer matrix and solid particles are insufficiently strong. Dewetting can be mitigated by coating the surface of solid particles with coupling agents, which form physical bonds with the polymer matrix (Yadav, Pant, & Das, 2020).

1.3 Scope of the Study

Since, degradation process is usually too slow to conduct normal aging studies in reasonable times; accelerated aging procedures are used to reduce the time scale for

such studies (Judge, 2003); (Biggs, 2009). Accelerated aging at higher temperatures was used to determine the behavior and performance of the sample in a shorter time. In this study, the physical and chemical effects of aging on a castable plastic bonded explosive (PBXN-109) whereby antioxidant and bonding agent contents were changed subjected to accelerated aging. For this purpose Shore A hardness, crosslink density, antioxidant content, tension, fourier transform infrared (FTIR) spectroscopy, dynamic mechanical analysis (DMA) and scanning electron microscopy (SEM) tests were carried out. The accelerated aging temperature was between 30°C and 80°C with aging time adjusted to thermal equivalent load of 10 years approximately for 60°C and higher temperatures. Although there are studies on the aging of energetic materials in the literature, the holistic approach intended to be put forward in this thesis is unfortunately not included in existing studies or is addressed from a limited perspective. This study aims to understand the physical and chemical effects of aging behavior and characterize it from a holistic perspective. It is evaluated that understanding the effect of antioxidant and bonding agent which is not included in every energetic material formulation but is known to have an important function, on aging behavior will enrich this goal.

CHAPTER 2

LITERATURE REVIEW

It is possible to categorize polyurethane-based energetic mixtures into two main groups: polymer bonded explosives and composite solid propellants. Non-energetic components used in polymer bonded explosives and composite solid propellants are often common. Since the aging of polyurethane-based energetic materials is generally explained in terms of the properties or behavior of the polymer structure, no distinction was made between explosives and propellants in the literature review. There are studies addressing different dynamics of aging in the aging of energetic materials and are explained in this section.

Aging of polyurethane leads to matrix hardening, primarily through crosslinking that occurs via double bonds present in its structure. Hasırcı et al. investigated the thermal aging of HTPB (hydroxyl-terminated polybutadiene) across various temperatures, assessing its physical, mechanical, and chemical changes. In this study, HTPB was aged at 50ºC, 65ºC, 80ºC, and 100ºC over 240 days, during which viscosity and molecular weight were monitored. Both properties increased with aging, while additional tests examined the mechanical properties and chemical structure of HTPB. FTIR analysis of aged HTPB revealed a rise in OH peaks, attributed to double bond breakage. The glass transition temperature also rised due to reduced free volume with aging. The aged binder was subsequently mixed with a curative (IPDI) and an antioxidant, forming a polyurethane structure upon curing. Tensile tests showed that elongation at break decreased while modulus increased with aging. These mechanical changes are attributed to the formation of crosslinks and increased OH functional groups of aged binder prior to mixing with curative. Additionally, lifetime prediction was conducted using the Arrhenius time-temperature relationship, with the time to 50% property deterioration used as the lifetime criterion. The study

estimated the lifetime of HTPB, and thus the polyurethane matrix, to be approximately 7 years (Hasırcı, Akbaş, & Aksoy, 1994).

In a separate study, Setyaningsih et al. investigated the impact of stabilizers on the thermal decomposition of aged solid propellant. The study examined how stabilizers influenced the thermal decomposition temperature over a 40-day storage period at 60 ºC for aged samples, compared to unaged samples. This analysis was conducted using a Differential Scanning Calorimetry (DSC) device. The Ozawa method was applied to determine kinetic parameters such as activation energy (E_a) and the pre-exponential factor (A). The composite solid propellant used in the study consisted of HTPB as the binder, IPDI as the curing agent, DOA as the plasticizer, and ammonium perchlorate (AP) as the oxidizer. AO 2246, a type of hindered phenol stabilizer, was added in varying amounts: 0%, 0.2%, 0.5%, and 1% by weight of the binder. Results indicated that aged propellants showed higher activation energy, reflecting reduced reactivity. Additionally, increasing the stabilizer content raised the activation energies for both aged and unaged samples to some extent. The optimal stabilizer concentration appeared to be 0.5% by binder weight, as further increases did not significantly affect the activation energies of either aged or unaged propellants (Setyaningsih, Juwono, & Supriyatno, 2017).

Adel et al. searched the service life prediction of AP/Al/HTPB solid rocket propellant, focusing on its softening aging behavior. The study included accelerated aging at 65ºC for 231 days, alongside normal aging at 25±3ºC with less than 50% relative humidity over an 8 years period. Mechanical properties were assessed through tensile testing, which showed that tensile strength and Young's modulus initially increased but gradually declined with aging. The aging process involved various reactions such as post-curing, oxidative crosslinking, chain scission, and hydrolysis. Initially, post-curing and oxidative crosslinking increased tensile strength and modulus, but chain scission and hydrolysis later softened the propellant, making it more flexible. Both normal and accelerated aging exhibited similar aging trends. The study estimated the shelf life of the propellant to be approximately 13 years, using the Arrhenius approach and a pre-determined modulus value as the life

criteria (Adel & Liang, 2019). However, in this thesis, the systematic softening aging mechanism mentioned in this source was not observed for lifespan determination. Therefore, an approach based on the hardening behavior of aging, predominantly discussed in various literature sources, was utilized. It was also noted that the softening behavior observed in this study emerged after 2 years, with hardening due to crosslink observed prior to that.

Ahmadi et al. explored the relationship between laser-induced breakdown spectroscopy (LIBS) and dynamic mechanical analysis (DMA) to evaluate the aging effects on plastic bonded explosives (PBX). The study examined the aging of fifteen cast-cured PBX samples at 60°C and 70ºC over five time intervals within a 29-day period. LIBS analysis revealed that CN band intensities decreased with aging, attributed to increased crosslinking, while AlO intensities rose due to oxidation. DMA measurements of storage modulus and tan δ indicated that tan δ decreased as chain mobility was reduced by increased crosslinking. The study found a strong correlation between the results from LIBS and DMA, indicating consistent findings across both methods (Ahmadi, Keshavarz, & Atabak, 2019).

Gorji et al. compared the Berthelot and Arrhenius methods for predicting the shelf life of a propellant. Aging experiments were performed at 313, 323, 333, and 343 K, with a 2.2% reduction in triethylamine concentration chosen as the shelf-life criterion. This level of depletion was reached within one year across all temperatures. The activation energy of the propellant was determined to be approximately 65 kJ/mol using the Arrhenius approach to assess depletion rates at each temperature. Shelf-life estimates at 293 K were found to be 5.7 years using the Arrhenius approach and 3.93 years using the Berthelot approach (Gorji & Mohammadi, 2013).

Wang et al. investigated the tensile behavior of thermally aged HTPB propellant at low temperatures under dynamic loading. Propellant samples underwent accelerated aging for over 98 days at 343.15 K with less than 10% relative humidity in a load-free condition. The effects of aging on tensile behavior were analyzed using an Instron testing machine, and microscopic damage was examined via SEM. Models

and numerical master curves were used to determine the tensile mechanical properties of the HTPB propellant under varying conditions of temperature, strain rate, and aging duration. Results showed that both temperature and strain rates significantly influenced tensile properties and SEM observations due to oxidative crosslinking. Additionally, the strain at maximum tensile stress was used as the failure criterion for further analysis (Wang, Qiang, Wang, & Wang, 2019).

Shekhar et al. examined the stress-strain behavior of aged composite solid propellants. Samples were aged at ambient conditions over an extended period, and two propellant types cartridge-loaded and case-bonded were analyzed. Tensile test results indicated that, with aging, tensile strength increased while strain decreased for both types of propellants. Findings revealed that cartridge-loaded composite propellants aged at a slower rate than case-bonded ones, leading to the conclusion that cartridge-loaded propellants have a longer shelf life (Shekhar, 2012).

Yongqiang et al. studied the effect of antioxidants on the storage performance and life prediction of HTPB composite propellants. The tensile strength and maximum elongation of aged samples containing varying antioxidant levels were measured, with a specific strain value chosen as the life assessment criterion. Using the Arrhenius approach and tracking the rate of change in strain values, the propellant lifetimes were estimated. Results showed that propellants with higher antioxidant content had longer predicted lifetimes, as antioxidants act as barriers to oxidative crosslinking in the polymer (Yongqiang, Jian, Jianzhuang, & Xin, 2019) .

Wojnar et al. used a dynamic mechanical analyzer (DMA) to determine the master curve of an aged composite propellant. Samples were aged at 50ºC and 60ºC for periods from one to eight weeks, with accelerated aging estimated to correspond to about six years of natural aging at room temperature. DMA analyses were conducted using double cantilever beams. From the stress relaxation curves, master curves for each aging temperature were developed using the time-temperature superposition method and WLF equations. The results showed that samples aged for longer durations and at higher temperatures exhibited higher relaxation modulus, consistent

with the increased crosslinking occurring during aging (Wojnar, Miller, & & Ghiassi, 2019).

Zhang et al. investigated the thermal decomposition kinetics of a naturally aged composite propellant using DSC. The propellant samples were stored in sealed plastic packages and naturally aged under ambient conditions for over 20 years. DSC scans at various heating rates were performed, and the decomposition kinetic parameters were determined using the Kissinger and Ozawa methods. The results indicated that the kinetic parameters derived from the naturally aged propellant were smaller than those obtained from DSC curves of samples aged under laboratory conditions using similar numerical approaches (Zhang & Zheng, 2018).

Dalby et al. used a multiscale model to predict the lifetime of solid rocket motors with HTPB binder-based propellants. The modeling was performed using Ansys Fluent. The multiscale model incorporated both chemical and physical effects of aging to provide reliable lifetime predictions. A key finding of the study was that aging cannot be simplified into a single reaction with one activation energy, as doing so could lead to inaccurate lifetime predictions. The model accounted for a range of reactions, starting from the molecular scale, where processes like chain welding and scission due to oxidation, debonding of binder/filler ionic bonds from hydrolysis, and plasticization from water and plasticizer migration occur. It extended to the macroscopic scale, predicting changes in the binder's mechanical properties. The connection between these scales was established through structure-property relationships from polymer physics and experimental data from the propellant manufacturer (Dalby & Caraës, 2015).

Gonçalves et al. investigated the shelf life of HTPB/AP-based solid composite propellant by analyzing chemical kinetic parameters obtained through DSC and burn rate tests. The goal of the study was to gather information to potentially extend the shelf life of propellants currently in use for up to 10 years. The aging process was simulated using the Large-Scale Atomic/Molecular massively parallel simulator software. Using heating rates of 5ºC, 10ºC, and 15ºC and applying the Arrhenius

approach with Kissinger and Ozawa kinetics, activation energy and other kinetic parameters were determined. The computational simulation revealed the ability of propellant molecules to rearrange when subjected to compressive forces, leading to the breaking of original chemical bonds and the formation of new ones. This increase in crosslink, which causes a shrinkage in volume, was identified as a potential aging characteristic, possibly leading to fractures and cracks within the propellant mass in a rocket motor. Based on the results, it was concluded that the propellant had not yet aged (Gonçalves, Iwama, Domingues, & Rocco, 2020).

Yıldırım et al. studied the aging of solid rocket motors, focusing on the critical thermal and pressure loading conditions that occur during shipping, storage, and firing. Finite element analysis was used for the structural analysis, and the simulations were conducted using ABAQUS software. The study focused on HTPB-based propellant within a fiberglass casing. Stress and strain distributions of the propellant were determined through the analysis. The maximum hoop stress at the surface of the propellant and the bond stresses at the interface between the liner and propellant were identified as the primary causes of cracking and debonding, and were defined as failure criteria. Both aged and unaged motors were analyzed. The results showed that the maximum hoop strain values were similar for both aged and unaged propellants. However, bond stress increased with aging, leading to the conclusion that bond stress at the liner interface is the most critical factor for determining the shelf life of a motor with solid composite propellant (Yıldırım & Özüpek, 2011).

Shekhar used both the Arrhenius and Berthelot equations to predict the shelf life of solid composite propellants. Accelerated aging, conducted for approximately one year at 60ºC with less than 20% humidity, was used to achieve higher degradation rates. Mechanical tests, including measurements of elongation, were performed at regular intervals. A reduction of more than 50% in elongation from its initial value was used as the lifetime criterion. The results from the Arrhenius and Berthelot equations were compared. The Arrhenius equation showed an exponential variation, while the Berthelot equation followed a power-law variation. The Arrhenius approach depended on activation energy, while the Berthelot approach relied on a 10

ºC reaction rise factor. From the elongation data, an activation energy of 72.8 kJ/mol and a 10 ºC reaction rise factor of 2.4 were found, both of which predicted a shelf life of 20 years under ambient conditions (Shekhar, 2011).

Villar studied the thermal aging of HTPB-IPDI-based polyurethane as a function of the NCO/OH ratio. Samples were aged in air ovens at 50°C, 60°C, 65°C, and 70°C for periods ranging from 1 to 34 weeks. Dumbbell specimens were used for uniaxial tension tests, and swelling tests were also performed on the aged samples. A correlation was established between swelling ratio, elastic modulus, and FTIR spectra. The results showed that as the NCO/OH ratio increased, elastic modulus and hardness increased, while elongation decreased. The changes observed in the infrared spectra of the aged samples were linked to the breakage of double bonds and the buildup of carbonyl groups. Kinetic analysis revealed that an increasing NCO/OH ratio, which corresponds to more urethane linkages, accelerated the oxidation process. The changes in both chemical and mechanical properties indicated that oxidative crosslinking is the primary mechanism behind the degradation of the HTPB binder (Villar, Cicaglioni, Diniz, Takahashi, & Rezende, 2011).

Cerri et al. investigated the aging of solid composite propellant using DMA measurements. The study employed DMA in torsion mode to assess the aging behavior of three HTPB-based SRP formulations with different aluminum particle sizes and contents. Accelerated aging was conducted at temperatures between 60°C and 90°C, with aging times adjusted to simulate a thermal equivalent load of 15 to 20 years at 25°C. The loss factor curves were modeled using Gaussian functions to provide a molecular or microscopic interpretation of the phenomena occurring in the binder. Aging of the propellant formulations was tracked by analyzing two parameters: the areas of the second and third transition peaks and the corresponding temperatures of the Gauss peaks. The modeling revealed that the glass transition temperature (T_g) of the second apparent peak ($T_{g\text{-}rest}$) reflected two distinct molecular phenomena, each represented by different transition temperatures. Additionally, the cause of crosslinking was attributed to oxidative attacks on the amino groups of the bonding agent for AP (Cerri S. , Bohn, Menke, & Galfetti, 2013).

CHAPTER 3

EXPERIMENTAL

In this thesis study, which deals with aging behavior of energetic materials, PBXN-109 explosive and its derivatives are the formulations to be studied. Accelerated aging was applied for all formulations. The aging period was determined as 8 months. STANAG 4666 (NATO Standardization Office, 2015) was taken as reference in determining the aging time as 8 months. This document provides guidance for the aging assessment of polymer bonded explosives. The aim of this agreement is to standardize accelerated aging and testing protocol by which aged samples of PBXs using inert or energetic binders can be assessed and compared. Single temperature aging and testing protocol is described to allow comparisons to be made between aged samples. However, in this study, five different aging temperatures (30°C, 50°C, 60°C, 70°C, 80°C) were selected for aging of nominal PBXN-109 formulation. In this report it is called as R1 (formulation 1). R2 is the formulation with more antioxidant content. R3 is the formulation that does not contain bonding agent. Formulation details are stated on Table 3.1 below.

Table 3.1 Aged explosive formulations

Content (%)	*R1 (Reference)*	*R2*	*R3*
RDX (CXM-7)	64.00	64.00	64.00
Aluminum	20.00	20.00	20.00
HTPB (1 % AO)	7.446	7.349	7.695
DOA	7.371	7.275	7.618
DHE	0.260	0.260	0.000
TPB	0.020	0.020	0.020
IPDI	0.877	0.869	0.645
AO2246	0.026	0.227	0.023
AO Total	0.100	0.300	0.100

3.1 Explosives Production

For this study, three production runs, each yielding approximately 20 kg of polymer bonded explosive, were conducted in 5-gallon capacity planetary mixers. Planetary mixers, which consist of a central blade and another blade performing a planetary rotation around it, are utilized for the production of high-viscosity mixtures such as composite solid propellants or polymer bonded castable explosives (Figure 3.1).



Figure 3.1. Explosive production in a planetary mixer

These mixers operate in a batch system. During the production of each of the R1, R2 and R3 formulations, the materials were sequentially added to the mixer, and mixing was performed in specific steps. The overall production process involves material addition followed by mixing. The mixer is equipped with a heated jacket, and mixing is typically carried out at temperatures between 50°C - 60°C. This elevated temperature enhances material mobility and consequently, mixing efficiency. Initially, liquid components (HTPB, IDP, DOA, DHE) are added to the mixer. After a specific mixing period to ensure homogeneity of the liquid components, the solid materials (CXM-7, Al) are introduced. The solid materials are not added all at once but rather in several divided additions with interdispersed mixing steps. Mixing continues until the solid materials form a sufficiently homogeneous blend with the liquid polymer. Finally, the curing agent IPDI is added, and the final mixing is performed. Although IPDI is a liquid, it is added at the end to prevent premature initiation of the polyurethane reaction. Immediately after IPDI addition, the curing

reaction with HTPB commences during the final mixing stage, leading to an increase in the material's viscosity. The mixture is typically cast into test molds for this study, and often into munitions for practical application. Excessive increase in viscosity can impede the casting process, potentially resulting in air voids within the casing or test molds. These air voids can lead to undesirable sensitivity reactions and inaccurate test results. Therefore, maintaining an optimal viscosity (not exceeding 10000 poise) during casting is crucial. The viscosity of three formulations were below 5000 poise. Even when the viscosity is within acceptable limits, munitions or test molds are subjected to vacuum and vibration during casting to minimize air entrapment. Air voids within munitions pose safety risks under various maintenance conditions (dropping, hot-cold temperature cycles, fire exposure, etc.). Air trapped in these voids can undergo adiabatic compression, creating localized hot spots within the material. These hot spots can initiate a process of adiabatic self-heating, potentially leading to detonation reactions. Munitions or test molds are filled within a vibrating and vacuum-capable chamber. To facilitate the deaeration of air bubbles, the filling chamber is also heated via hot water circulation through its jacketed structure. While elevated temperature accelerates curing, it also aids in the removal of air voids during filling, in conjunction with vibration and vacuum assistance. Following the completion of the mixing and casting processes for all three formulations, the conditioning step was initiated. Conditioning is the period in which the mixture completes its curing reaction before undergoing the post-curing process. This typically spans one week and is conducted within a temperature range of 50°C - 65°C.

3.2 Explosives Sample Preparation

All aged samples for three different formulations belong to single batch production for every formulations. After curing, explosives are placed in the form of a block in a plastic package and artificially aged at the prescribed temperatures and durations in ovens. Figure 3.2 shows a sample block for aging temperature of 80°C at t_0.

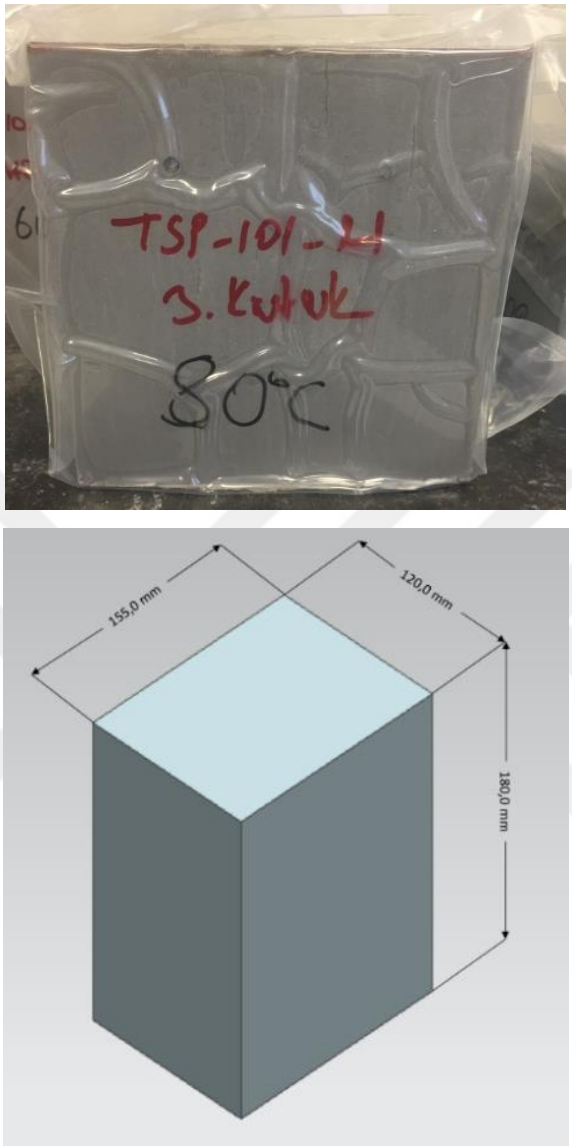


Figure 3.2. Explosive block sample in plastic package and its dimensions

At each testing period during aging a minimum depth of 20 mm removed from all surfaces of the bulk sample. Although explosive blocks were wrapped with plastic packages, the removal of surface layer is intended to minimize aging effects on surface due to the ease of exposure of atmospheric effects (i.e. humidty) on surface which can influence quality of the bulk. Aged PBX sample blocks should be large

enough to readily extract samples from the layers for testing purposes as shown in Figure 3.3.

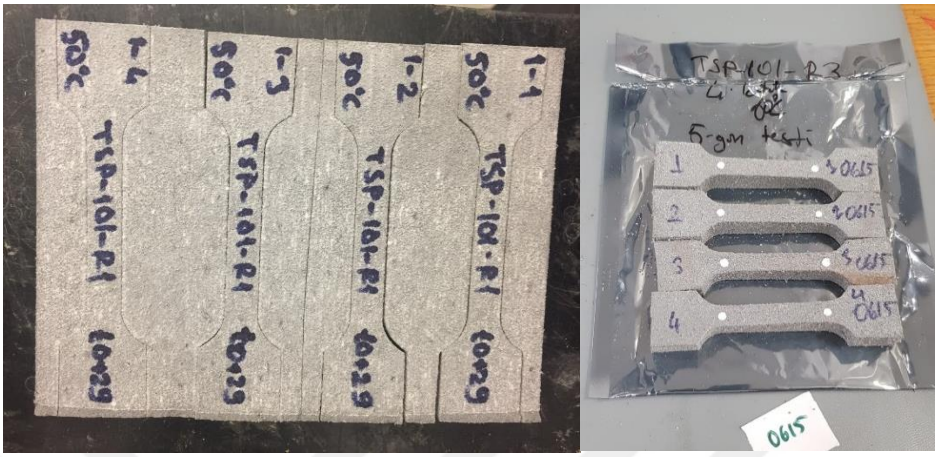


Figure 3.3. Dog-bone shaped tensile test specimens prepared from sliced explosive composite layers

3.3 Aging Procedure

During the 8-months aging period, tests were conducted at various time intervals specific to each temperature. These intervals are detailed in Table 3.2, which outlines the testing times for the respective temperatures. However, DMA, SEM and FTIR analyses were not performed for all temperatures and times given in the Table 3.2 The initial row (t_0) represents the baseline testing performed prior to the commencement of the aging period. Subsequent rows (t_1 through t_7) indicate the duration of aging. A dash (-) indicates that no testing was performed at that specific time point for the given temperature. Accelerated aging was applied across all temperature levels for the nominal PBXN-109 formulation (R1), whereas aging for the R2 and R3 formulations was conducted solely at 60°C only. The rationale behind employing multiple aging temperatures for the R1 formulation was to examine and better understand the impact of temperature-dependent aging on material properties. In contrast, the R2 formulation, characterized by a modified antioxidant ratio, and the R3 formulation, lacking a bonding agent, were aged at a single temperature

(60°C) to evaluate the specific effects of antioxidant content and bonding agent presence on aging behavior.

Table 3.2 Aging temperatures and test intervals for the R1, R2 and R3 formulations (60°C only for R2 and R3)

Test Times	*80°C (days)*	*70°C (days)*	*60°C (days)*	*50°C (days)*	*30°C (days)*
t_0 (initial)	**t_0**	**t_0**	**t_0**	**t_0**	**t_0**
t_1	5	9	16	29	52
t_2	9	16	29	52	94
t_3	**16**	29	52	94	**135**
t_4	29	**52**	94	**135**	170
t_5	**52**	94	**135**	170	**240**
t_6	-	**135**	170	**240**	-
t_7	-	-	**240**	-	-

Test times are post-production t_0, 5^{th}, 9^{th}, 16^{th}, 29^{th}, $52^{nd,}$ 94^{th}, 135^{th}, 170^{th} and 240^{th} days. Test time intervals were determined as logarithmically. As temperature decreases, time rate of change of properties with aging decreases. Hence, first test times (t_1) after post productions (t_0) are intentionally selected at increasing order as temperature decreases. Therefore, the initial test times (t_1) after production (t_0) were deliberately selected in increasing order as temperature decreased. At higher temperatures, rapid changes in properties are expected, leading to shorter test times. Consequently, as the temperature decreases, the final test time (or aging time) is extended to ensure convergence with the results obtained from high-temperature aging at the end of the testing period. Therefore, higher temperatures involved more frequent testing intervals within the 8-month period to capture the accelerated aging effects. For instance, the 80°C samples were tested more frequently in the initial stages compared to the 30°C samples, which had test times with longer intervals.

Aging times were calculated using the time-temperature equivalent load principle. The increase / decrease of temperature by 10°C increases / decreases the reaction rate constants by an average factor F of 3, the range often is between 2 to 4. This factor was deduced from the work of Van'T Hoff, who compiled and compared

reaction rates obtained at different temperatures (Bohn M. , 2009). Higher values of F are possible, up to 6. The generalized form of this observation is written as Eq.(1) and gives the temperature parameterization of the reaction rate constant with H as pre-factor and ΔT_F as temperature interval related to the used factor F.

$$k(T) = H.F^{\frac{T}{\Delta T_F}} \qquad \text{Eqn. (1)}$$

$$\frac{k_2(T_2)}{k_1(T_1)} = F^{(T_2-T_1)/\Delta T_F} = \frac{t_1(T_1)}{t_2(T_2)} \qquad \text{Eqn. (2)}$$

Eq. (2) corresponds to the generalized Van't Hoff rule. For practical application the following formulas containing units are useful as Eq. (3).

$$t_E = t_T.F^{\frac{T_T-T_E}{\Delta T_F}}/365.25 \qquad \text{Eqn. (3)}$$

1 year = 365.25 days

t_E in-use time in years at temperature T_E

t_T test time in days at test or aging temperature T_T

T_T test or aging temperature

T_E in-use temperature

F acceleration or deceleration factor per 10ºC temperature change

ΔT_F temperature interval assigned to actual value of factor F, mostly 10ºC

In accordance with STANAG 4666 (NATO Standardization Office, 2015), the acceleration factor (F) was determined using Eq. (3), based on the assumption that an 8-month aging period at 60°C is equivalent to a 10-12 year shelf life. Utilizing the calculated F factor of 2.23, the accelerated aging times required to simulate 10 years of storage under ambient conditions, a typical lifetime criterion for these material types (Naseem, Yerra, Murthy, & Ramakrishna, 2021) were computed for

80°C, 70°C, and 60°C. For the 50°C and 30°C conditions, the final accelerated aging duration was selected to correspond to a minimum of 10 years of natural aging time (240 days) at the 60°C accelerated aging temperature. The time-temperature equivalences for accelerated aging relative to 25°C reference temperature are presented in Table 3.3. This table tells us that the effects of aging that would normally take many years to occur at a standard temperature (25°C, roughly room temperature) can be achieved much faster by exposing the material to higher temperatures. The table clearly illustrates how sensitive the aging process is to temperature changes. Even a relatively small increase in temperature can significantly reduce the time it takes for aging effects to become apparent. For example, approximately 5 days of exposure at 80°C is roughly equivalent to 1.1 years at 25°C. Similarly, 170 days at 50°C would have a similar aging effect as 3.5 years at 25°C.

Table 3.3 Equivalent isothermal aging durations at elevated temperatures for predicting long-term behavior at 25°C

Accel. Aging at 80ºC (Day)	*Equiv. Aging at 25ºC (Year)*	*Accel. Aging at 70ºC (Day)*	*Equiv. Aging at 25ºC (Year)*	*Accel. Aging at 60ºC (Day)*	*Equiv. Aging at 25ºC (Year)*	*Accel. Aging at 50ºC (Day)*	*Equiv. Aging at 25ºC (Year)*	*Accel. Aging at 30ºC (Day)*	*Equiv. Aging at 25ºC (Year)*
0	0	0	0	0	0	0	0	0	0
5	1.1	9	0.9	16	0.7	29	0.6	52	0.21
9	2.0	16	1.6	29	1.3	52	1.1	94	0.38
16	3.6	29	2.9	52	2.4	94	1.9	135	0.55
52	11.7	52	5.3	94	4.3	135	2.7	170	0.70
-	-	94	9.5	135	6.1	170	3.5	240	0.98
		135	13.6	170	7.7	240	4.9	-	-
-	-	-	-	240	10.9	-	-	-	-

Crosslink density, antioxidant content, tensile strength, hardness, FTIR, DMA and SEM analyses were performed on the aged samples. The specific tests performed and their corresponding time points are detailed in Table 3.4. Table outlines which characterization tests were performed on aged samples and at which time intervals (denoted by t_0, t_1, t_2, etc.) under various accelerated aging temperatures (80°C, 70°C,

60°C, 50°C, and 30°C). Tests were not conducted at every aging interval. The exact days (t) on which the tests were carried out at each temperature are listed in Table 3.2.

Table 3.4 Conducted tests and schedule for each aging temperatures for all temparatures (60°C only for R2 and R3)

Tests	*80°C*	*70°C*	*60°C*	*50°C*	*30°C*
Crosslink Density	t_0, t_1, t_2, t_3, t_4, t_5	t_0, t_1, t_2, t_3, t_4, t_5, t_6	t_0, t_1, t_2, t_3, t_4, t_5, t_6, t_7	t_0, t_1, t_2, t_3, t_4, t_5, t_6	t_0, t_1, t_2, t_3, t_4, t_5
Antioxidant Measurement	t_0, t_1, t_2, t_3, t_4, t_5	t_0, t_1, t_2, t_3, t_4, t_5, t_6	t_0, t_1, t_2, t_3, t_4, t_5, t_6, t_7	t_0, t_1, t_2, t_3, t_4, t_5, t_6	t_0, t_1, t_2, t_3, t_4, t_5
Tension Test	t_0, t_1, t_2, t_3, t_4, t_5	t_0, t_1, t_2, t_3, t_4, t_5, t_6	t_0, t_1, t_2, t_3, t_4, t_5, t_6, t_7	t_0, t_1, t_2, t_3, t_4, t_5, t_6	t_0, t_1, t_2, t_3, t_4, t_5
Hardness	t_0, t_1, t_2, t_3, t_4, t_5	t_0, t_1, t_2, t_3, t_4, t_5, t_6	t_0, t_1, t_2, t_3, t_4, t_5, t_6, t_7	t_0, t_1, t_2, t_3, t_4, t_5, t_6	t_0, t_1, t_2, t_3, t_4, t_5
FTIR	t_0, t_2, t_3, t_5	t_0, t_2, t_4, t_6	t_0, t_3, t_5, t_7	t_0, t_2, t_4, t_6	t_0, t_1, t_3, t_5
SEM	t_0, t_3, t_5	-	t_0, t_5, t_7	-	t_0, t_3, t_5
DMA	t_0, t_2, t_4, t_5	-	t_0, t_3, t_5, t_7	-	t_0, t_1, t_3, t_5

3.4 Test Methods

3.4.1 Hardness Measurement

Hardness tests were carried out with Bareiss brand Shore A type durometer device (Figure 3.4). Shore A hardness provides a straightforward measurement of a rubber material's response to a standardized pressing force. Of the various hardness scales,

Shore A utilizes a steel indenter shaped like a truncated cone for its measurements. Within the Shore A hardness scale, an inverse relationship is observed between material hardness and penetration depth. Specifically, a Shore A hardness value of 0 corresponds to a maximum penetration depth of 2.5 mm, whereas a value of 100 indicates a penetration depth of 0 mm (International Organization for Standardization, 2003). The device has been carefully placed in direct contact with the sample as shown in Figure 3.4.

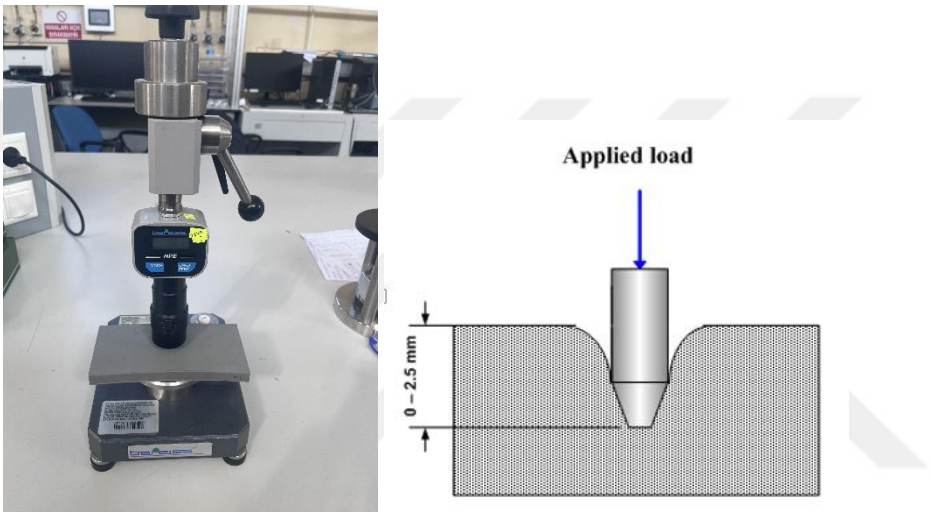


Figure 3.4. Shore A hardness measurement and illustriation of indenter through material

Hardness measurements were performed on each side of 12.5 mm thick rectangular samples extracted from aged blocks. These samples were prepared by removing a 20 mm surface layer from aged blocks at each aging interval. Each individual measurement was completed within 15 seconds. Since hardness testing involves averaging multiple readings, results inherently include a margin of error defined by standard deviation. For every test sample, a minimum of ten measurements (five per side) were performed at different locations, and the average value was calculated. The measurement locations on one side of the sample are illustrated in Figure 3.5.

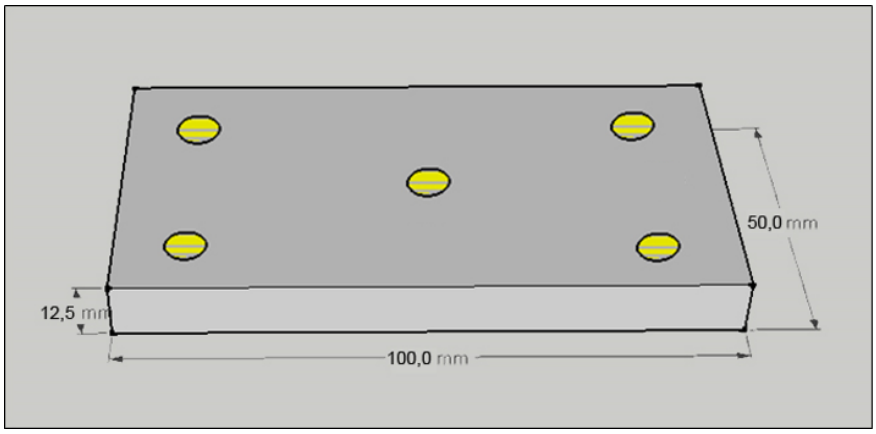


Figure 3.5. Shore A hardness measurment locations on sample

3.4.2 Crosslink Density Measurement

Crosslink Density measurement is based on STANAG 4666 (NATO Standardization Office, 2015). At crosslink density measurement a sample of the polymer bonded explosive with a known volume is swollen in toluene at a stable and known temperature (ideally room temperature). The soluble or extractable content is a key parameter for assessing the degree of crosslink or chain scission in a crosslinked polymer. A higher fraction of non-crosslinked polymer chains results in a greater soluble fraction. When crosslink is dominant, an insoluble macroscopic gel forms. This fraction includes all extractable components, such as plasticizers and antioxidants. Test set up and its components are shown in Figure 3.6.

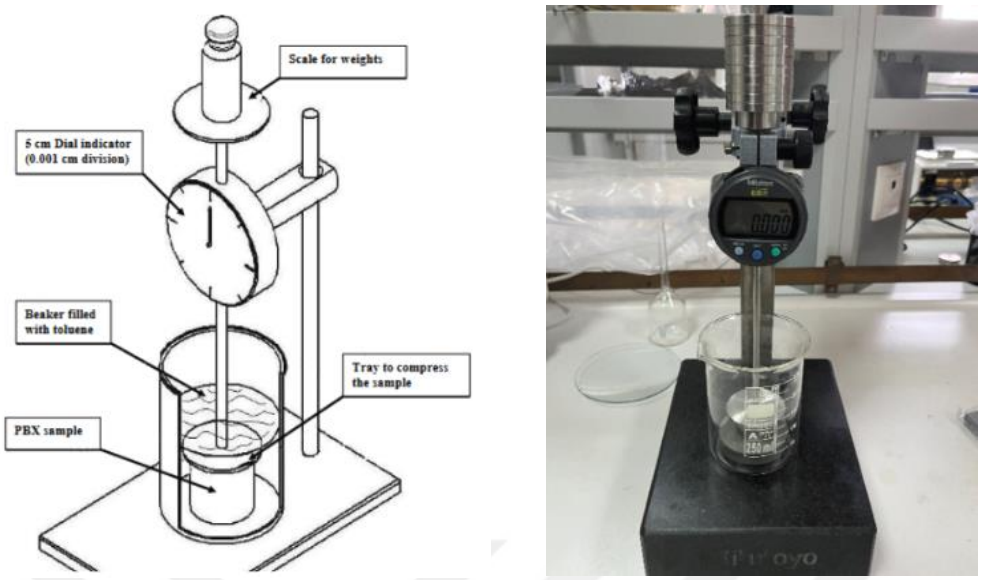


Figure 3.6. Crosslink density measurement test set-up and its components

To study the swelling behavior of PBX samples, precise discs (1.5 cm high, 2.5 cm diameter) were prepared. Each disc was fully immersed in 60-100 ml of toluene within a beaker to ensure consistent swelling throughout the experiment. The samples remained submerged until they reached a stable swelling point (equilibrium). This equilibrium was confirmed by monitoring the sample's weight every 30 seconds for 5 minutes; a stable weight indicated equilibrium. After reaching this stable swollen state (typically taking about one week), compression measurements were conducted. These measurements involved gradually applying weights, ranging from 40 to 400 grams, onto the swollen sample and recording the resulting vertical displacement for each added weight. Figure 3.7 illustrates an example of how displacement changes with applied weight for the R1 formulation.

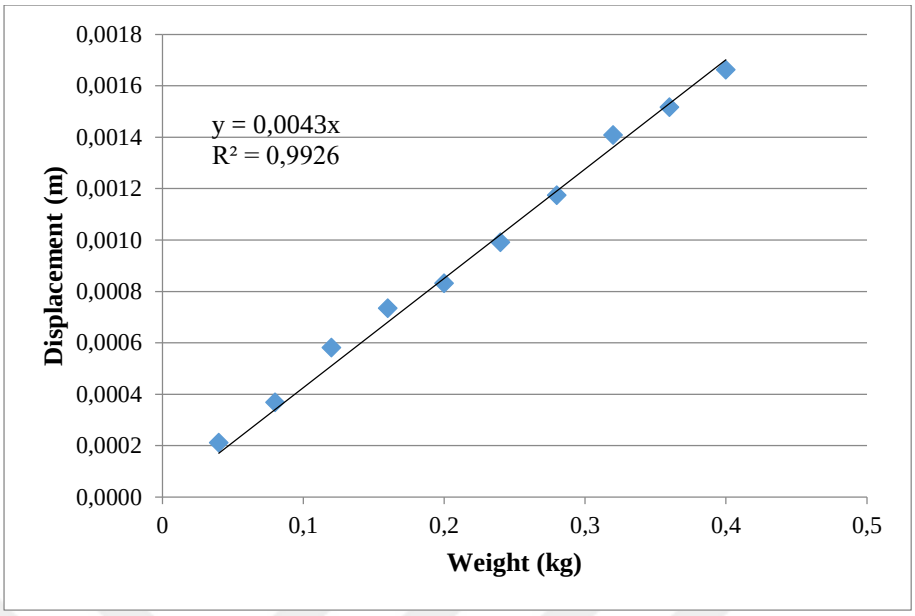


Figure 3.7. A representative load-displacement curve for a tested sample, used to ascertain the compression modulus necessary for crosslink density measurement

Following each weight application and displacement recording, the weight was removed, and the swollen PBX sample was allowed to recover its equilibrium shape in the toluene for 2 to 5 minutes. To ensure accurate measurements, the initial zero displacement reading might have been recalibrated, particularly after applying heavier weights. The compression testing was stopped once a satisfactory plot of weight against displacement was obtained, usually after ten data points. This data was then plotted to create a weight versus deflection graph. The compression modulus (S), a measure of the swollen material's stiffness, was determined from this graph. This modulus was subsequently used to calculate the crosslink density (the degree of interconnectedness within the material) using a formula (Eqn. 4) derived from the Flory-Rehner theory (Flory & Rehner Jr, 1943). To ensure the reliability of the results, these measurements were conducted on at least two separate PBX samples.

$$C = \frac{h_0 S}{3 A_0 R T} \ (mole/m^3) \qquad \text{Eqn. (4)}$$

Where,

h_o : Height of the sample (m)

A_o : Area of the cross section (i.e. circular face) (m^2)

R : Gas constant (8.315 J/mole.K)

T : Temperature (K)

S : Slope of the displacement vs. weight plot x 9.807 m/s^2 (N/m)

C : Crosslink density ($mole/m^3$)

3.4.3 Antioxidant Measurement

The method utilizes solutions obtained after maceration of the PBX in any suitable solvent according to the formulation. The determination of antioxidant content is measured by high performance liquid chromatography (HPLC) using an internal standard procedure. The test procedure involves two main steps: preparation of the solution and extraction. First, 10 mg of antioxidant and 10 mg of internal standard are weighted to 0.1 mg precision. Then, these are dissolved in 50 ml of methanol. If needed, dilution to a larger volume is acceptable as long as the mass to volume ratio is maintained. In the second step, approximately 5 g of polymer bonded explosive is cut into 2 to 3 mm pieces and 10 mg of internal standard is extracted in 50 ml of methanol. Mixture is agitated for at least 6 hours, then it is allowed to settle for a few minutes. 10 to 15 ml of the supernatant are taken and centrifuged or filtered to achieve a clear solution. Finally, 3 µl of the prepared solution is injected into the HPLC, ensuring that both the standard and sample solutions are injected under identical operating conditions. Antioxidant content is determined by calculating the peak areas obtained from HPLC. Mobile phase of acetonitrile (80%) and water (20%) with a flow rate of 3 ml/min and injection volume of 1 µl and 30°C column temperature were operating parameters of HPLC.

3.4.4 Tension Test

Tensile tests were conducted on aged molds by cutting them into standard dog-bone-shaped specimens for each testing interval. During analysis, stress and strain values at the point of maximum load were used to assess elongation. The typical dimensions of the dog-bone samples are illustrated in Figure 3.8.

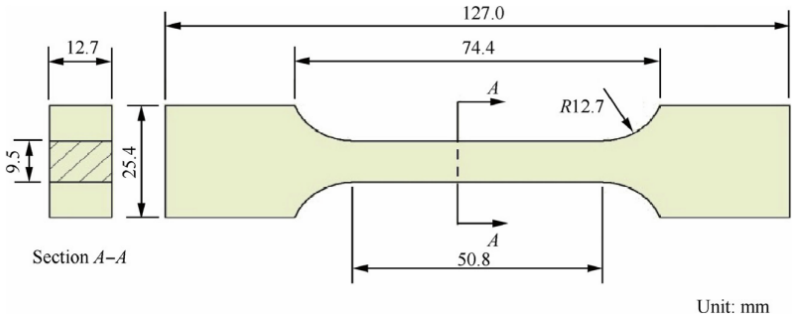


Figure 3.8. Standard dimensions for uniaxial tensile specimen (Adel & Liang, 2019)

Due to the inherent variability of the explosive material and the composite structure, as well as potential inconsistencies in sample preparation, tensile test results may display unexpected patterns. To account for this, each test result represents the average of four dog-bone specimens. Testing was carried out using an Instron universal testing machine at test temperature of $25 \pm 2°C$ and a cross-head speed of 50 mm/min.



Figure 3.9. Instron universal testing machine

3.4.5 Fourier Transform Infrared Spectroscopy (FTIR) Measurements

FTIR spectroscopic analysis was carried out with a Perkin Elmer Spectrum 100 device equipped with Attenuated Total Reflectance (ATR) with spectral range of 4000 – 450 cm^{-1} and 1 cm^{-1} resolution. This test aims to analyze the changes in selected functional groups due to aging. With this test, it is aimed to observe the aging behavior of carbonyl (C=O) group in the polyurethane structure.

3.4.6 Dynamic Mechanical Analysis (DMA) Tests

Dynamic mechanical measurements were carried out in tension mode using a DMA instrument of type DMA850 manufactured by TA Instrument. Tests were conducted in temperature sweep mode with a strain amplitude of 0.1% (in order to stay in linear viscoelastic range), frequency of 1 Hz, temperature range of -100°C to 100°C, and heating rate of 3°C/min. Sample dimensions were 10 mm wide, 5 mm thick and 50 mm long. The viscoelastic properties (tan (d), storage modulus (E')) of the material as a function of aging were investigated via DMA. Tests were performed at the

temperatures and times indicated in Table 3.4. Figure 3.10 illustrates the sample placement within the instrument.

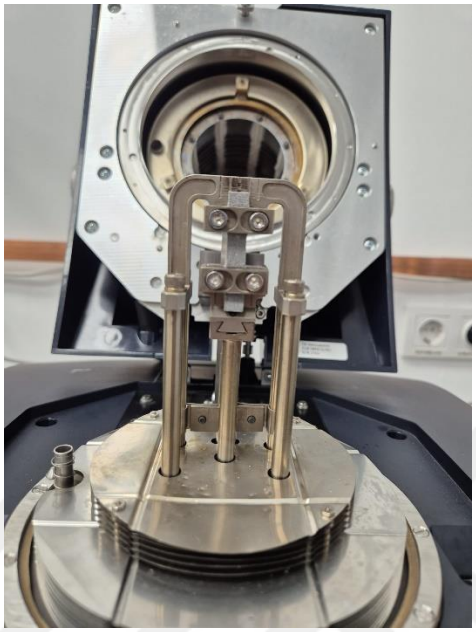


Figure 3.10. Sample in tension clamp at DMA

3.4.7 Scanning Electron Microscopy (SEM) Analysis

SEM analyzes were performed on the rupture interfaces of the dog bones remaining from the tension tests with a Zeiss Evo 40 model Scanning Electron Microscope located in Ankara University. This test aims to observe the physical interaction between solid filling materials and polymer structure due to aging. The samples were examined at 20 kV accelerating voltage and between 100x to 1000x magnification ranges.

This research focuses on analyzing the fracture interfaces of post-tensile test specimens as a function of aging. The ultimate goal of this study is to characterize the influence of aging on polymer-filler interactions based on the findings.

CHAPTER 4

RESULTS AND DISCUSSION

4.1 Shore A Hardness

Hardness measurements were conducted over a period of time for each temperatures, with data points representing the mean hardness values at each time interval stated in Table 3.2. In each hardness measurement, at least 10 hardness measurements were conducted from the test sample at different points and the average value is calculated within a certain standard deviation. Figure 4.1. illustrates the temporal evolution of Shore A hardness for the R1 formulation under isothermal aging conditions at varying temperatures whereas Figure 4.2 and Figure 4.3 represents evolution of Shore A hardness at 60°C. Error bars on the plots indicate the standard deviation of measurements, providing a measure of data variability.

The data for the R1 (Figure 4.1) reveals a general trend of increasing hardness over time, and temperature. Specifically, higher aging temperatures (i.e. 80°C) appear to accelerate the increase in Shore A hardness compared to lower temperatures (i.e. 60°C). The initial hardness (t_0) values and the subsequent increase in hardness suggest a time-dependent hardening of the R1 formulation. These findings highlight the impact of both aging time and temperature on the viscoelastic properties of the material.

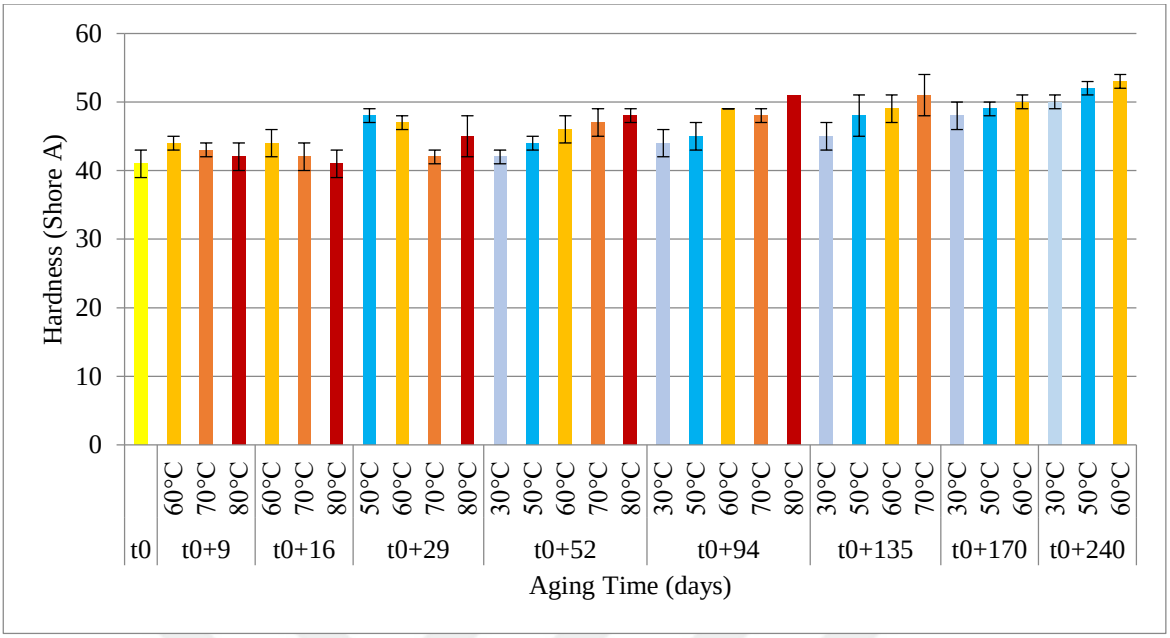


Figure 4.1. Shore A hardness change as a function of the aging time at all aging temperatures for the R1 formulation

While both the R2 and R3 formulations exhibit some variability in hardness measurements over time (Figure 4.2 and Figure 4.3), a general tendency towards increased hardness with aging is evident for R2, similar to R1. In contrast, the R3 formulation displays greater instability in hardness values. This increased fluctuation is proposed to be a consequence of inadequate polymer-filler interaction due to the absence of a bonding agent, leading to non-uniform distribution of the solid filler within the matrix for R3.

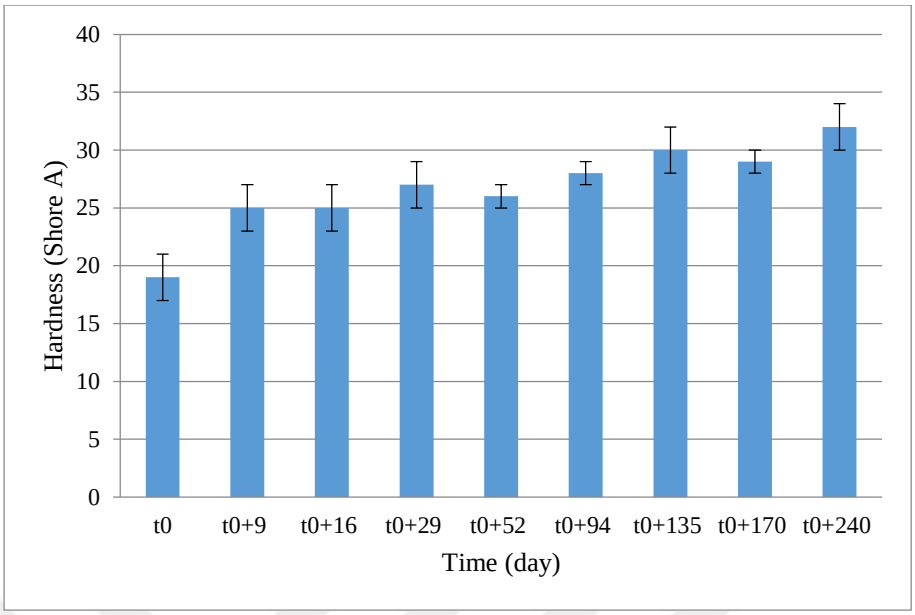


Figure 4.2. Shore A hardness change as a function of the aging time at 60°C for R2 formulation

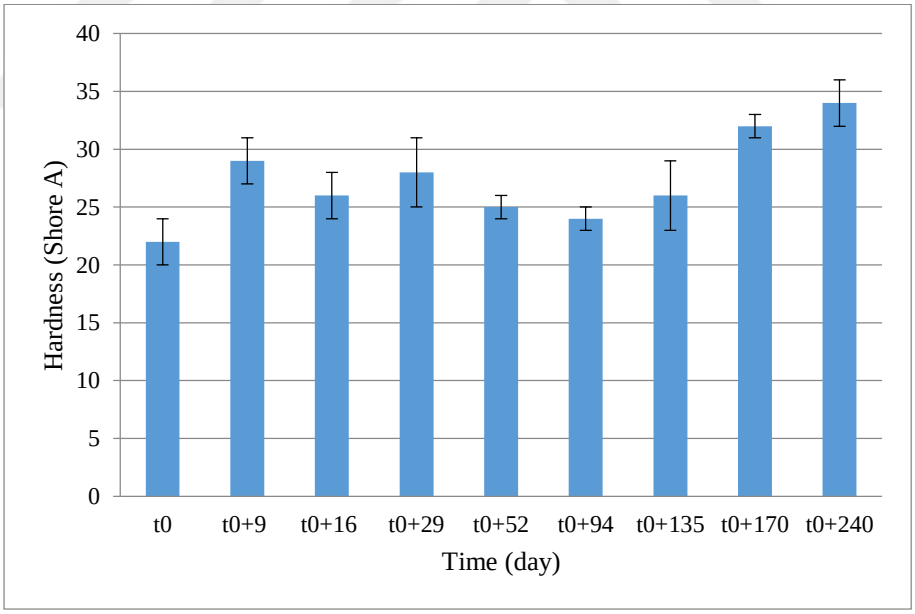


Figure 4.3. Shore A hardness change as a function of the aging time at 60°C for R3 formulation

Despite the general trend of increasing hardness as a function of aging time and temperature, some fluctuations are observed for all three formulations. To minimize

moisture influence during aging, the material was plastic package-sealed. However, a 24-hour conditioning period at room temperature was implemented before testing commenced. Although the effect is anticipated to be small, some moisture exposure is likely to ocur during this period.

In the 30-day aging study conducted by Lai et al. at 20°C and 60°C temperatures and 77% relative humidity, it was observed that the hardness value decreased. The reason for this is explained as the degradation of the binder and the rupture of polymer chains due to hydrolysis because of humidity. No difference was observed between the hardness at 20°C and 60°C temperatures, and it was evaluated that this situation was due to the dominance of the effect of humidity over temperature. In addition, it was stated in that study that while the migration of plasticizers due to aging and the resulting increase in hardness were expected, the effect of humidity was more dominant, causing a decrease in hardness (Lai, Dong, Kong, Qu, & Xiao, 2021).

Brown suggested that Shore hardness measurements can vary due to factors such as the operator performing the measurement, the duration of the measurement, and deviations from perfect elastic behavior of the material, particularly in polymer structures containing fillers (Brown R. , 2006). Mohamed and Aggas posited that uncertainties in Shore hardness tests may arise from the flatness of the measuring surface, resolution, repeatable measurement capability of the instrument used, and the influence of temperature on the instrument's transducer (Mohamed & Aggag, 2003).

The observed fluctuations in hardness data were analyzed in light of potential causes identified in the literature. Instrument planarity, resolution, and the response of device transducers to environmental conditions are also possible, but less probable, contributing factors. Given that the instrument used acquires measurements via a stand without operator-applied force, operator error is not considered a likely cause. Furthermore, the measurement duration was standardized at 15 seconds, precluding measurement time-related errors. The prevailing assessment suggests that these fluctuations are primarily attributable to the inherent heterogeneity of the material.

Since the R1, R2 and R3 formulations are different formulations and cured at different times, they have different initial hardness values. Therefore, the effect of AO and bonding agent on hardness could not be distinguished.

4.2 Crosslink Density

The crosslink density measurements are carried out with reference to STANAG 4666 (NATO Standardization Office, 2015) and took approximately one week for each sample measurement according to the relevant standard. In the graphs of crosslink density change with time (Figure 4.4-Figure 4.8), the data are the average of at least two tests and the error bars represent standard deviations.

An analysis of the aging-dependent variation graphs of crosslink density for the R1 formulation indicates a general increasing trend up to the final data point at all temperatures except 70°C. Since crosslinking and bond scission are competing phenomenas (Bohn M. , 2009); (Bohn & Cerri, 2010); (Kumar, Commereuc, & Verney, 2004), at temperatures other than 70°C, crosslink density continues to increase until reaching a certain point, beyond which bond scission becomes the dominant mechanism, leading to a decline in crosslink density. The absence of this behavior in the last test data at 70°C, along with the fluctuations observed in the overall data trend beyond the last data points, suggests that multiple underlying factors may be influencing these results. These factors could include variations in material microstructure, measurement uncertainties, or localized differences in the degradation kinetics of the polymer network. When the maximum crosslinking density values obtained at each temperature for the R1 formulation are examined, it is observed that higher maximum crosslinking density is achieved at lower temperatures. This is thought to be due to the tendency for chain scission at higher temperatures prevailing over the tendency for crosslinking.

As detailed in Section 3.4.2, the crosslink density measurements take approximately 1 week and the test sample reaches the equilibrium state and its weight is confirmed by confirming that it is fixed. Since the amount of soluble material extracted here corresponds to a small portion of the total mass, it is necessary to use a balance with appropriate sensitivity and to make measurements with utmost care to determine the equilibrium state. Another element within the scope of the test process is the determination of the displacement of the material with the weights applied to the material and the waiting period until the material returns to its initial state after the weights are removed. As a result of not waiting long enough, the slope of Figure 3.7, and therefore the crosslink density, may have been calculated incorrectly due to the material not being in its pre-measurement condition. Wang et. al. (Wang, Chang, & Zhang, 2016) also stated in their study that the swelling method is open to error due to long test times and test details that require attention.

Another reason for the oscillations in the data may be the exposure of the material to humidity. Although the materials are stored in plastic packages to minimize exposure to atmospheric conditions during the aging process, it is known that there is no humidity control in the ovens and these packagings are not 100% moisture-proof. Polyurethane (PU) undergoes hydrolysis when exposed to water due to the presence of ester groups in its backbone (Adel & Liang, 2019); (Schollenberger & Stewart, 1971). Research has shown that ester groups degrade more rapidly than urethane linkages (Xie, et al., 2019). This reaction leads to chain scission, producing two chain ends one containing a hydroxyl group and the other a carboxyl (COOH) group. The carboxyl group, being acidic, acts as a catalyst, further accelerating the degradation process (Brown, Lowry, & Smith, 1980).

Another potential reason could be that, due to the inherently heterogeneous composite structure of the material, the tested sample may not have been representative enough to exhibit the theoretically expected behavior at the given aging duration. This discrepancy could arise from variations in the material's microstructure, distribution of constituents, or localized inhomogeneities, which may affect the aging response and crosslinking dynamics. In the extraction method, the

plasticizer within the sample also dissolves. Given that plasticizers have a relatively low molecular weight and are not chemically bonded to the polyurethane structure, they exhibit significant mobility within the material, particularly under aging conditions. This migration is influenced by several factors, including temperature fluctuations, mechanical stress, and oxidative degradation, all of which can alter the polymer network over time. As plasticizers diffuse or leach out of the material, they can lead to changes in the mechanical properties, flexibility, and overall stability of the polymer matrix. Moreover, the redistribution or depletion of plasticizers within the polymer structure introduces an additional variable that may affect measurement outcomes, particularly in relation to sample homogeneity. Variations in plasticizer concentration across different regions of the sample may result in inconsistencies in crosslink density measurements or other analytical assessments (Judge, 2003). Consequently, plasticizer mobility should be carefully considered as a critical factor when interpreting experimental results, as it can contribute to deviations in data and impact the overall reliability of the analysis.

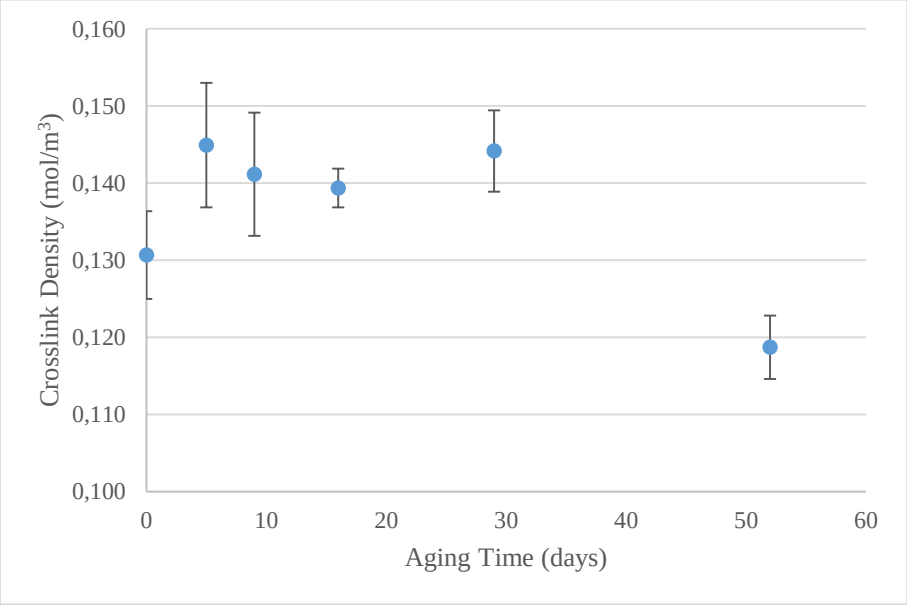


Figure 4.4. Crosslink density change as a function of the aging time at 80°C for the R1 formulation

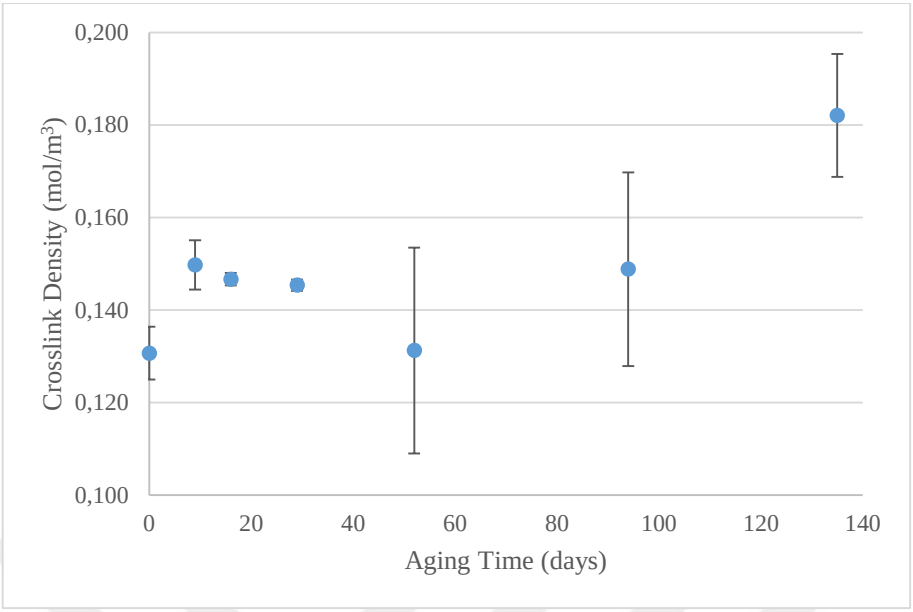


Figure 4.5. Crosslink density change as a function of the aging time at 70°C for the R1 formulation

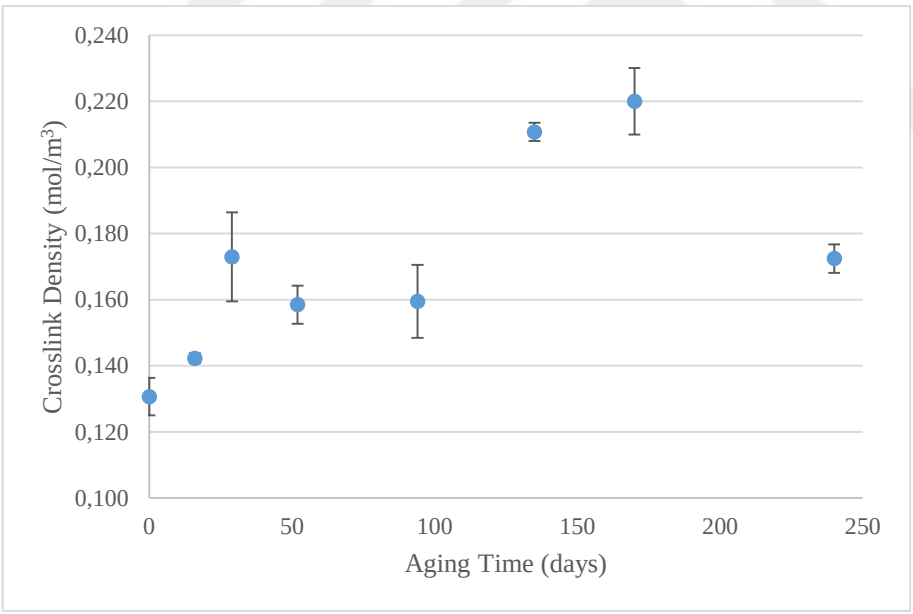


Figure 4.6. Crosslink density change as a function of the aging time at 60°C for the R1 formulation

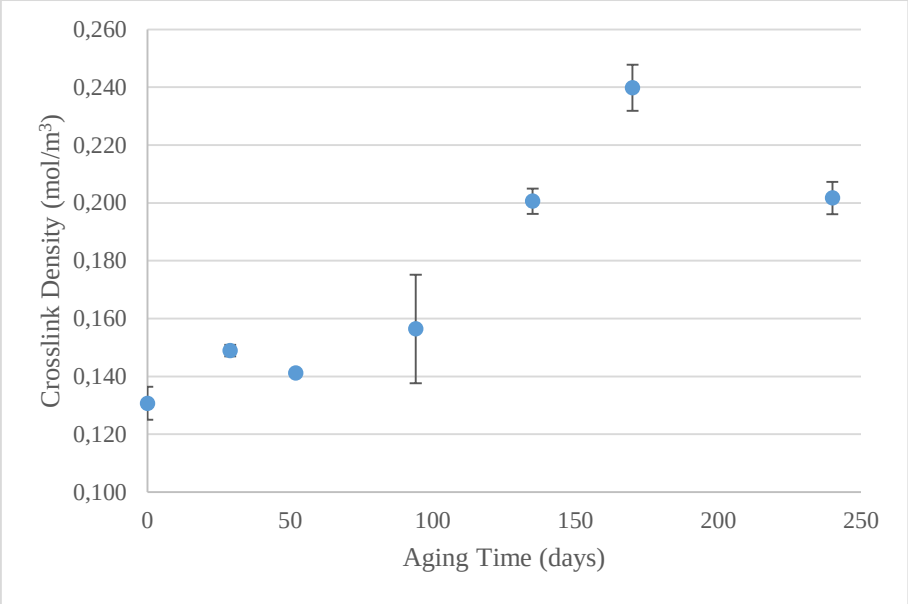


Figure 4.7. Crosslink density change as a function of the aging time at 50°C for the R1 formulation

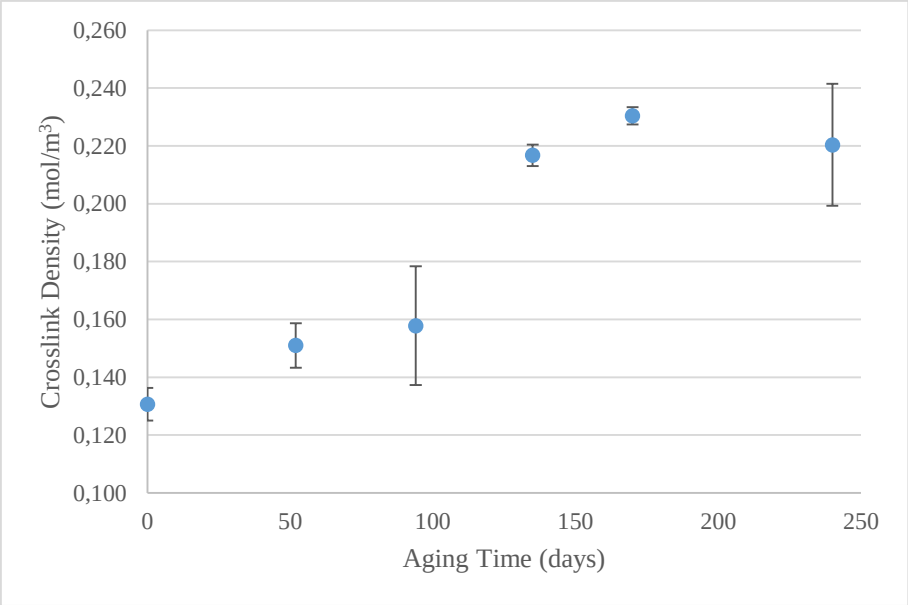


Figure 4.8. Crosslink density change as a function of the aging time at 30°C for the R1 formulation

An analysis of the crosslinking variation in the R2 formulation (Figure 4.9) reveals a distinct trend compared to the R1 formulation, where crosslinking initially decreases before subsequently increasing. This behavior can be attributed to the higher antioxidant content in the R2 formulation, which plays a crucial role in inhibiting the early-stage crosslinking process. As expected, the presence of antioxidants suppresses the formation of additional crosslinks in the initial phase, thereby allowing chain scission reactions to dominate. During this stage, polymer backbone cleavage occur more prominently, leading to a reduction in crosslink density. However, once antioxidant drops to a certain level, the crosslinking process begins to regain dominance, contributing to a gradual increase in crosslink density. At this stage, the availability of reactive sites and the reduction in antioxidant efficiency may facilitate further crosslinking. Finally, the chain scission mechanism once again becomes the predominant factor, likely due to the cumulative effects of prolonged thermal aging and oxidative degradation within the polymer network.

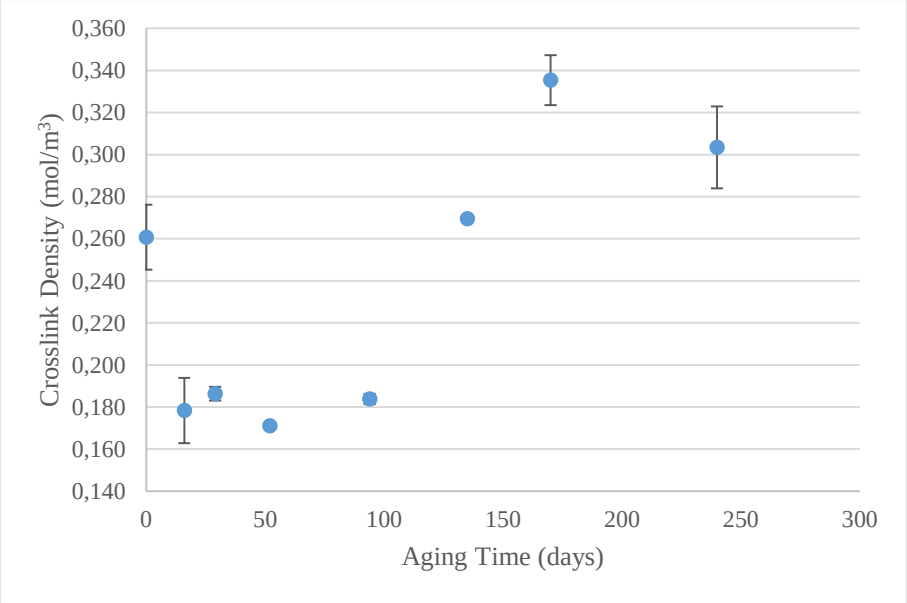


Figure 4.9. Crosslink density change as a function of the aging time at 60°C for the R2 formulation

The high initial crosslink density observed in the R3 formulation (Figure 4.10) compared to the R1 formulation can be attributed to its higher olefin content, as it

does not contain a bonding agent (Table 3.1). The presence of greater number of double-bond containing structures (i.e. higher olefin content) enhances the material's predisposition toward crosslinking by providing more reactive sites for polymerization and network formation. This structural characteristic facilitates the formation of a highly interconnected polymer network at an accelerated rate. Conversely, the R1 formulation contains a higher proportion of hydantoin and polar functional groups, which influence the crosslinking dynamics differently. The presence of these polar groups alters the chemical environment, leading to a more restricted interaction between oxygen and the olefinic sites, thereby limiting the extent to which oxygen can initiate crosslinking. As a result, the availability of reactive double bonds is reduced in the R1 formulation, leading to a comparatively slower crosslinking rate in the initial phase.

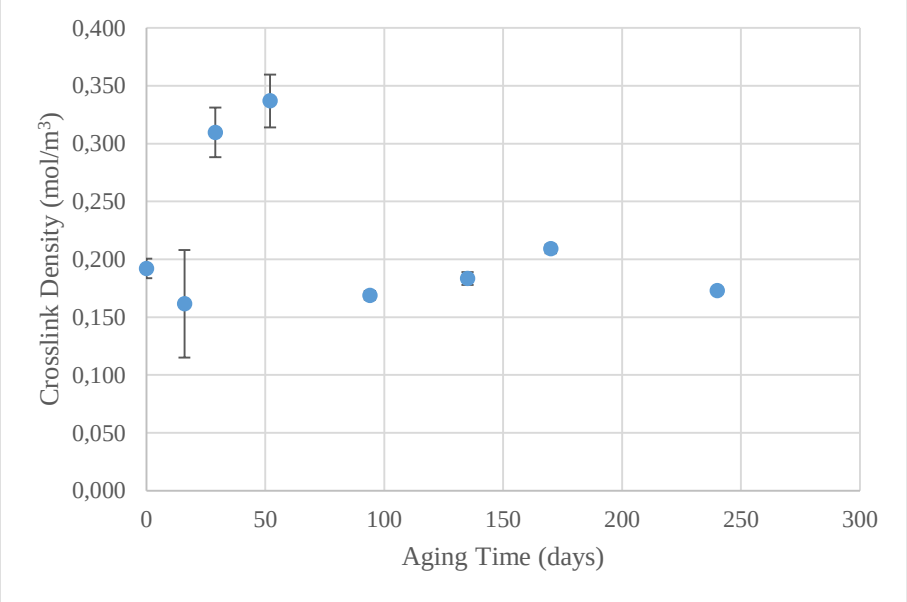


Figure 4.10. Crosslink density change as a function of the aging time at 60°C for the R3 formulation

The crosslinking data for the R3 formulation exhibit considerable complexity and lack a distinct trend. This irregularity is likely attributed to the absence of a bonding agent in the formulation, which weakens the polymer-filler interactions and, consequently, leads to issues related to homogeneity. As a result, variations in the

crosslinking data may stem from structural inconsistencies within the material. Therefore, due to the absence of a bonding agent, it is not possible to systematically analyze or draw definitive conclusions regarding its impact on the crosslink density behavior during the aging process.

4.3 Antioxidant Content

Antioxidants break the degradation chain by donating H- atoms to free radicals. Therefore, it could prevent those radicals from propagating the chain reaction. The chemical structure of such anti-oxidant includes pendant phenols or aromatic amines. 2,2'-Methylenebis, which is called as AO2246, is phenolic antioxidant used in the formulations in this study. It binds to HTPB using IPDI as a bridge and prevents the chain reaction by donating hydrogen to the radicals as shown in Figure 4.11. Meanwhile, AO2246 can improve the mechanical properties by integrating into the polymer matrix through its –OH functional groups.

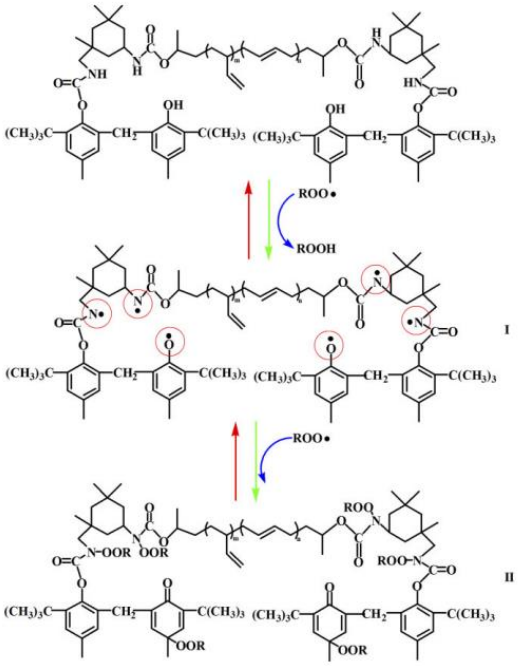


Figure 4.11. Radical Attack Prevention of Antioxidant at HTPB-IPDI Polyurethane Structure (Wang, Zhang, Liu, & Hao, 2015)

Primary antioxidants are the most widely utilized in composite propellants due to their ability to inhibit oxidative reactions at the initial stages. The depletion of antioxidants is intrinsically linked to the oxidative crosslinking process, as their consumption accelerates the progression of thermal oxidative degradation (Eslam, Sherif, Ahmed, & Hosam, 2020).

When examining the change in antioxidant levels due to aging for the R1 formulation (Figure 4.12) , it is observed that the antioxidant content decreases over time at all temperatures. Additionally, it is evident that this decline is more pronounced with increasing temperature. Higher temperatures accelerate the rate of antioxidant depletion. The initial antioxidant content in the R1 formulation was found to be lower than the theoretically expected value of 0.1%. This discrepancy can be readily attributed to a competitive reaction between the IPDI curing agent and the phenolic hydroxyl groups of the antioxidant, leading to a portion of the AO being grafted onto the polymer chain and consequently becoming inaccessible for subsequent extraction.

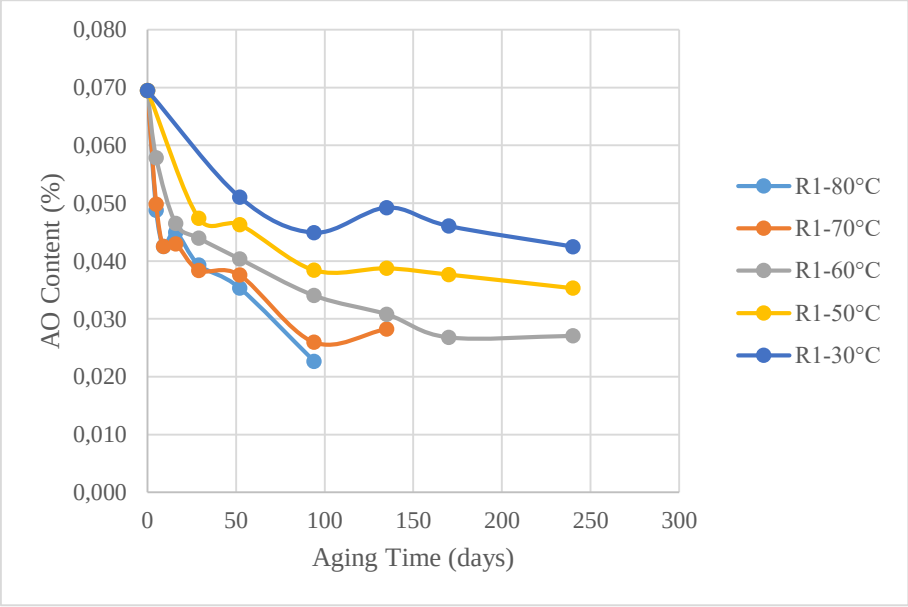


Figure 4.12. Antioxidant content change of the R1 formulation as a function of aging time at different temperatures

Celina et al. explored the correlation between aging-induced antioxidant depletion and mechanical characteristics. In this investigation, the antioxidant AO2246 was employed, and its consumption kinetics were quantified at temperatures of 50°C, 65°C, 80°C, 95°C, and 110°C using gas chromatography. The results revealed a direct proportionality between antioxidant consumption rate and temperature, with higher rates observed at elevated temperatures and lower rates at reduced temperatures. The antioxidant consumption profile of the R1 formulation demonstrated consistency with these findings. In addition, Celina's research indicated that for a constant target mechanical property (elongation) affected by aging across varying temperature regimes, lower free antioxidant concentrations were detected at higher temperatures, while higher concentrations were observed at lower temperatures. Three potential explanations exist for the observed behavior of AO at Celina's work. Firstly, the AO may exhibit exceptional efficacy in inhibiting degradation at elevated temperatures, even at low concentrations. Secondly, the AO could participate in a grafting reaction, possibly involving its hydroxyl group or radical recombinations, thereby preventing its extraction. This grafting to the polymer backbone might still offer some thermo-oxidative protection, while simultaneously hindering AO quantification through the employed extraction technique. Thirdly, due to the complex degradation profile, potentially influenced by spatial heterogeneity and localized oxidation may occur, effectively bypassing the protective effects of the overall antioxidant concentration (Celina, J.M., Winters, Assink, & Minier, 2006).

In another aging study (Epure, Grigorıu, Tiganescu, Iorga, & Marin, 2022) utilizing AO2246, it was observed that while crosslink density increased during a 3-month aging process at 60°C, there was no significant alteration in AO content. This phenomenon is postulated to be attributable to either the antioxidant becoming bound to the polymer chain, as also noted in Celina's (Celina, J.M., Winters, Assink, & Minier, 2006) work, thus preventing its extraction, or to regional heterogeneity within the test samples.

In degradation kinetics study of Setyaninggsih et al., that was conducted using DSC and the Ozawa model, it was observed that an increase in antioxidant concentration led to a rise in the material's activation energy. This elevation in activation energy indicates enhanced resistance of the material to degradation (Setyaningsih, Juwono, & Supriyatno, 2017).

This thesis study suggests that the observed antioxidant behavioral changes due to aging can be explained by a decrease in the antioxidant's reaction tendency from high to low temperatures, i.e. by reaction kinetics. On the other hand, errors arising from the extraction technique would be expected to manifest across all temperatures. Furthermore, although exceptional data exhibiting concerns regarding homogeneity were obtained, there is no systematic data behavior attributable to homogeneity that would affect the overall data trend for each temperature.

Considering the antioxidant consumption rate (Figure 4.13), the rate of decrease in the amount of AO of the R2 formulation, which has a high antioxidant content, is higher than the R1 and R3 formulations. This situation is interpreted as the reaction tendency of excess antioxidant in R2 with free oxygen attacking from air.

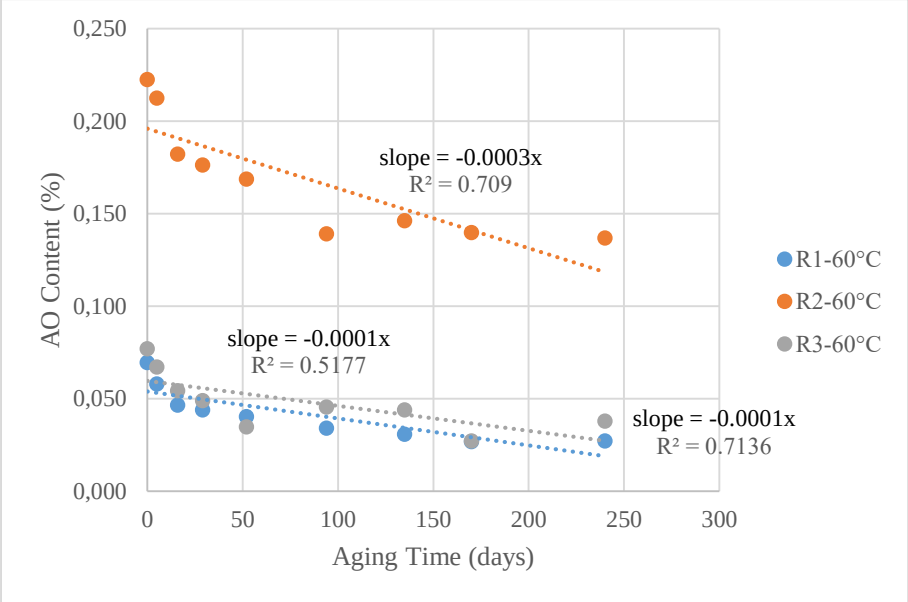


Figure 4.13. AO depletion rate of the R1, R2 and R3 formulation at aging temperature of 60ºC

Considering the increased antioxidant consumption at high temperatures**,** as observed in Celina's study (Celina, J.M., Winters, Assink, & Minier, 2006), and the elevated degradation activation energy due to high antioxidant content, as stated in Setyaningsih's work (Setyaningsih, Juwono, & Supriyatno, 2017), it is an expected outcome that the R2 formulation**,** which has a high antioxidant content, will exhibit rapid antioxidant consumption behavior to prevent oxidative degradation. It is also understood that the R1 and R3 formulations**,** having the same antioxidant content, display similar antioxidant consumption behavior.

4.4 Tensile Properties

Tensile tests were conducted by subjecting dog-bone specimens, prepared in accordance with STANAG 4666 Method 2A, to uniaxial tension at a crosshead speed of 50 mm/min (NATO Standardization Office, 2015). Elongation, a parameter often specified as a lower limit for explosives, is primarily utilized as a shelf life determination criterion in aging analyses (Shekhar, 2011) ; (Yongqiang, Jian, Jianzhuang, & Xin, 2019). A decrease in the material's elongation capability is expected to correlate with an increase in crosslink density. The changes in elongation at maximum load for the R1 formulation as a function of aging time are illustrated in the graphs below (Figure 4.14-Figure 4.18). The elongation values presented in the graphs represent the average of four dog-bone specimens tested at each aging time. Standard deviation error bars are also included. High standard deviations were observed in some elongation data. This is attributed to potential internal localized damage within the test specimen or the inherently heterogeneous nature of the material. Despite the deviating trends at certain test times for some aging temperatures, it is generally reasonable to state that the elongation values decrease with time across all temperatures for R1 formulation.

Beyond the standard deviations, although not altering the overall trend in time-dependent elongation behavior, data points exhibiting a contrary trend are also

present locally. This phenomenon could stem from localized defects or heterogeneity, as well as moisture effects.

The study by Torry and Cunliffe (Torry & Cunliffe, 2000) reported that high elongation values were obtained due to the plasticizing effect of moisture exposure, despite the material's tendency for high crosslink. Similarly, Judge's work (Judge, 2003) indicated that while elongation data generally showed a greater decreasing trend with increasing temperature, deviations from this trend were observed in relation to moisture content. Therefore, moisture exposure and localized defects may be plausible reasons explaining the occasional increases observed in the elongation data, which generally exhibits a decreasing trend over time.

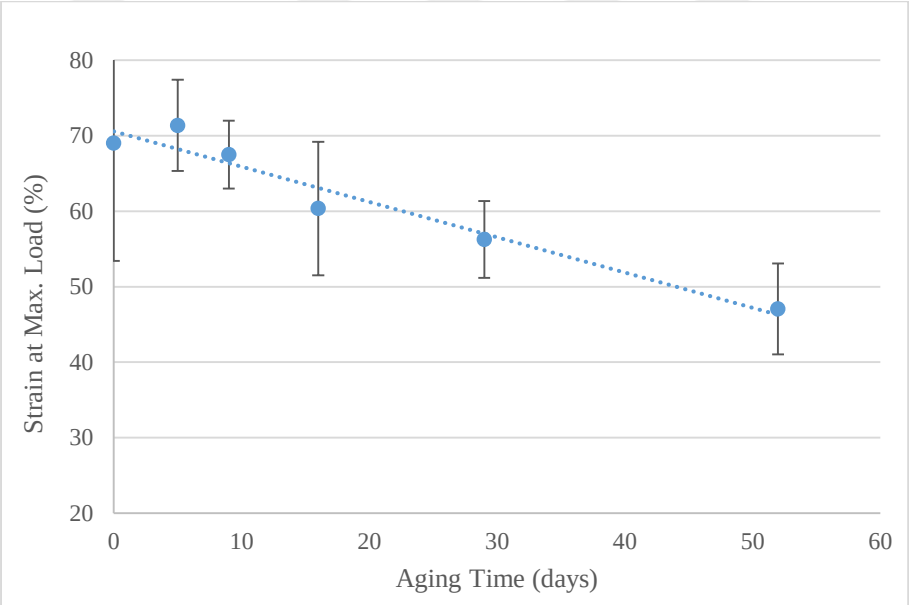


Figure 4.14. The strain at maximum load as a function of the aging time at 80°C for the R1 formulation

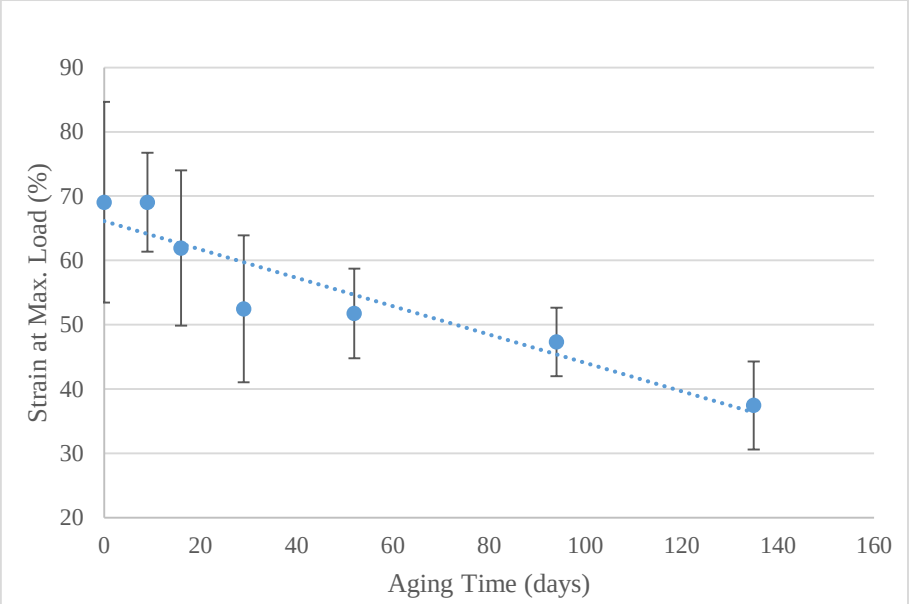


Figure 4.15. The strain at maximum load as a function of the aging time at 70°C for the R1 formulation

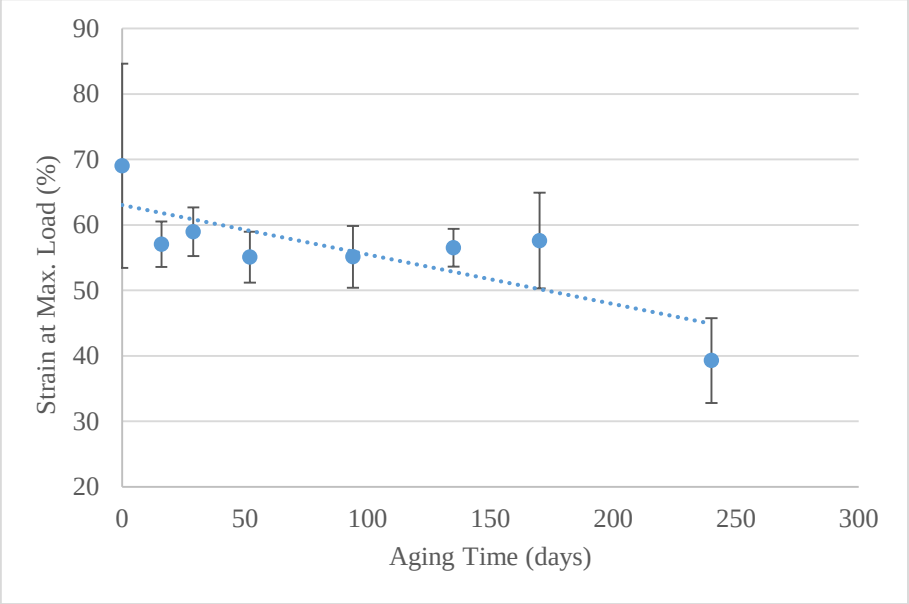


Figure 4.16. The strain at maximum load as a function of the aging time at 60°C for the R1 formulation

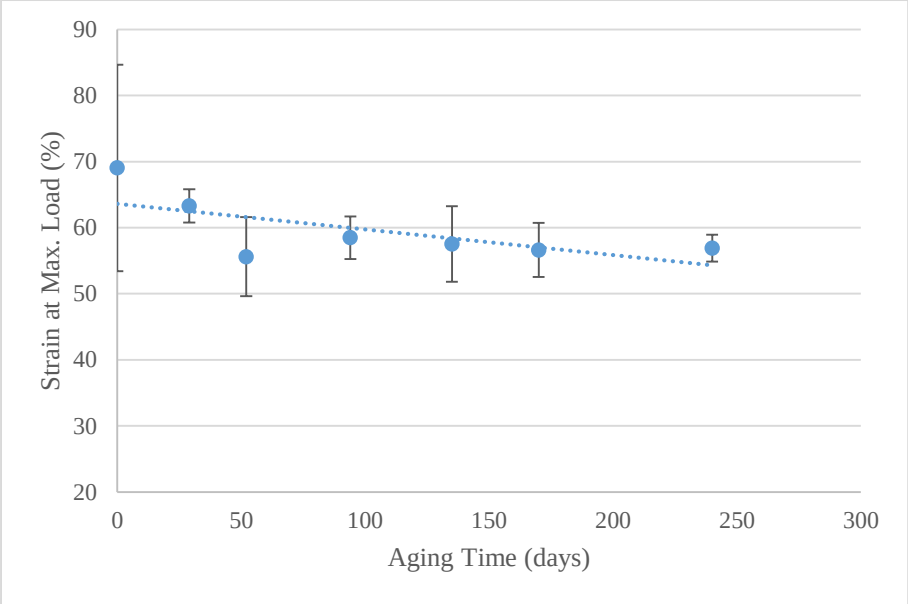


Figure 4.17. The strain at maximum load as a function of the aging time at 50°C for the R1 formulation

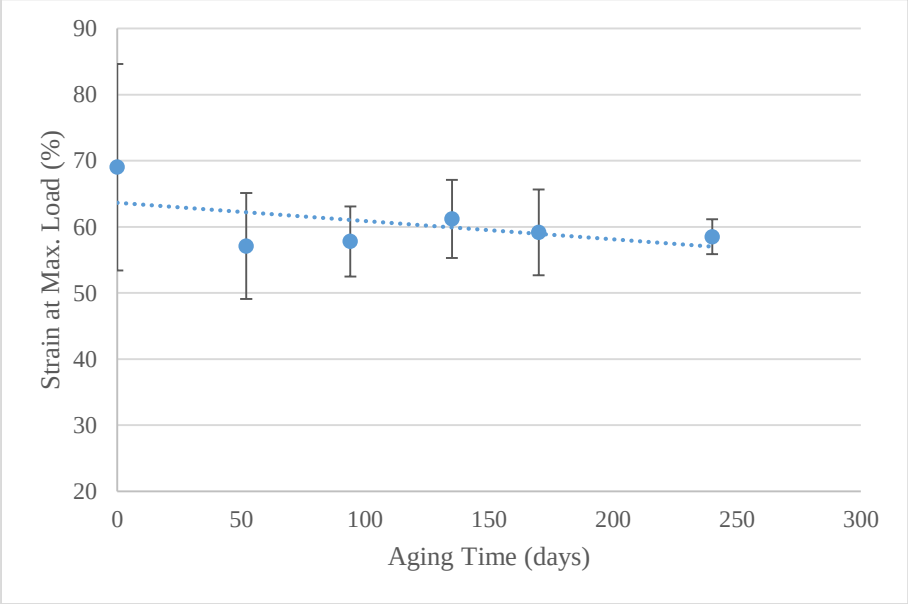


Figure 4.18. The strain at maximum load as a function of the aging time at 30°C for the R1 formulation

For the R1 formulation, when the time-dependent variation of average elongation values at maximum load across all temperatures is examined, it is observed that the

decrease in elongation increases with increasing temperature (Figure 4.19). It has been observed that the r^2 value increases from low to high temperatures. At low temperatures, material properties change more slowly, causing variations dependent on the material's heterogeneous structure to dominate over time-dependent changes. At high temperatures, faster changes occurring in the material's structure can mask measurement errors originating from material heterogeneity. This is considered to be the reason for the increase in the r^2 value towards higher temperatures. According to the results for R1, physical effects of aging may be the dominant mechanism during accelerated aging, which can cause significant decline of the strain at higher temperatures although oxidative crosslinking seems slower at higher temperatures. Plasticizer migration, filler/matrix interface fail (dewetting) due to thermal stress may be possible reasons of this behavior. Thermal accelerated aging leads to matrix hardening and a subsequent reduction in interfacial adhesive stress between filler particles and the matrix, attributed to thermal stress (Wang, Qiang, Wang, & Wang, 2019). This explains that the physical and chemical effects of aging may not always reinforce each other's effects, on the contrary, they may produce results that compete with each other. The study by Wang et al. (Wang, Chen, Qiang, & Fu, 2025) investigated age-related changes in crosslinking and tensile properties of composite propellant. No clear trend was observed in the alteration of crosslinking, a finding attributed to the simultaneous occurrence of crosslink formation and chain scission. However, changes were observed in tensile properties. Consequently, the study emphasized that crosslinking and chain scission did not have an impact on tensile properties. It was suggested that other physical factors, such as dewetting, could influence tensile properties. Conversely, the study by Nasem et al. (Naseem, Murthy, & Ramakrishna, 2020) indicates that chain scission diminish the elongation capacity. Consequently, when this phenomenon is considered in conjunction with the physical effects of aging at elevated temperatures, it elucidates the accelerated reduction in elongation with increasing temperature.

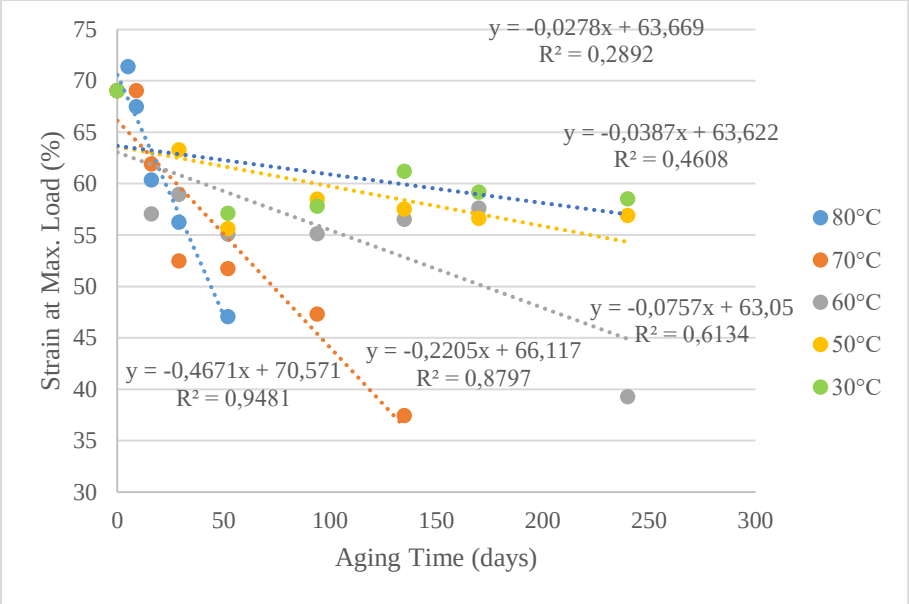


Figure 4.19. Time-rate of change of strain for the R1 formulation at different aging temperatures for the R1 formulation

When the elongation behavior of R1 and R2 formulations at 60°C is examined (Figure 4.20), it is seen that they show almost similar decreasing trend over time. Although the crosslink density behavior of these two formulations at 60°C was different, this difference did not show itself in the elongation behavior. It is understood that the excess antioxidant in the R2 formulation has no effect on the aging-related elongation behavior other than the initial elongation value. This shows that physical mechanisms of aging manifest themselves more dominantly in the tensile test than chemical aging mechanisms.

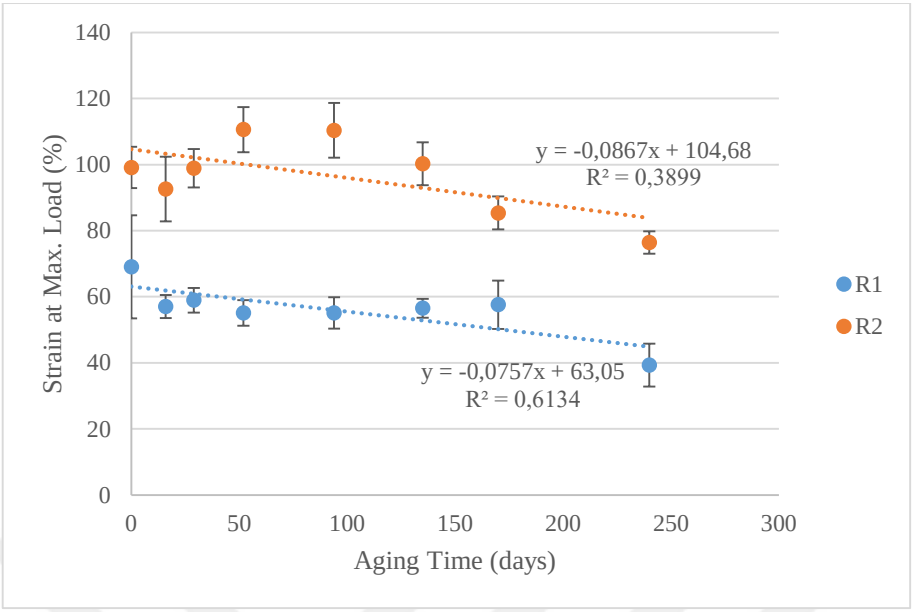


Figure 4.20. Time-rate of change of strain for the R1 and R2 formulations at 60°C aging temperature

The aging-induced elongation behavior of the R3 formulation showed a random trend (Figure 4.21). It is considered that the reason for this is that the polymer filler interaction cannot be achieved sufficiently due to the lack of bonding agent. The weak interaction between the polymer and the solid filling material caused the tensile stress of the material to remain at low levels and show a random distribution of strain during all aging periods.

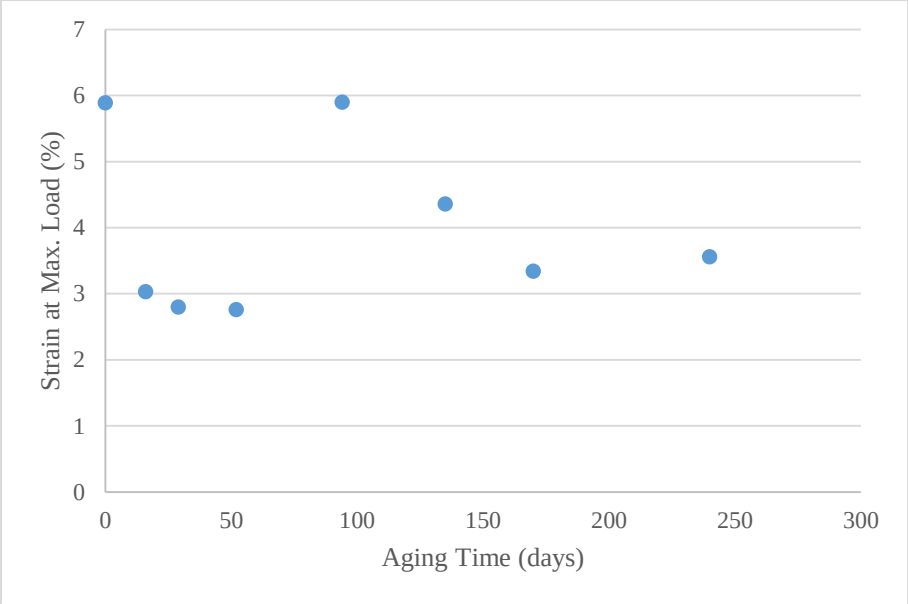


Figure 4.21. The strain at maximum load as a function of the aging time at 60°C for the R3 formulation

The temperature-dependent variation of the maximum stress value in the tensile properties of the R1 formulation was also investigated (Figure 4.22 - Figure 4.26). The stress values exhibited a similar trend to the crosslink density data. For all temperatures, the stress values increased with increasing crosslink density. However, with the exception of 70°C, a decrease in stress values was observed at the final test points, which coincided with a reduction in crosslink density, indicating an increase in bond scission.

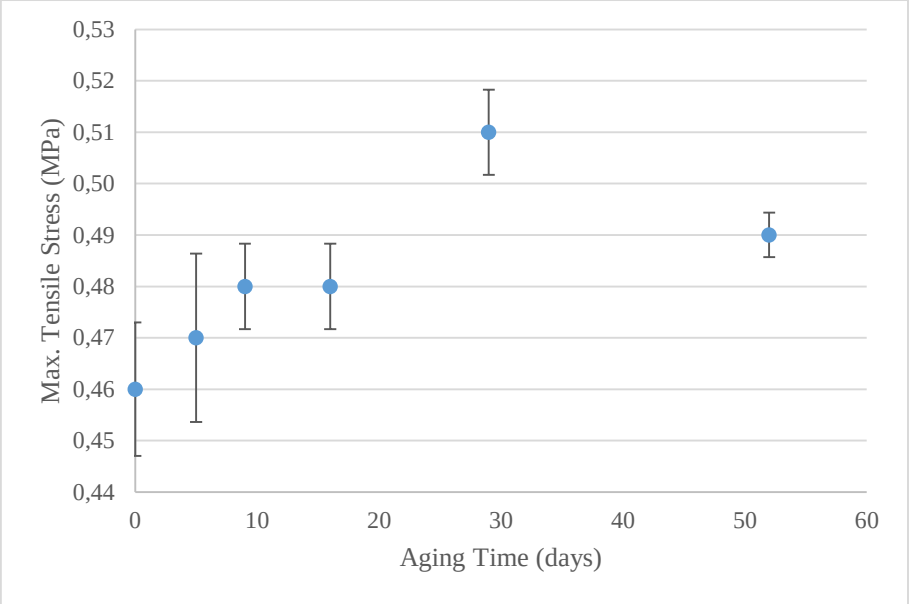


Figure 4.22. The maximum tensile stress as a function of the aging time at 80°C for the R1 formulation

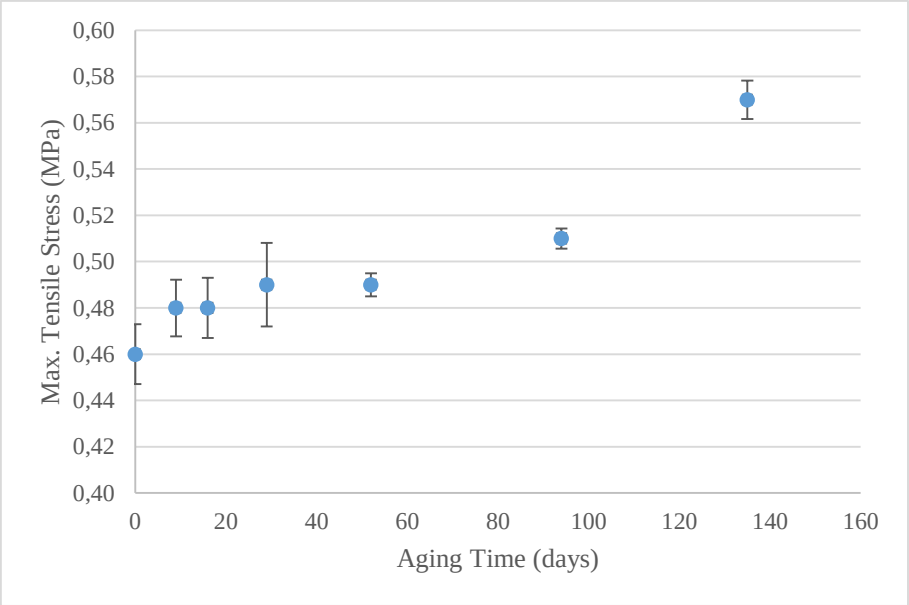


Figure 4.23. The maximum tensile stress as a function of the aging time at 70°C for the R1 formulation

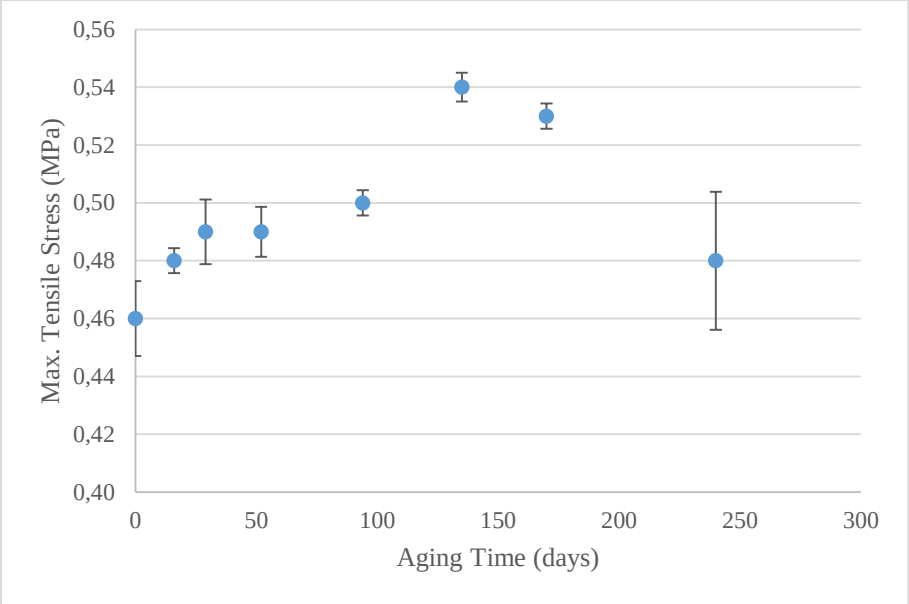


Figure 4.24. The maximum tensile stress as a function of the aging time at 60°C for the R1 formulation

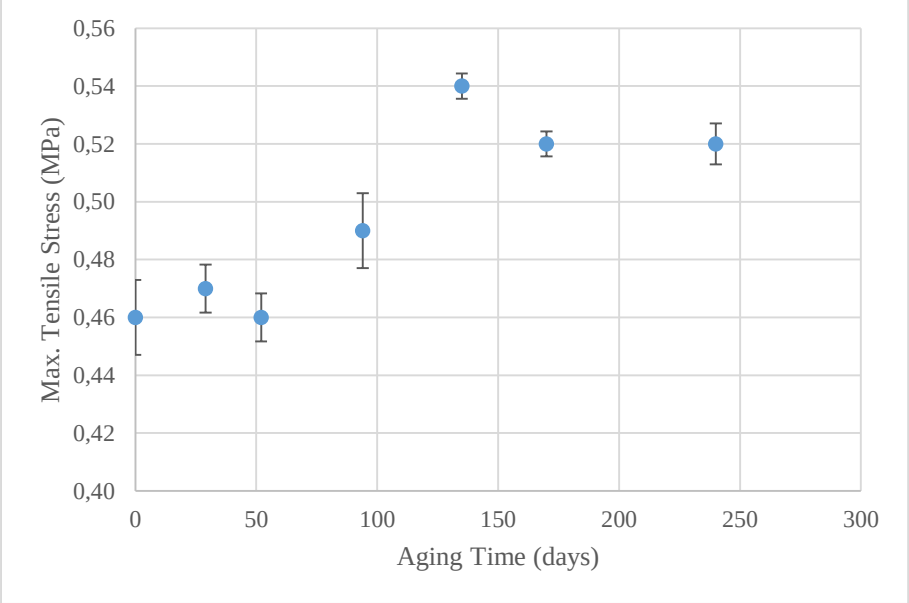


Figure 4.25. The maximum tensile stress as a function of the aging time at 50°C for the R1 formulation

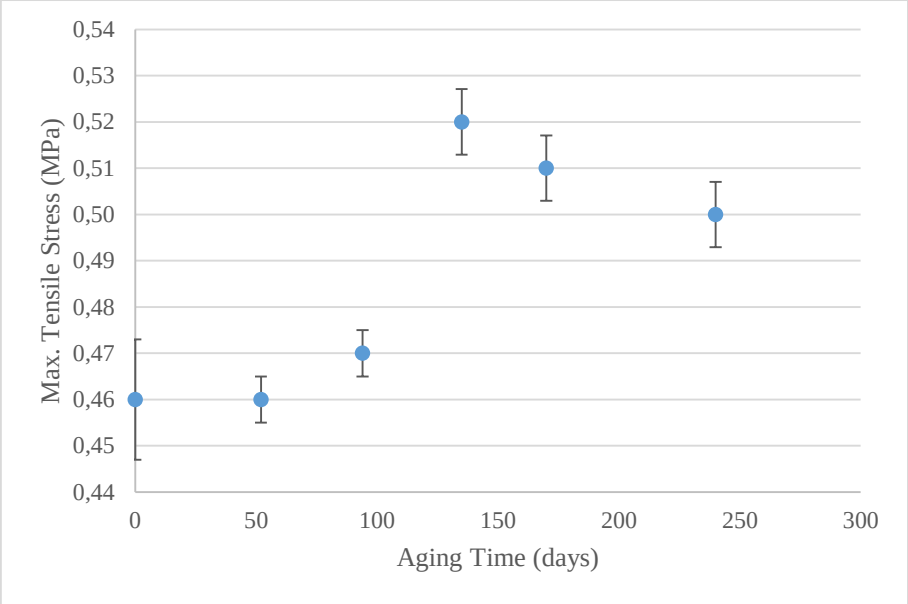


Figure 4.26. The maximum tensile stress as a function of the aging time at 30°C for the R1 formulation

4.5 FTIR Analysis

FTIR analyzes were performed for all test samples at times indicated in Table 3.4. The Figure 4.27 presents the functional groups corresponding to specific wavelengths in the FTIR spectrum of a typical polyurethane.

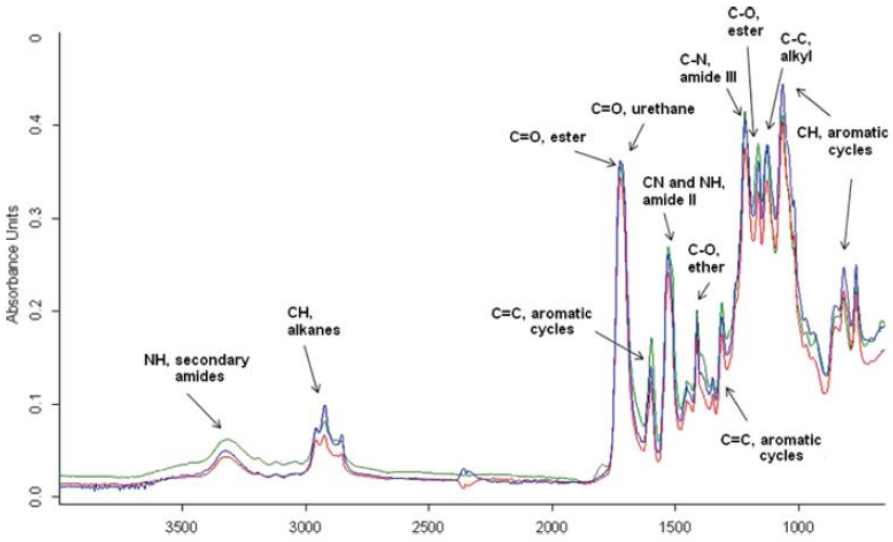


Figure 4.27. FTIR Spectrum of a Typical Polyurethane (Tcharkhtchi et al., 2014)

The t_0 time FTIR spectra of the R1, R2 and R3 formulations are given in Figure 4.28.

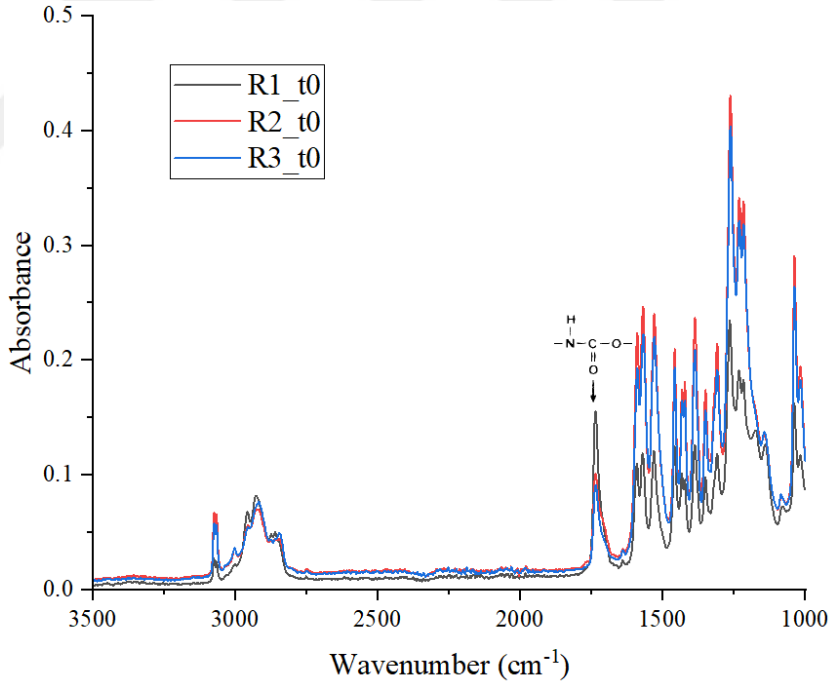


Figure 4.28. FTIR spectrum of the R1, R2 and R3 formulations at t_0

The objective is to analyze the designated functional group by examining the change in the inter chain distances of the polymer chains due to aging induced crosslinking or chain scission. It is known that the C=O groups in the urethane linkages present

on the polymer chains can engage in hydrogen bonding interactions with hydrogen atoms in urethane groups on adjacent chains (Figure 4.29). It is anticipated that the extent of hydrogen bonding interaction will increase as the polymer chains move closer to each other and decrease as they move further apart.

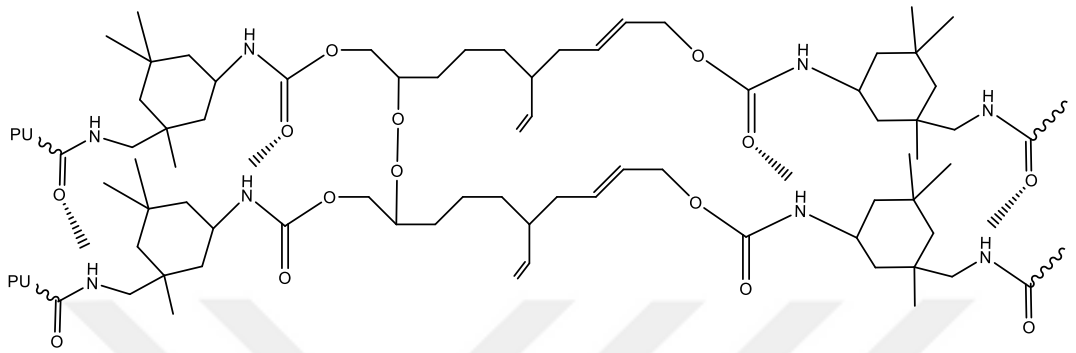


Figure 4.29. Schematic represantation of hydrogen bond interaction between crosslinked HTPB-IPDI polymer chains

C=O stretching vibration of urethane groups show themselves at around 1700 cm^{-1} absorption bands in the FTIR spectrum (Villar, Cicaglioni, Diniz, Takahashi, & Rezende, 2011); (Cao, Zhou, Jie, & & Li, 2016). The peak obtained in the urethane (C=O) region of the relevant spectrum was analyzed with the Origin program. Resolving the carbonyl peak in the urethane bond with the help of the Origin program (after baseline correction), auxiliary subpeaks forming the relevant peak were revealed. A curve fitting technique of nonlinear least squares optimization based on Gaussian curve shapes was used to fit the band outlines in the carbonyl region. The raw spectrum of the carbonyl region after aging at 60°C is exemplified in Figure 4.30.

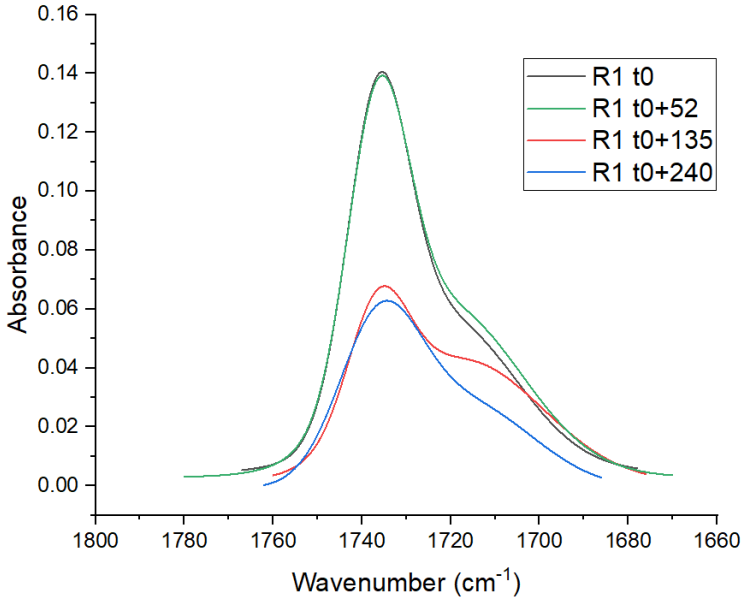


Figure 4.30. Carbonyl region spectrum change of the R1 formulation with aging at 60°C

Individual bands were assigned and quantified to determine the intensity ratio of different carbonyl bands. Deconvoluted two peaks in Figure 4.31 represent the energy levels of free carbonyl groups that interact with and do not interact with the amide group in different polymer chains. Among the peaks shown in green, the one seen at around 1720 cm^{-1} wavenumber corresponds to the interacting low energy carbonyl group, and the peak that shows itself at around 1740 cm^{-1} wavenumber (red curve) corresponds to the noninteracting (free) high energy carbonyl group.

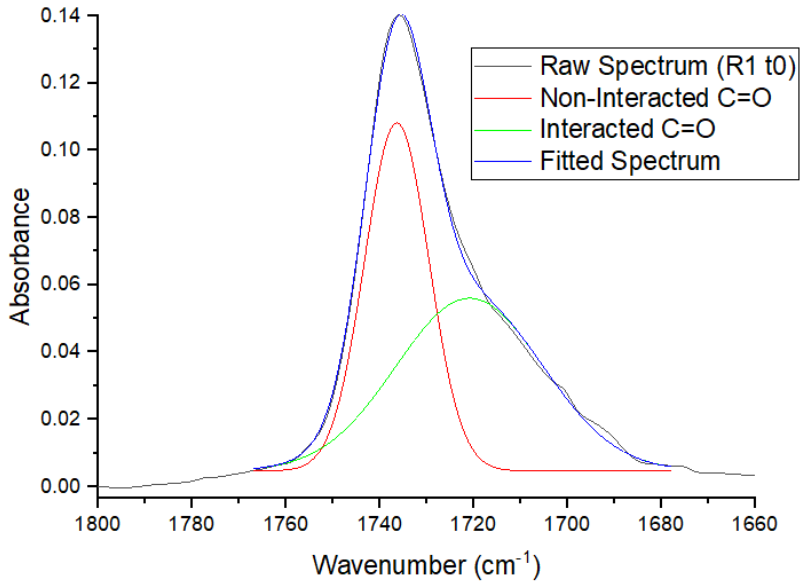


Figure 4.31. Peak analysis example plot of the R1 at time t_0

The difference between the energy levels (wavenumbers) of the interacting and free carbonyl groups is an indicator of how close the polymer chains are to each other; an output expected to increase or decrease with increasing crosslink density or chain scission due to aging. According to the Beer Lambert's Law a given peak is directly proportional to the concentration. Therefore, the areas of the interacting and free carbonyl peaks is a data that allows us to make inferences about the relative quantities of these groups in the total structure. The ratio of the areas of interacting and non-interacting carbonyl groups as a result of the spectrum analyzes of the tests performed at the aging times specified for FTIR in Table 3.4 is indicated in Table 4.1.

Table 4.1 The deconvoluted carbonyl spectrum area ratios (interacted/non-interacted) of the aged R1 formulation at different aging times

Temperatures	Aging Time	*Interacted Area*	*Non-Interacted Area*	*Interacted/Non-Interacted Area*
R1 (80°C)	t_0	2.01	1.78	1.13
	t_0+9	2.06	1.06	1.94
	t_0+16	1.92	0.90	2.23
	t_0+52	2.62	1.91	1.37
R1 (70°C)	t_0	2.01	1.78	1.13
	t_0+16	2.30	1.31	1.76
	t_0+52	2.12	0.80	2.62
	t_0+135	1.51	0.66	2.29
R1 (60°C)	t_0	2.01	1.78	1.13
	t_0+52	2.42	1.67	1.45
	t_0+135	1.86	0.72	2.58
	t_0+240	1.07	1.16	0.92
R1 (50°C)	t_0	2.01	1.78	1.13
	t_0+52	1.98	0.74	2.24
	t_0+135	1.90	0.90	2.68
	t_0+240	1.26	1.97	0.64
R1 (30°C)	t_0	2.01	1.78	1.13
	t_0+52	1.80	0.80	2.17
	t_0+135	1.88	0.73	2.58
	t_0+240	2.41	0.79	3.05

When the interacted/non-interacted area ratios in the table are examined, it is seen that the area ratios increase until the final aging time at all aging temperatures except 30°C. At 30°C the rate continued to increase. It is considered that this situation is a result of the hydrogen interaction with the C=O group in the polymer chains, which increase in crosslink density due to aging at all temperatures up to last test time except 30°C. At other temperatures other than 70°C, the decrease in the final aging time is considered to be a result of the chains moving away due to chain scission, as can be seen from the crosslink density test data for the same temperatures. As a result, crosslink density test results and interacted/non-interacted area ratio behavior for R1 formulation tend to be similar for all temperatures except 70°C. It is considered that this situation at 70°C may be due to the heterogeneity of the tested sample.

Table 4.2 shows the ratio of interacted carbonyl/non-interacted carbonyl areas for formulations R2 and R3. In the R2 formulation, the area ratio first decreased and then increased. This behavior is consistent with the crosslink density data for formulation R2. In other words, for the R2 formulation, the area ratio decreased due to the polymer chains moving away as a result of the decreasing crosslink density at the second test time. After the consumption of antioxidant in the R2 formulation, the area ratio continued to increase in parallel with the increase in crosslink density.

Table 4.2 The deconvoluted carbonyl spectrum area ratios (interacted/non-interacted) of the aged R2 and R3 formulations at different aging times at 60°C

Formulations	Aging Time	*Interacted Area*	*Non-Interacted Area*	*Interacted/Non-Interacted*
R2 (60°C)	t_0	1.72	0.96	1.79
	t_0+52	1.99	1.18	0.71
	t_0+135	1.01	1.43	1.69
	t_0+240	1.71	0.78	2.19
R3 (60°C)	t_0	1.19	0.95	1.25
	t_0+52	1.27	0.85	1.49
	t_0+135	0.92	0.75	1.23
	t_0+240	0.58	0.84	0.69

In the R3 formulation, the area ratio first increased and then showed a decreasing trend. This result is in parallel with the crosslink density behavior for the same aging times.

The literature lacks studies that have investigated the aging-related quantitative analysis of composite solid propellants or plastic bonded explosives via FTIR. In the study by Wang et al. on the characterization of antioxidants and thermo-oxidative aging resistance in natural rubber vulcanizates, the bonding structure of the antioxidant (AO2246), IPDI, and polyol (HTPB) was characterized using FTIR. The disappearance of the -NCO absorption peak at 2271 cm^{-1} and the appearance of peaks at 1480 cm^{-1} ($-CH_2-$ bending vibration of AO2246) indicated the reaction between -NCO groups in HTPB-IPDI and AO2246. The FTIR results confirmed the successful binding of AO2246 onto the HTPB-IPDI chains, leading to the formation

of the polymeric antioxidant HTPB-IPDI-AO2246 (Wang, Zhang, Liu, & Hao, 2015). The absence of the -NCO peak (2271 cm^{-1}) and the presence of the -CH_2- peak (1480 cm^{-1}) coming from the AO structure in the FTIR spectra shown in Figure 4.28 for R1, R2, and R3 formulations confirm the HTPB-IPDI-AO246 reaction, aligning with Wang's findings.

In the study of Villar et al. it was investigated the thermal aging of hydroxy-terminated polybutadiene isophorone diisocyanate (HTPB/IPDI) based polyurethane. It specifically examined how the NCO/OH ratio (1.0 and 0.85) affects the chemical and mechanical properties of the polyurethane during aging. Samples were aged in air ovens at 50°C, 60°C, 65°C, and 70°C for periods up to 34 weeks. An increase in absorption in the C=O stretching region was observed, indicating the formation of carbonyl groups. This increase was slightly more pronounced for the F1 formulation (1.0 NCO/OH ratio). The C=O stretching region showed an enlargement of the overlapping twin bands related to free and hydrogen-bonded vC=O at 1725 cm^{-1} and 1712 cm^{-1}, respectively. Higher NCO/OH ratio was found to accelerate the oxidation of HTPB-IPDI based polyurethanes during aging (Villar, Cicaglioni, Diniz, Takahashi, & Rezende, 2011). In parallel with Villar's reported FTIR findings concerning the hydrogen bonding interaction of the carbonyl group, this study also revealed these characteristic features (Figure 4.31). The obtained spectral areas were subsequently analyzed to perform a quantitative assessment related to aging as explained with Table 4.1 and Table 4.2.

4.6 Dynamic Mechanical Analysis

During Dynamic Mechanical Analysis (DMA) measurements, the applied energy absorbed by the specimen, comprises two distinct contributions. The first is a purely dissipative component, wherein energy is converted into heat through internal frictional mechanisms within the sample called viscous contribution. The second is utilized for molecular rearrangements within the binder network called elastic

contribution. As the temperature is scanned across different state regions, the glass transition region where changes in molecular arrangements occur.

In the tan(δ) vs. temperature plot, primary maximum, often referred as the main peak, corresponds to the glass transition of the hydroxyl terminated polybutadiene (HTPB) main chain segments, also known as soft segment units, where the large scale molecular motion of the main chain either initiates or ceases. The temperature at which this peak maximum occurs is designated as $T_{g,unrest}$. The secondary peak is attributed to localized motions within the short hard segment units (urethane groups) and/or within regions of the soft segments where mobility is significantly restricted due to the presence of fillers and binder-filler interactions. To emphasize this restricted mobility, the temperature corresponding to the maximum of the secondary peak has been termed as $T_{g,rest}$ (Cerri S. , Bohn, Menke, & Galfetti, 2013). Figure 4.32 illustrates these distinct hard/soft segments of HTPB-IPDI polyurethane chain.

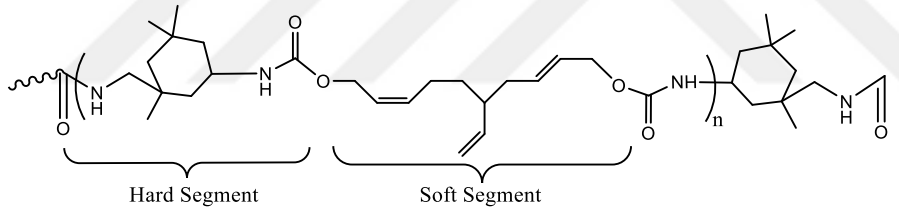


Figure 4.32. Hard and soft segment regions at IPDI-HTPB polyurethane chain structure

Aging-dependent tan(δ) curves for the R1 formulation and the variation of $T_{g,unrest}$ with aging time at 80°C are presented in Figure 4.33 and Figure 4.34 respectively. As $T_{g,unrest}$ is a negative value, a decrease in the bar graph visually represents an increase, while an increase signifies a decrease for all $T_{g,unrest}$ plots. Accordingly, for the R1 formulation aged at 80°C, the $T_{g,unrest}$ initially increases, then decreases, and finally shows an increasing trend. At this temperature and times, the crosslink density was observed to increase for 9th and 29th days, but decrease on 52nd day. Evaluating these findings, the $T_{g,unrest}$ data for 9th day consistently show an increase, aligning

with the crosslink density data. However, the $T_{g,unrest}$ data for 29th and 52nd days exhibit a trend contrary to the crosslink density. Based on the crosslink density data, the $T_{g,unrest}$ value should increase on 29th day and decrease on 52nd day.

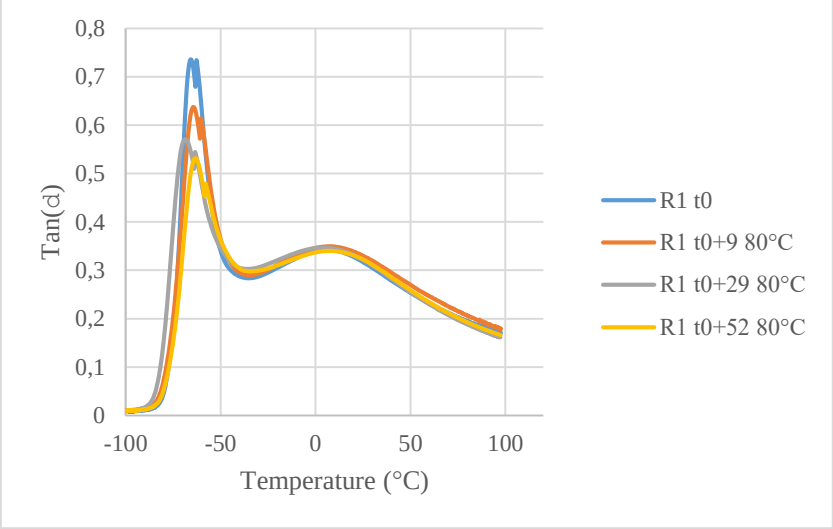


Figure 4.33. Tan (δ) change of the R1 formulation at 80°C aging temperature as a function of temperature sweep at different aging times

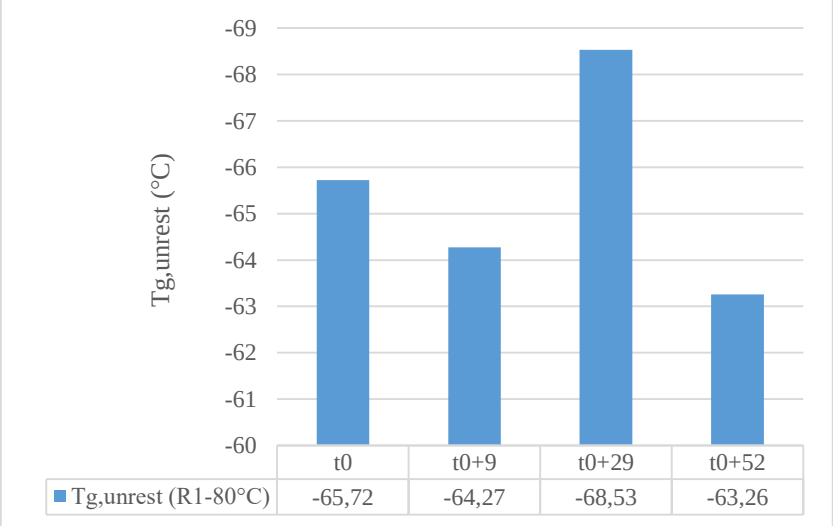


Figure 4.34. Change of $T_{g,unrest}$ as a function of aging time for the R1 formulation aged at 80°C

When the storage modulus (E') of the R1 at 80°C was examined with respect to aging, it was observed that the storage modulus increased with aging (Figure 4.35-

Figure 4.36). This situation is consistent with the increasing crosslink density of the R1 formulation. However, while a decrease in modulus was expected due to the reduced crosslink density on 52nd day, this was not observed.

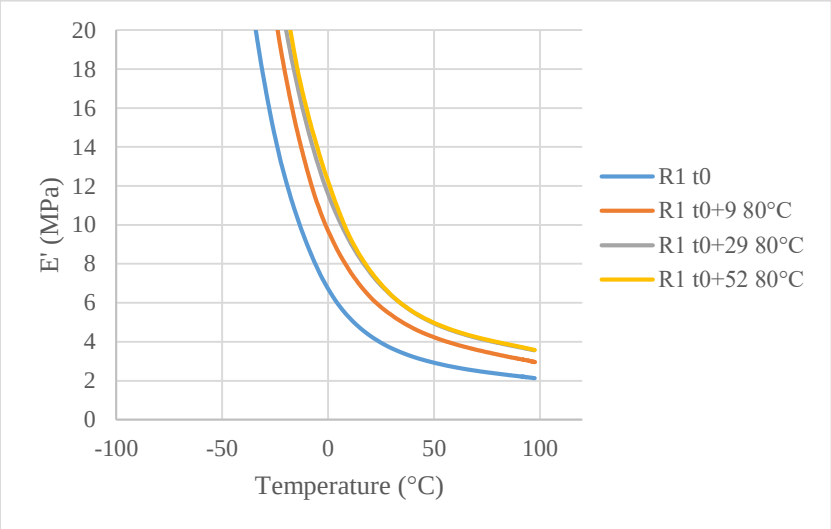


Figure 4.35. Storage modulus (E') as a function of temperature for the R1 formulation aged at 80°C

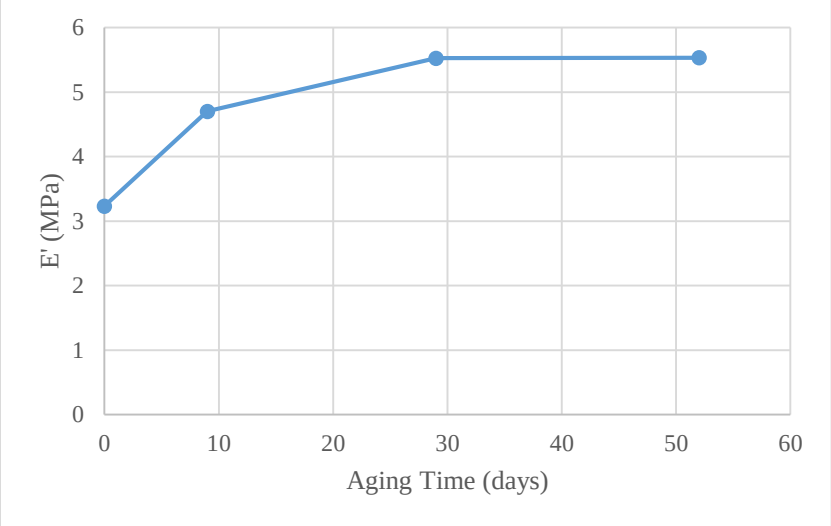


Figure 4.36. Storage Modulus (E', at 40°C) as a function of aging time for the R1 formulation aged at 80°C

Aging-dependent tan(δ) curves for the R1 formulation and the variation of $T_{g,unrest}$ with aging time at 60°C are presented in Figure 4.37 and Figure 4.38 respectively.

Accordingly, for the R1 formulation aged at 60°C, the $T_{g,unrest}$ initially increases, then decreases, and finally shows an increasing trend. At these temperatures and times, the crosslink density was observed to increase on 52nd and 135th days, but decrease on 240th day. Evaluating these findings, the $T_{g,unrest}$ data for 52nd day consistently show an increase, aligning with the crosslink density data. However, the $T_{g,unrest}$ data for 135th and 240th days exhibit a trend contrary to the crosslink density. Based on the crosslink density data, the $T_{g,unrest}$ value should increase on 135th and decrease on 240th days.

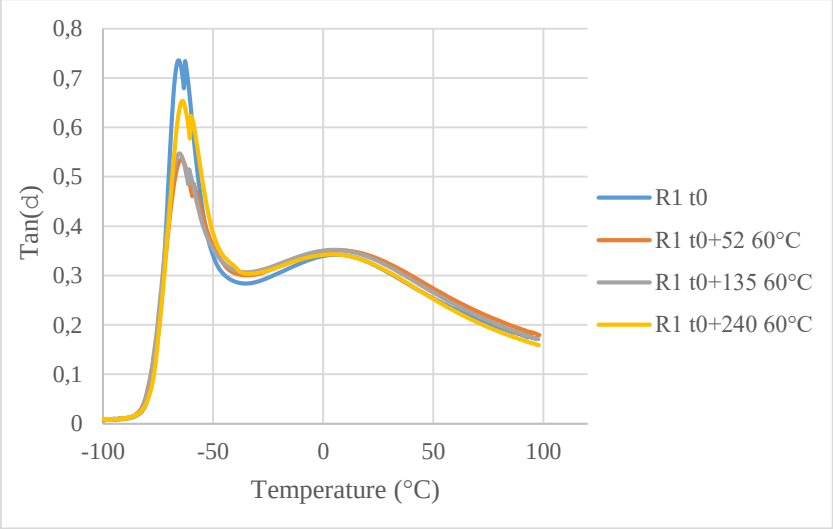


Figure 4.37. Tan (δ) change of the R1 formulation at 60°C aging temperature as a function of temperature sweep at different aging times

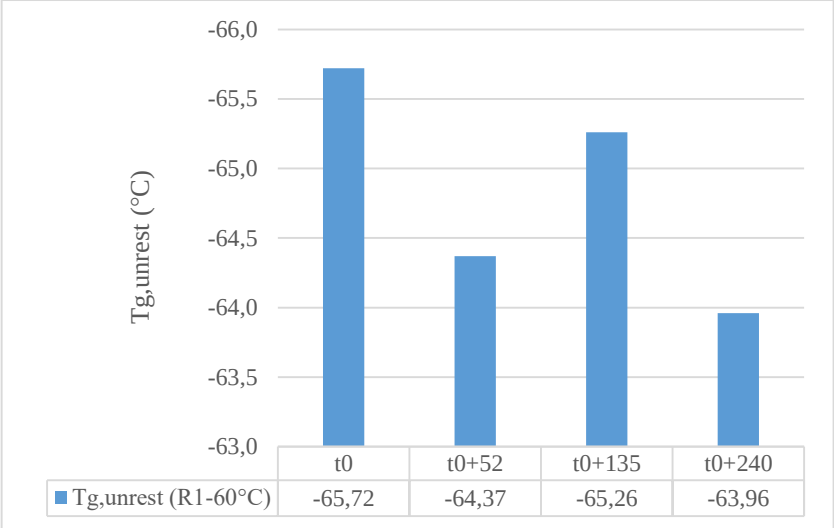


Figure 4.38. Change of $T_{g,unrest}$ as a function of aging time for the R1 formulation aged at 60°C

Examination of the temperature-dependent storage modulus (E') values for the R1 formulation aged at 60°C for various durations reveals an increase in storage modulus on 52nd and 135th days, followed by a decrease on 240th day (Figure 4.39 - Figure 4.40). This behavior is consistent with crosslinking behavior.

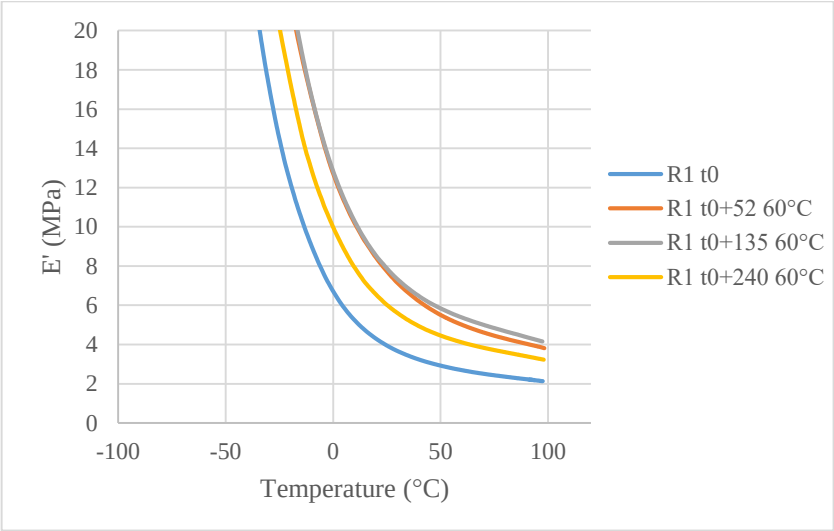


Figure 4.39. Storage modulus (E') as a function of temperature for the R1 formulation aged at 60°C

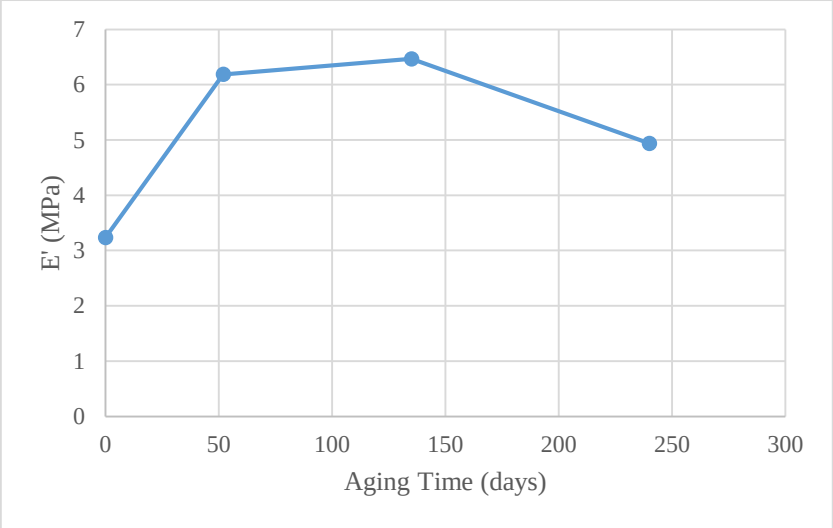


Figure 4.40. Storage Modulus (E', at 40°C) as a function of aging time for the R1 formulation aged at 60°C

Aging-dependent tan(δ) curves for the R1 formulation and the variation of $T_{g,unrest}$ with aging time at 30°C are presented in Figure 4.41 and Figure 4.42 respectively. Accordingly, for the R1 formulation aged at 30°C, the $T_{g,unrest}$ increases up to last data point, and finally it shows a decreasing trend. At these temperatures and times, the crosslink density was observed to increase for 52nd and 135th days, but decrease on 240th day. Evaluating these findings, the $T_{g,unrest}$ data seems to align with the crosslink density data.

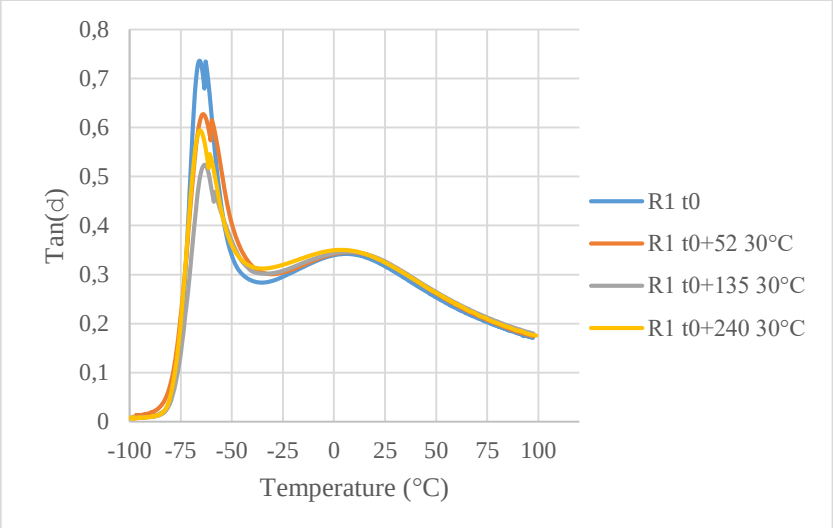


Figure 4.41. Tan (δ) change of the R1 formulation at 30°C aging temperature as a function of temperature sweep at different aging times

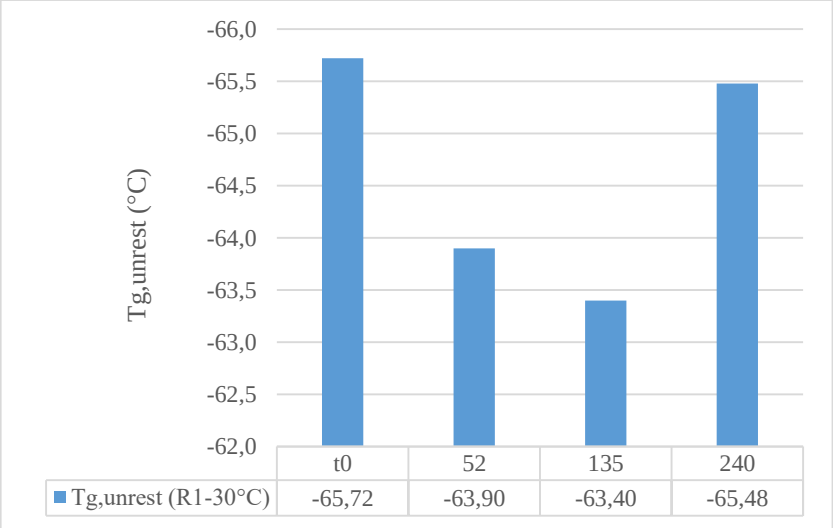


Figure 4.42. Change of $T_{g,unrest}$ as a function of aging time for the R1 formulation aged at 30°C

Examination of the temperature-dependent storage modulus values for the R1 formulation aged at 30°C for various durations reveals an increase in storage modulus on 52nd and 135th days, followed by a decrease on 240th day (Figure 4.43-Figure 4.44). This behavior is consistent with the material's crosslinking behavior.

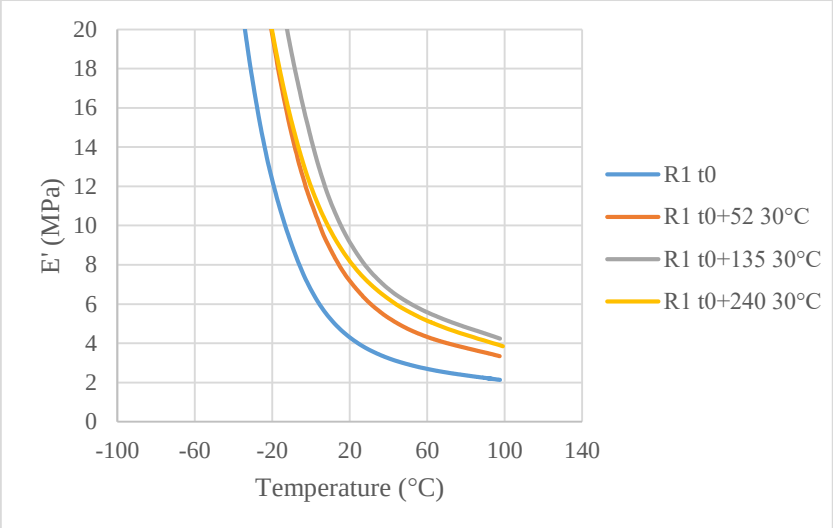


Figure 4.43. Storage modulus (E') as a function of temperature for the R1 formulation aged at 30°C

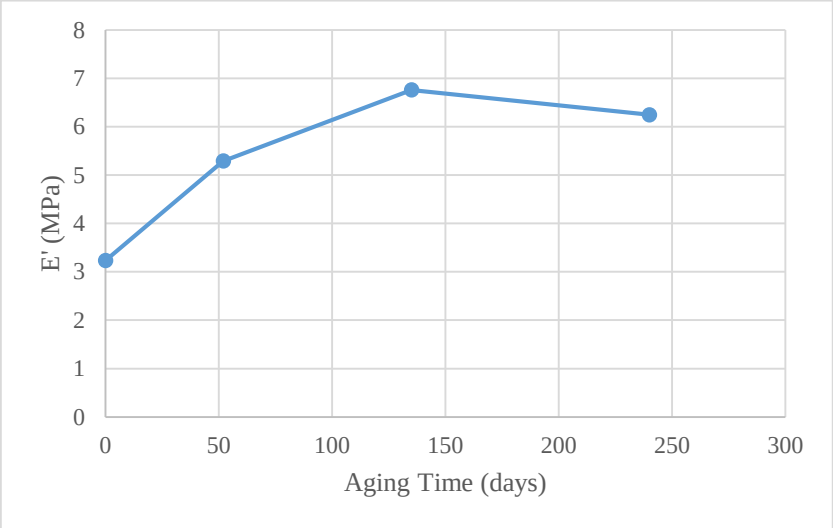


Figure 4.44. Storage Modulus (E', at 40°C) as a function of aging time for the R1 formulation aged at 30°C

Aging-dependent tan(δ) curves for the R2 formulation and the variation of $T_{g,unrest}$ with aging time at 60°C are presented in Figure 4.45 and Figure 4.46 respectively. Accordingly, for the R2 formulation aged at 60°C, the $T_{g,unrest}$ decreases up to last data point, and finally it shows an increasing trend. The crosslink density was observed to decrease for 52nd day. Therefore, a decrease in $T_{g,unrest}$ at this time is

understandable. However, the continued decrease in $T_{g,unrest}$ on 135th day, while crosslinking was increasing, contradicts the crosslinking data. On 240th day, an increase in $T_{g,unrest}$ was observed, which is consistent with the increased crosslinking compared to 52nd day. Evaluating these findings, the $T_{g,unrest}$ data seems to align with the crosslink density other than data of 135th day.

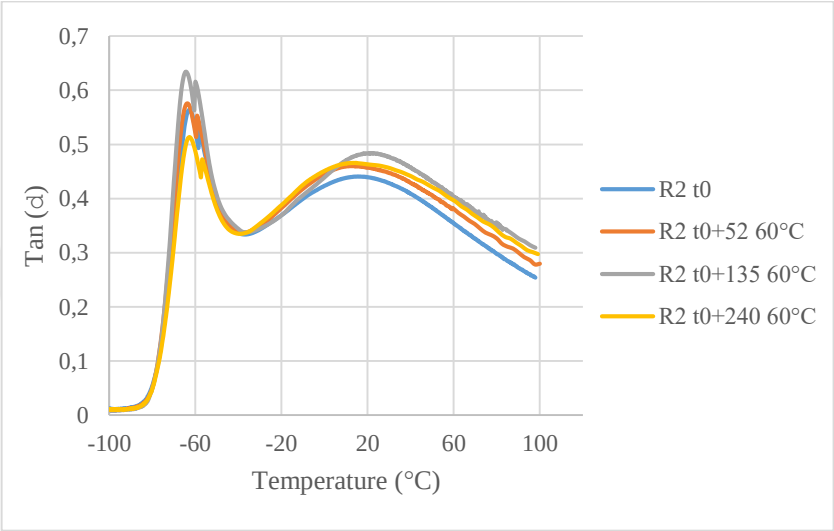


Figure 4.45. Tan (δ) change of the R2 formulation at 60°C aging temperature as a function of temperature sweep at different aging times

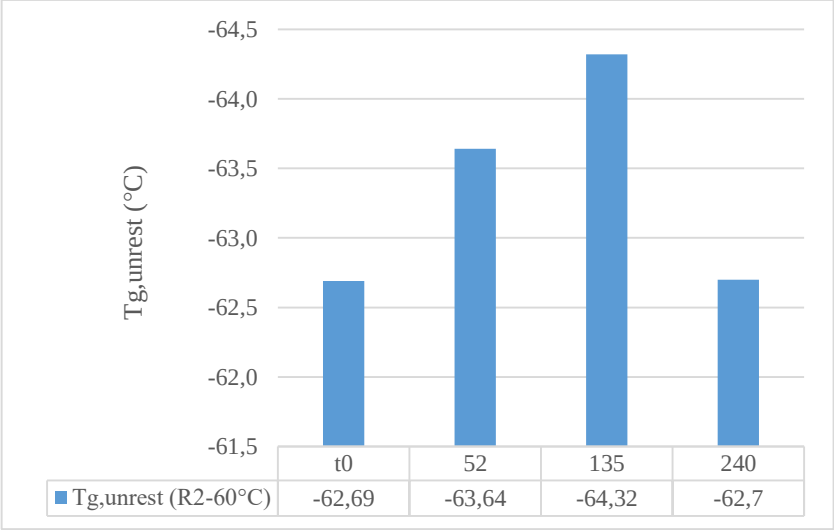


Figure 4.46. Change of $T_{g,unrest}$ as a function of aging time for the R2 formulation aged at 60°C

The storage modulus value exhibited a decrease on 52nd day. Contrary to expectations of an increase, it continued to decline on 135th day (Figure 4.47-Figure 4.48). On 240th day it increased in accordance with crosslink density data. With the exception of the 135th day data, the observed storage modulus (E') behavior consistently correlated with the crosslinking data.

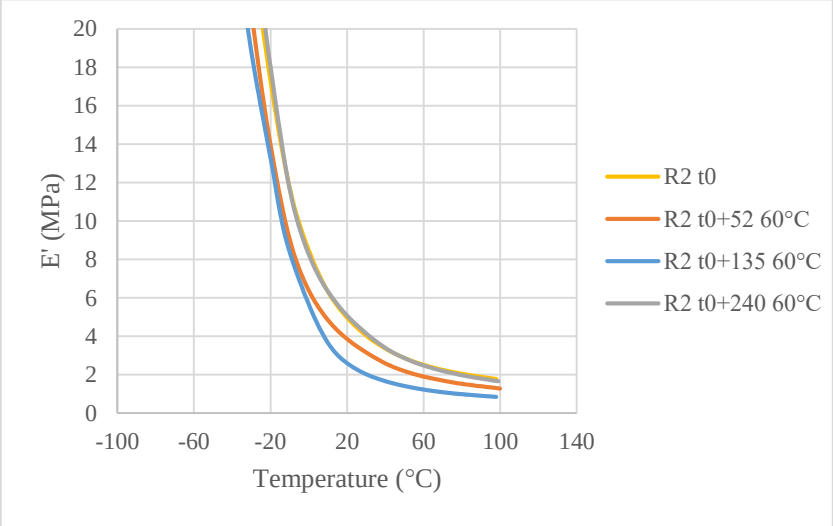


Figure 4.47. Storage modulus (E') as a function of temperature for the R2 formulation aged at 60°C

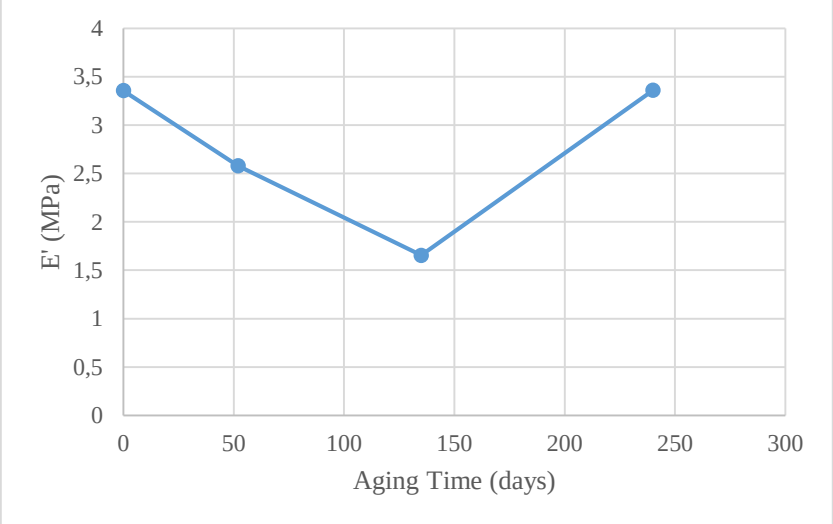


Figure 4.48. Storage Modulus (E', at 40°C) as a function of aging time for the R2 formulation aged at 60°C

Aging-dependent tan(δ) curves for the R3 formulation and the variation of $T_{g,unrest}$ with aging time at 60°C are presented in Figure 4.49 and Figure 4.50 respectively. Accordingly, for the R3 formulation aged at 60°C, the $T_{g,unrest}$ decreases on 52nd day, increases at 135th day and finally decreases for last test time of 240th day. On 52nd day, the decrease in $T_{g,unrest}$ despite an increase in crosslinking presents a contradiction**.** For 135th day, a decrease in $T_{g,unrest}$ would be expected since crosslinking decreased compared to 52nd day**.** However, the 135th day $T_{g,unrest}$ value was observed to increase**.** When evaluating the 240th day $T_{g,unrest}$ data**,** an increase was noted, even though a decrease was anticipated (relative to 52nd day) due to the crosslinking data being lower than that of 52nd day. In summary, the $T_{g,unrest}$ behavior of R3 formulation is inconsistent with the crosslinking data. It is hypothesized that the absence of a bonding agent in the R3 formulation contributes to the material's inherent tendency towards greater heterogeneity, thereby impacting the reliability of the measurements.

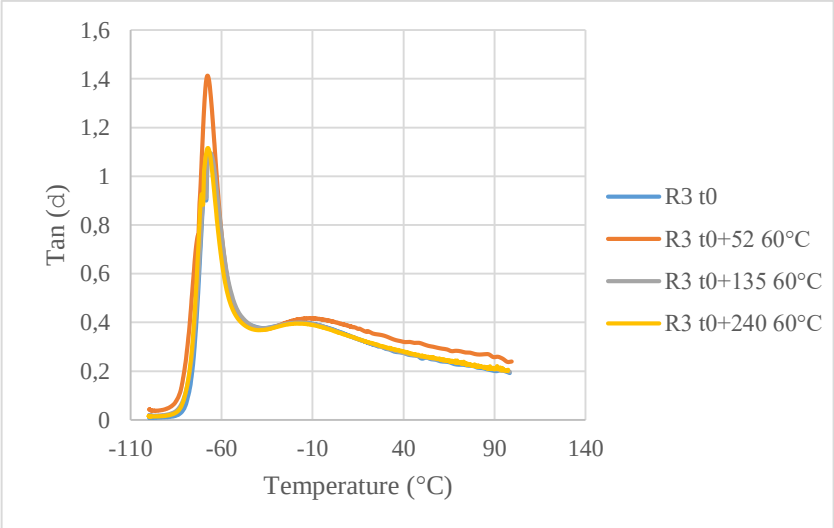


Figure 4.49. Tan (δ) change of the R3 formulation at 60°C aging temperature as a function of temperature sweep at different aging times

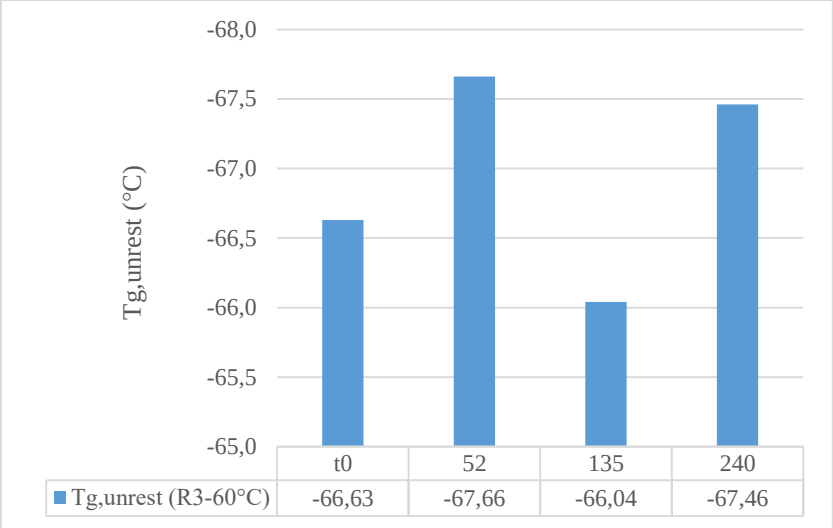


Figure 4.50. Change of $T_{g,unrest}$ as a function of aging time for the R3 formulation aged at 60°C

Examination of the temperature-dependent storage modulus values for the R3 formulation aged at 60°C for various durations reveals an equality as temperature increases (Figure 4.51-Figure 4.52). The temperature range corresponding to the second peak in the tan(δ) vs. temperature graph, where the storage modulus equalize, characterizes the interaction between the hard urethane segments and the HTPB backbone with the filler materials. Since the R3 formulation does not contain a bonding agent, the binder-filler interaction does not differ for various aging times.

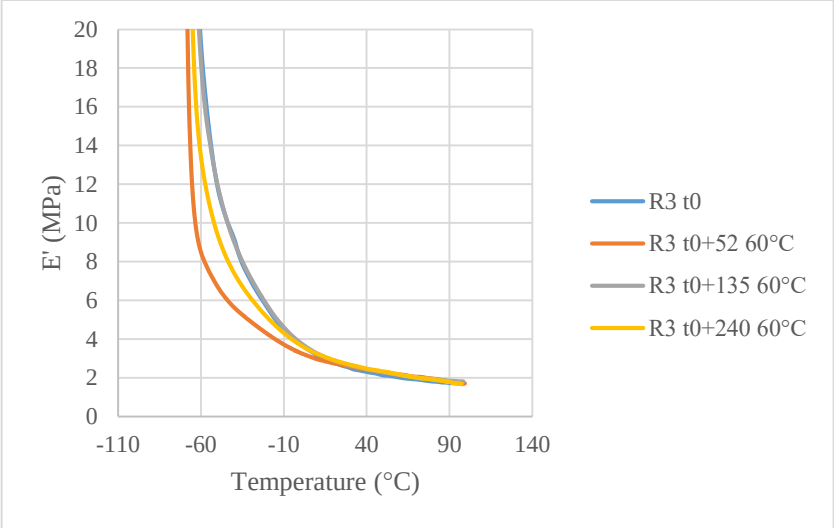


Figure 4.51. Storage modulus (E') as a function of temperature for the R3 formulation aged at 60°C

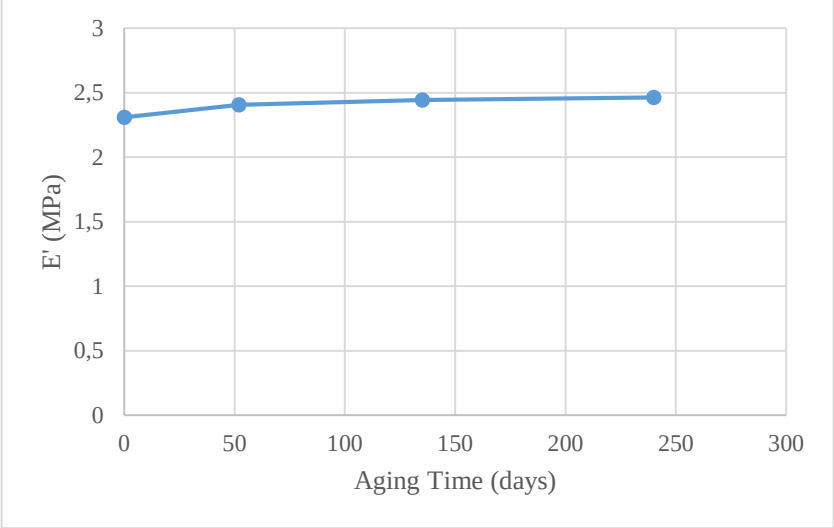


Figure 4.52. Storage Modulus (E', at 40°C) as a function of aging time for the R3 formulation aged at 60°C

DMA analysis results were evaluated in conjunction with the crosslink density test results. When assessing the DMA analyses in terms of changes in tan(d), $T_{g,unrest}$, and storage modulus (E') values, it was observed that the behavior of storage modulus largely aligned with the crosslinking behavior, with a few exceptions (R1-80°C on 52nd day, R2-60°C on 135th day). Although the $T_{g,unrest}$ behavior appeared

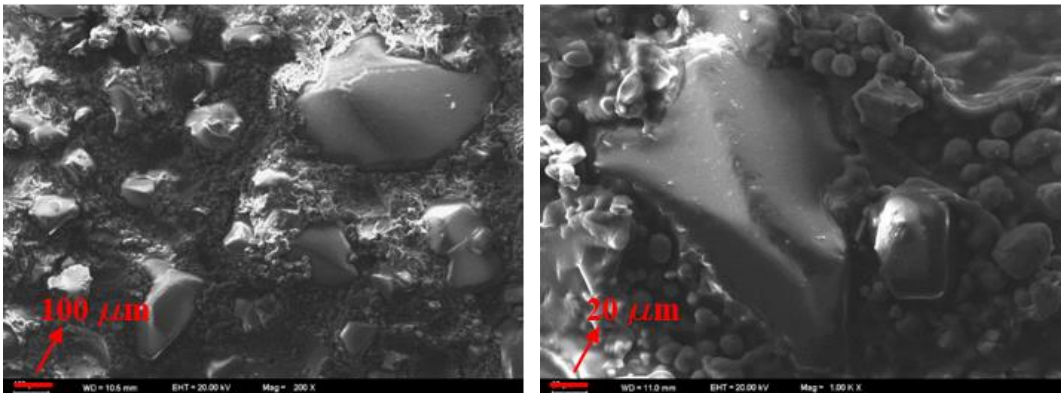
inconsistent with the crosslink density behavior across all temperatures, it's important to note that $T_{g,unrest}$ values at each aging temperature were considerably close to one another (within ± 2°C), with the exception of the R1 formulation at 80°C on 29th day. Therefore, the obtained $T_{g,unrest}$ values can be considered within the limits of measurement error. Consequently, it can be stated that the obtained $T_{g,unrest}$ values were not significantly different from each other, except for this single outlier. However, this conclusion unfortunately does not correlate with the increasing or decreasing crosslink density data and the reason for this discrepancy remains unclear.

4.7 SEM Analysis

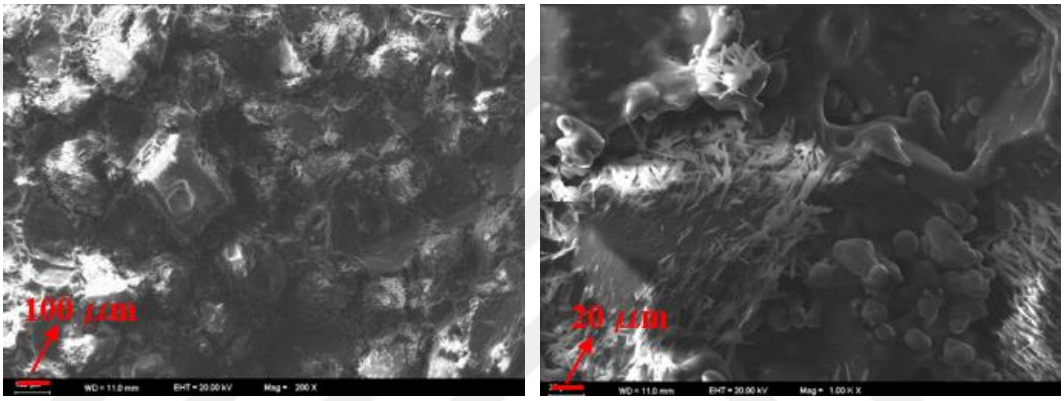
Polymer bonded explosive is a type of elastomer that is heavily filled with particles, meaning it is created by incorporating fine solid particles (such as RDX or Al) into an elastomeric matrix. As a result, the fracture mechanisms (or microscopic damage) in the explosive typically involve failure at the filler/matrix interface (also known as dewetting) and tearing of the matrix. Over time, during thermal accelerated aging, the matrix becomes harder, and the adhesive stress at the interface between the RDX particles and the matrix decreases due to thermal stress. As a result, the likelihood of adhesive interface failure (or dewetting) increases as the aging time progresses or temperature increases (Wang, Qiang, Wang, & Wang, 2019). Hence, with SEM analysis it is aimed to visualize the rupture interface of the material due to aging. All the images clearly shows a heterogeneous surface. There are distinct, relatively large, angular particles embedded within a finer, more continuous matrix phase. This is characteristic of a composite material where filler particles are dispersed within a binder.

When the 30ºC aging images of the R1 formulation are examined (Figure 4.53), it is seen that there is still a strong interaction between the polymer and the filler material suggesting that no significant change was observed at the polymer-solid-filler interface due to aging at this temperature. There are numerous rod-like or needle-like structures around particles, likely representing polymer at all aging times.

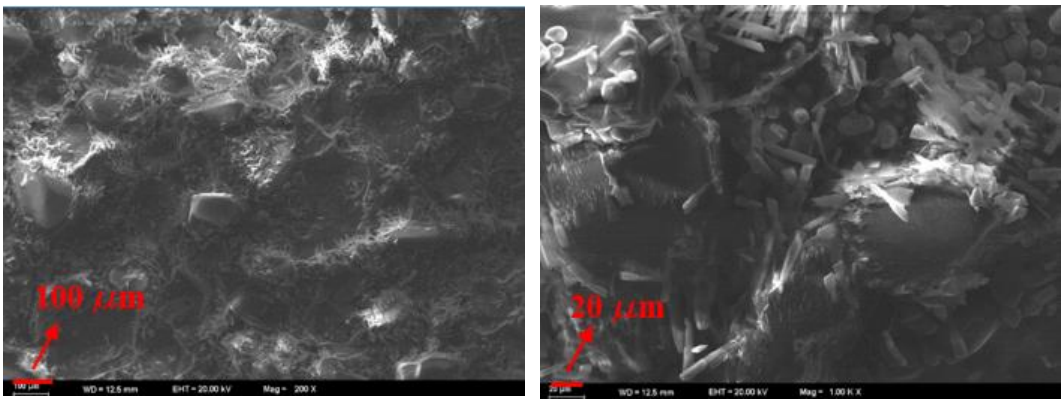
Although the crosslink density increased more at low temperatures, no distinct separation was observed between the solid filler and the polymer. This is because, as in the tensile test, the physical effects of aging (i.e. low thermal stress between polymer and filler) dominate the chemical effects.



$R1_{t0}$



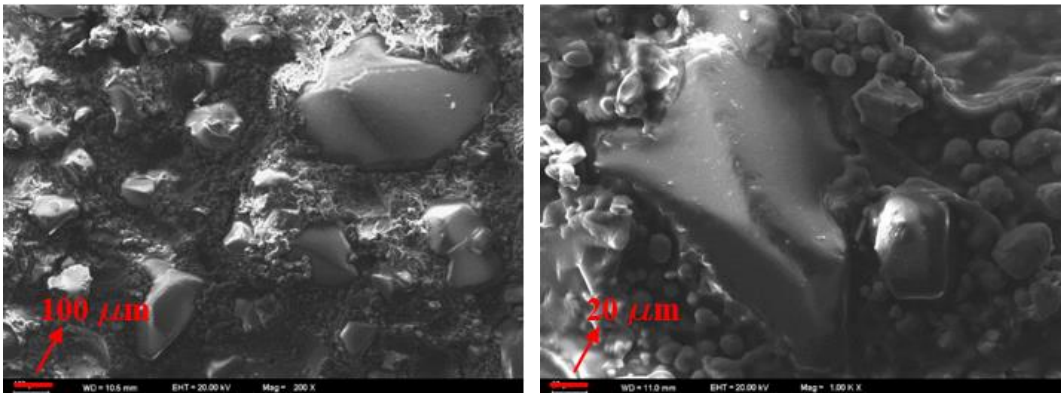
$R1_{t0+135}$-30°C



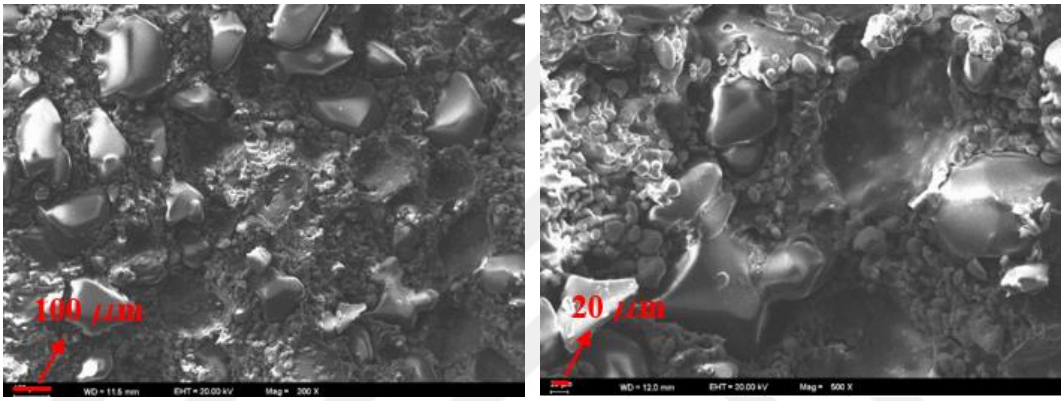
$R1_{t0+240}$-30°C

Figure 4.53. SEM images of the time-dependent fracture surfaces of the dog-bone specimens remained after tensile testing of the R1 formulation, aged at 30°C

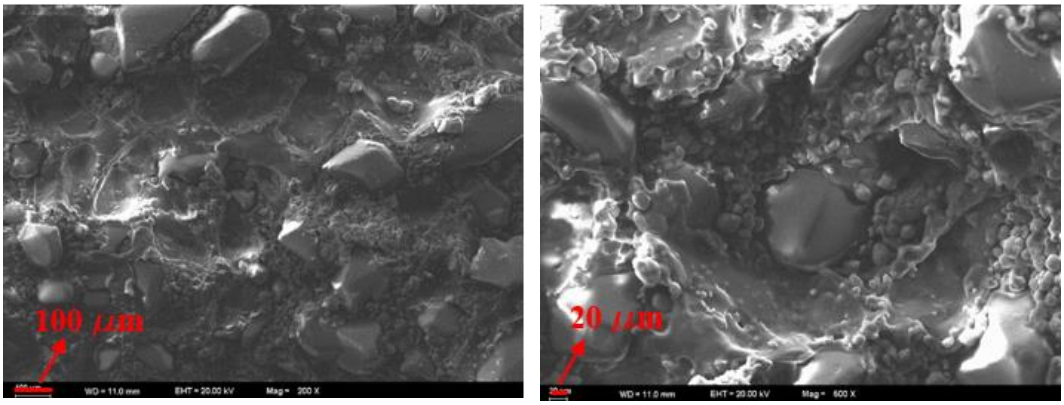
In the 16th and 52nd day aging images of 80ºC aging temperature (Figure 4.54), it is understood from the polymer pieces on the solid filler that the rupture occurred from within the polymer material itself. Rougher areas with voids suggest ductile tearing, potentially in polymeric phase. This situation shows that in the nominal R1 formulation using the bonding agent, there is a strong bond between the solid material and the polymer even at high temperatures. There are numerous small spherical or irregular particles distributed in the matrix. Some larger particles appear to be partially embedded, suggesting possible interfacial debonding.



$R1_{t0}$



$R1_{t0+16}$-80ºC

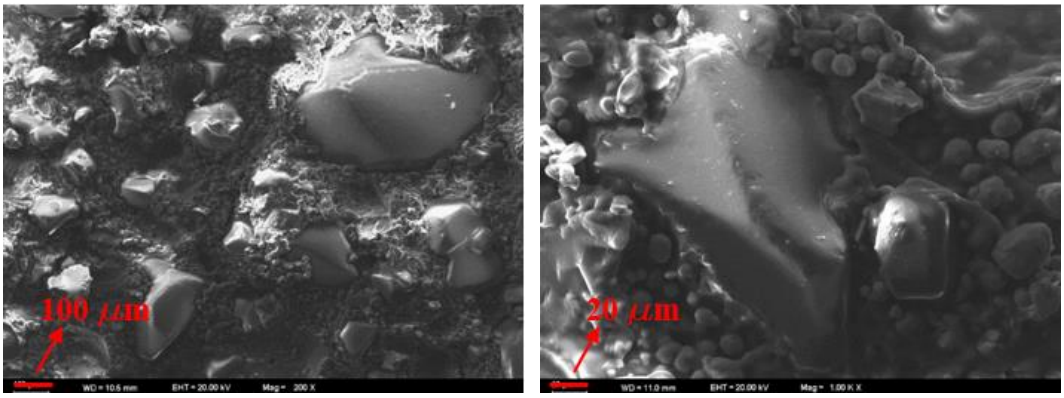


$R1_{t0+52}$-80ºC

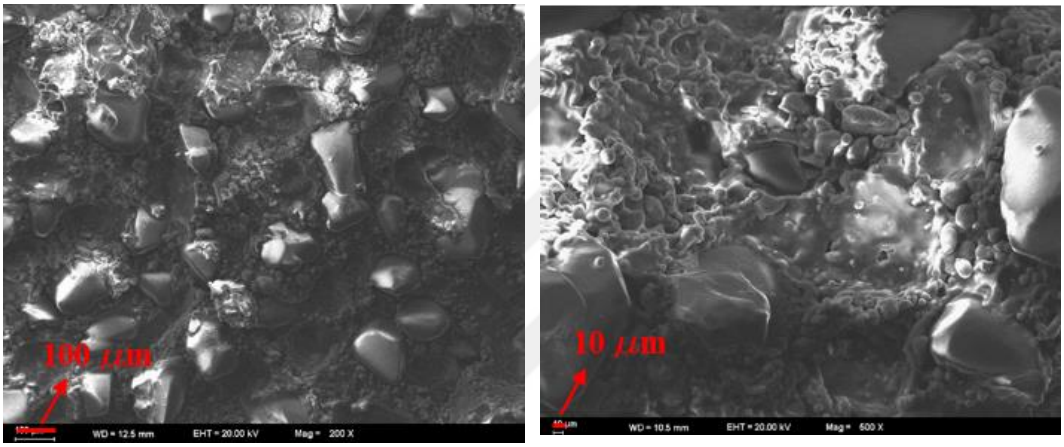
Figure 4.54. SEM images of the time-dependent fracture surfaces of the dog-bone specimens remained after tensile testing of the R1 formulation, aged at 80°C

When the rupture interface images of R1, R2 and R3 formulations (Figure 4.55-Figure 4.57) are examined for 60°C temperature, it is seen that the R2 formulation which has highest antioxidant content, has the best polymer-filler material interaction. The surface shows a rugged, ductile fracture pattern, suggesting a toughened matrix (Figure 4.56). Numerous small spherical or irregular particulates are embedded within the matrix. The reason for this is that the polymer ages more slowly for the same temperature in the R2 formulation due to its higher antioxidant content, and therefore the interaction between the polymer and the filler material remains high.

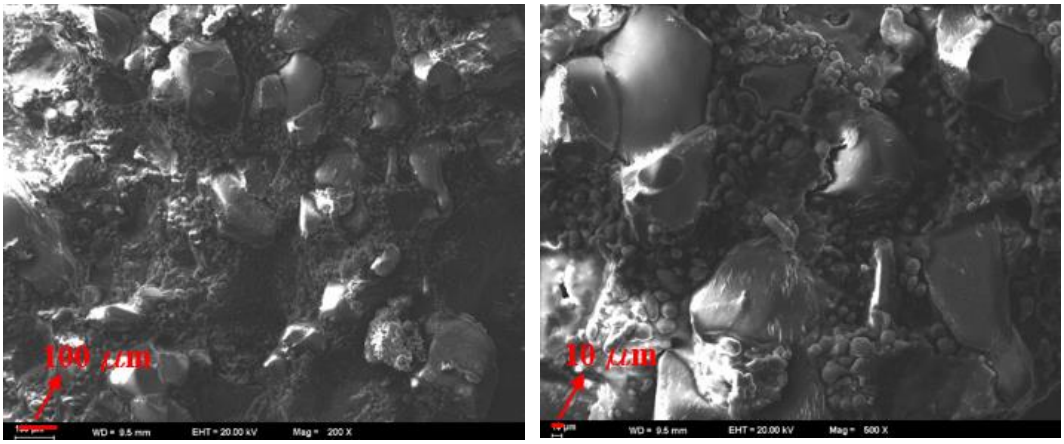
In the R3 formulation without bonding agent, it is clearly seen for all aging times that the polymer and filler interface is very clearly separated (Figure 4.57). It can be seen that the filler particles seems to have pulled away from polymer matrix, creating voids or gaps at the interface. These voids can reduce the mechanical integrity of the composite, especially under tensile or impact loading. This debonding suggests that the adhesion between the filler and the binder was not strong enough to withstand the stress during rupture. The extent of debonding could be a critical factor in the overall mechanical properties and failure behavior of the polymer bonded explosive.



$R1_{t0}$

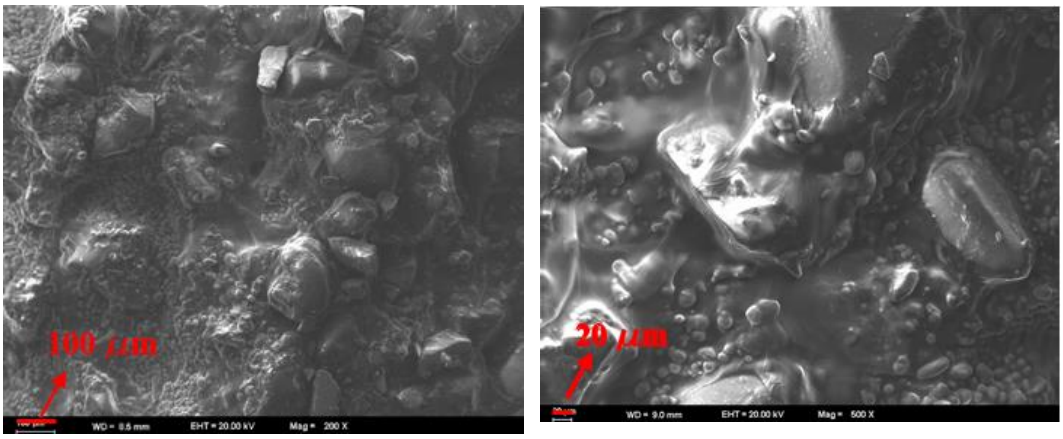


$R1_{t0+135}$-60ºC

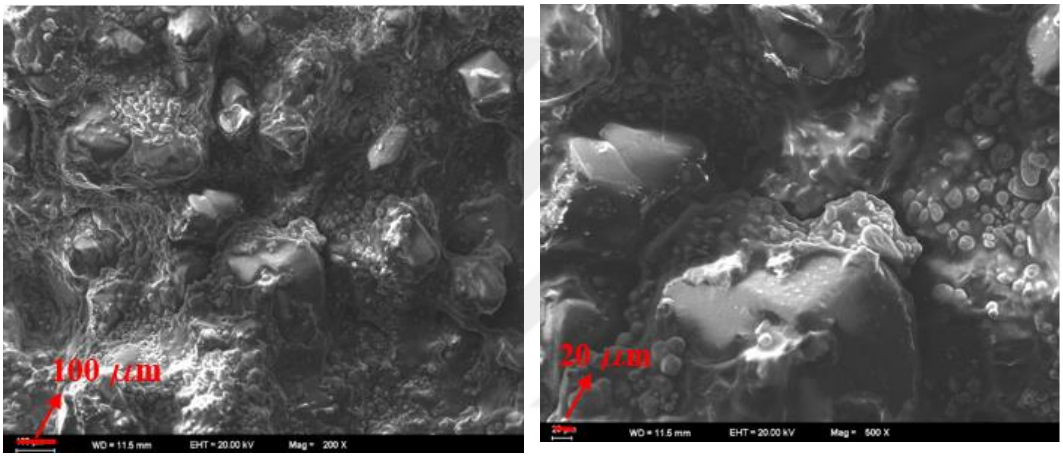


$R1_{t0+240}$-60ºC

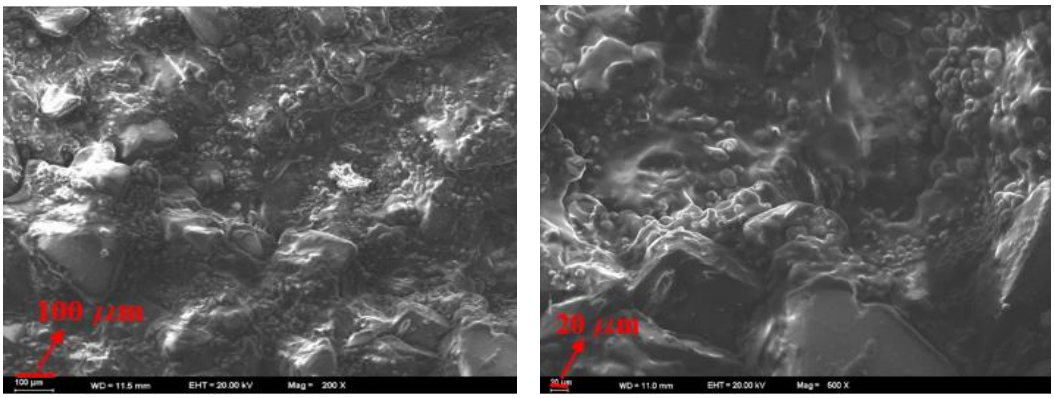
Figure 4.55. SEM images of the time-dependent fracture surfaces of the dog-bone specimens remained after tensile testing of the R1 formulation, aged at 60°C



$R2_{t0}$

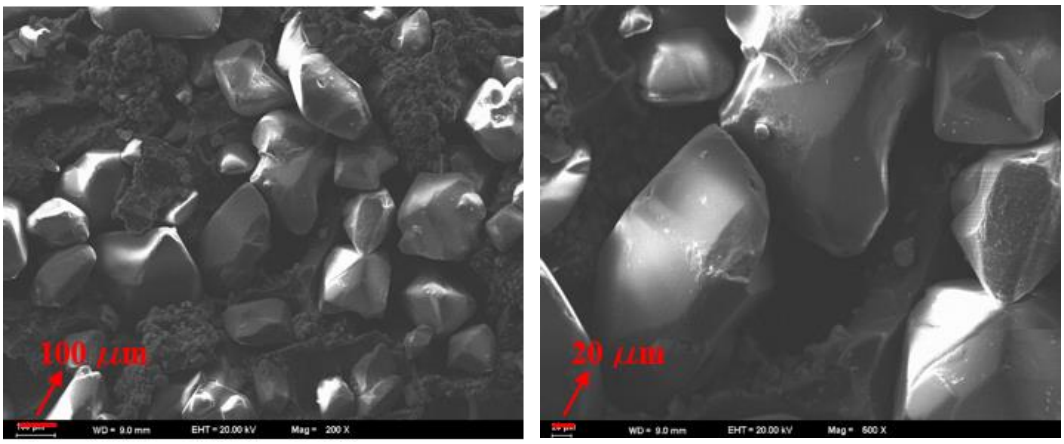


$R2_{t0+135}$-60ºC

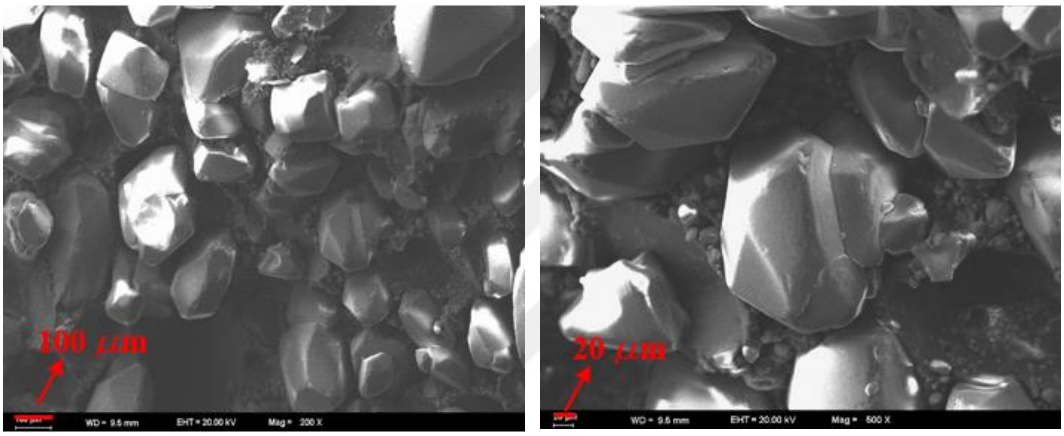


$R2_{t0+240}$-60ºC

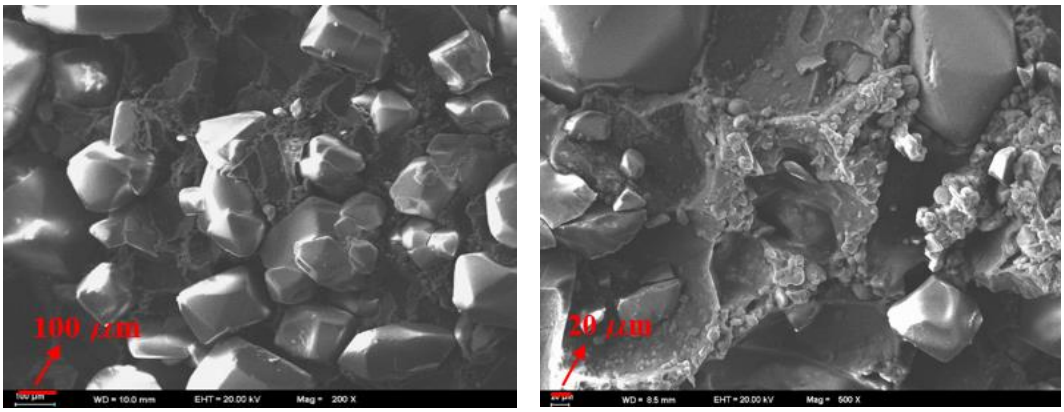
Figure 4.56. SEM images of the time-dependent fracture surfaces of the dog-bone specimens remained after tensile testing of the R2 formulation, aged at 60°C



$R3_{t0}$



$R3_{t0+135}$-60ºC



$R3_{t0+240}$-60ºC

Figure 4.57. SEM images of the time-dependent fracture surfaces of the dog-bone specimens remained after tensile testing of the R3 formulation, aged at 60°C

4.8 Comparison of Crosslink Density, Tension, FTIR and DMA Test Results

From Figure 4.58 to Figure 4.62 presents the strain at maximum load, storage modulus (E'), the crosslink density, and FTIR analysis results for the R1 formulation at aging temperatures of 80°C, 60°C and 30°C while 60°C data presented for R2 and R3 as a function of aging time. The absence of figures for 70°C and 50°C for R1 is due to the unavailability of complete property data to make comparisons at these temperatures. Table 3.4 presents a summary of the tests performed, specifying the corresponding aging temperatures and durations. The data were normalized by multiplying with specific coefficients to ensure observable scales on the graphs.

When comparing data trends, it's hypothesized that an increase in crosslinking will lead to the closer proximity of polymer chains. Consequently, an increase in hydrogen bonding interactions is expected, resulting in an increase of the carbonyl area (interacted carbonyl area/non-interacted carbonyl area). Similarly, an increase in crosslinking is anticipated to raise the storage modulus, which is a measure of the material's elastic behavior. In this context, the data trends for crosslink density, storage modulus, and carbonyl area are expected to show mutually supportive increases or decreases. Regarding elongation data (strain at max. load), while it's influenced by chemical changes like crosslinking or chain scisson, the physical effects of aging (dewetting, thermal stress, plasticizer diffusion), as explained in Section 4.4, are considered to be more dominant than the chemical effects. Therefore, a general decreasing trend in elongation data is expected. While a general decrease in elongation behavior is observed, local increases seen in some graphs might be attributed to a decrease in crosslinking. Although the physical effects of aging cannot be entirely separated from crosslinking, this hypothesis is based on physical response of temperature on aging. The results discussed in the relevant sections of the thesis and summarized in this section are explained with the graphs from Figure 4.58 to Figure 4.62.

In Figure 4.58, trends in the data indicate similar patterns among the crosslink density, FTIR carbonyl interactions, and the storage modulus (E') changes. This trend is further supported by the strain at maximum load data, where an increase in the crosslink density, storage modulus, or the carbonyl interactions corresponds to a decrease in elongation. While the decrease observed in the crosslink density and carbonyl interactions on 52nd day is attributed to chain scission, a corresponding decrease in storage modulus and increase in elongation was not observed. The continued decrease in the strain at maximum load is thought to be due to reduced filler-polymer interaction resulting from increased thermal stress within the material as explained in Section 4.4. This highlights the need to consider the coupled physical and chemical effects of aging on the material, suggesting that for the R1 formulation at 80°C, physical changes are predominant over chemical changes. Despite no decrease in the storage modulus on 52nd day, the absence of an increasing trend at this point suggests it could mark the onset of a decline.

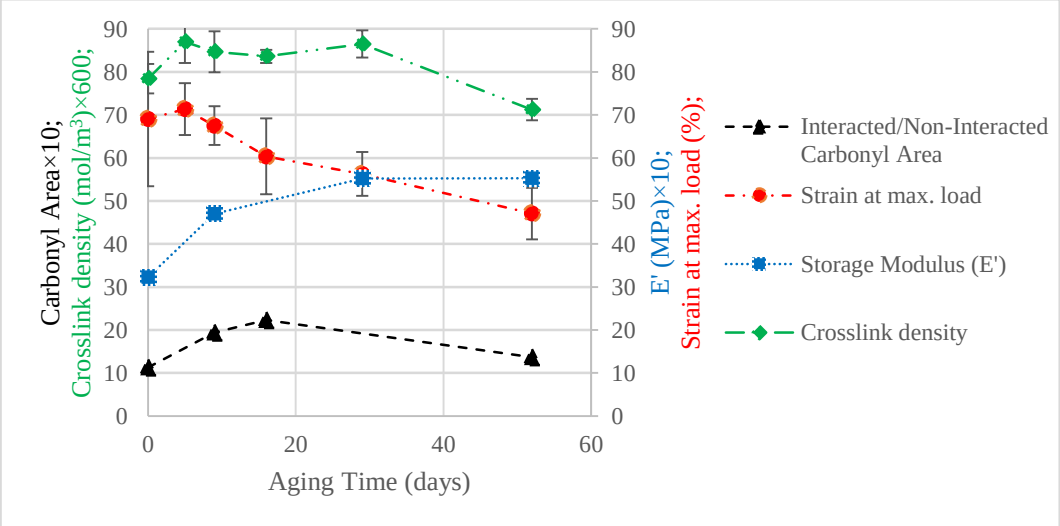


Figure 4.58. Property change of the R1 formulation as a function of time at 80°C

Figure 4.59 presents the strain at maximum load, storage modulus (E'), the crosslink density, and FTIR analysis results for the R1 formulation at aging temperature of 60°C, as a function of aging time. It's seen that the aging behavior of the R1 formulation at 60°C exhibits analogous trends for all characteristics, driven by the

same causes as its behavior at 80°C. Furthermore, the lack of a decrease in modulus observed at the last data point at 80°C aligned with the reduction in crosslink density and carbonyl area at 60°C.

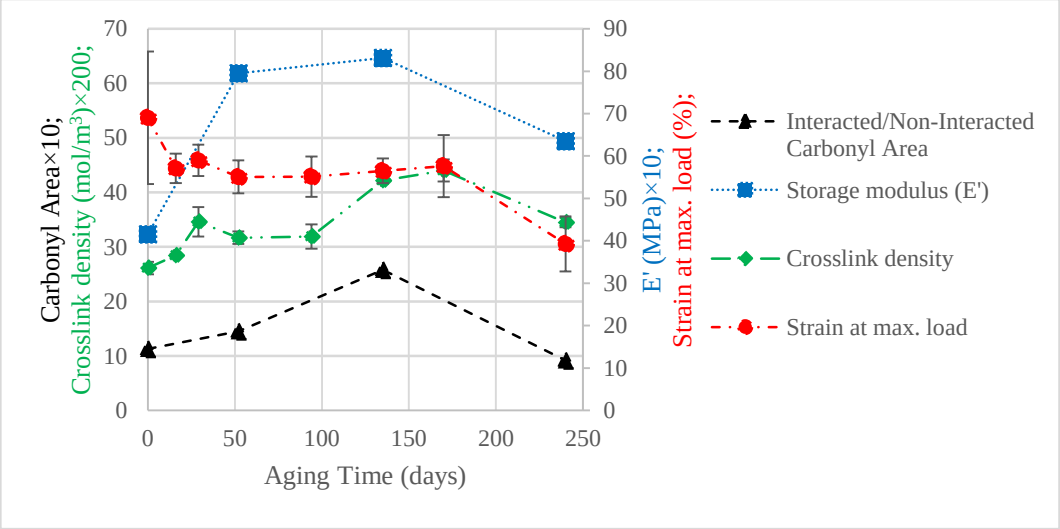


Figure 4.59. Property change of the R1 formulation as a function of time at 60°C

Figure 4.60 presents the strain at maximum load, storage modulus (E'), the crosslink density and FTIR analysis results for the R1 formulation at aging temperature of 30°C, as a function of aging time. Generally, carbonyl content and crosslinking show an increasing trend, while strain at max. load decreases, confirming these observations. The storage modulus data also increased in parallel with the crosslink density data until the last measurement. However, considering that the crosslink density data generally show an increasing trend when examining the difference between the first and last data points, it can be concluded that all test data are almost consistent with each other.

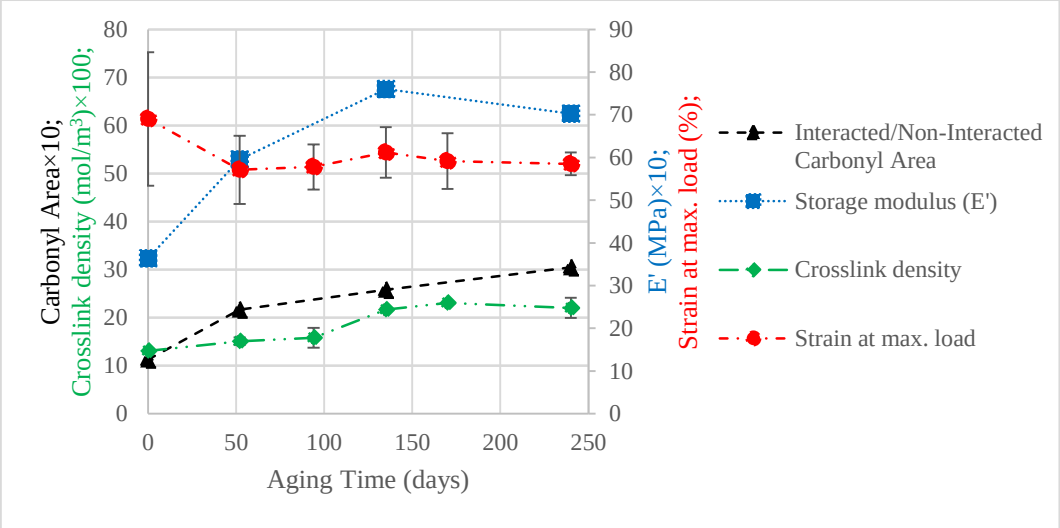


Figure 4.60. Property change of the R1 formulation as a function of time at 30°C

Figure 4.61 presents the strain at maximum load, storage modulus (E'), the crosslink density and FTIR analysis results for the R2 formulation at aging temperature of 60°C, as a function of aging time. For the high antioxidant R2 formulation, the storage modulus decrease correlates with the trends observed in the crosslink density, carbonyl interaction, the strain at maximum load excluding the storage modulus data of 135th day. This means that a reduction in the crosslink density is consistent with a decrease in the storage modulus, an increase in the strain at maximum load, and a decrease in the carbonyl interaction. Conversely, the opposite trends in these properties would also likely exhibit a similar correlation as can be seen from the trends obtained after 94th day.

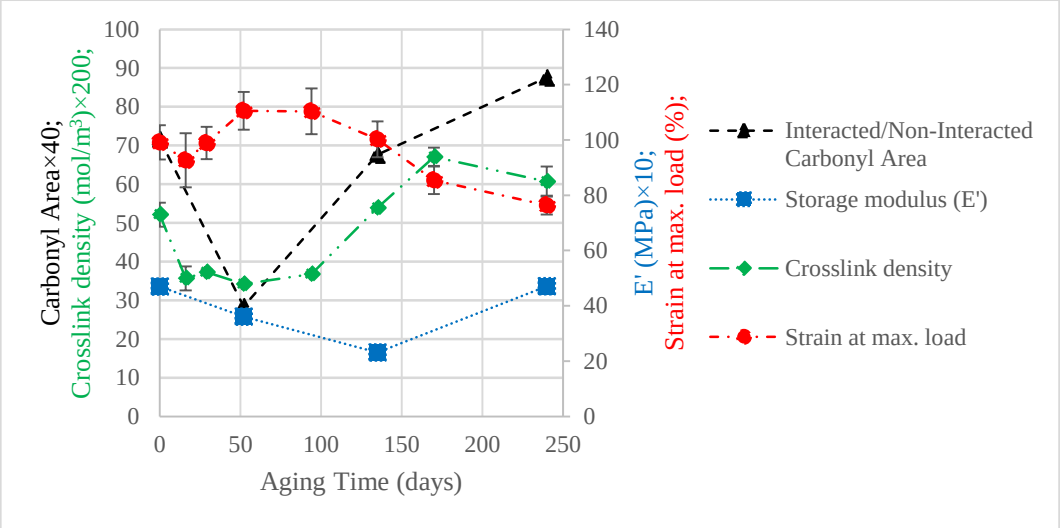


Figure 4.61. Property change of the R2 formulation as a function of time at 60°C

Figure 4.62 presents the strain at maximum load, storage modulus (E'), the crosslink density and FTIR analysis results for the R3 formulation at aging temperature of 60°C as a function of aging time. In the R3 formulation (formulation lack of bonding agent), the trends in the crosslink density and the carbonyl interaction are mutually supporting: either increase or decrease in parallel. The strain at maximum load data further supports this, inversely correlating with the crosslink density (i.e. the strain at maximum load decreases as the crosslink density increases, and vice versa). Although crosslinking and elongation data seems to confirm each other from chemical point of view, it is evaluated that the elongation behavior of the R3 formulation is mostly due to the interaction between the polymer and the filler since it does not contain a bonding agent. Consequently, the crosslink density, strain at maximum load, and the carbonyl interaction behaviors are seemed to be consistent. The storage modulus, however, exhibits a largely stable trend, which is likely due to the relatively constant filler-polymer interaction in this bonding agent-free formulation throughout aging.

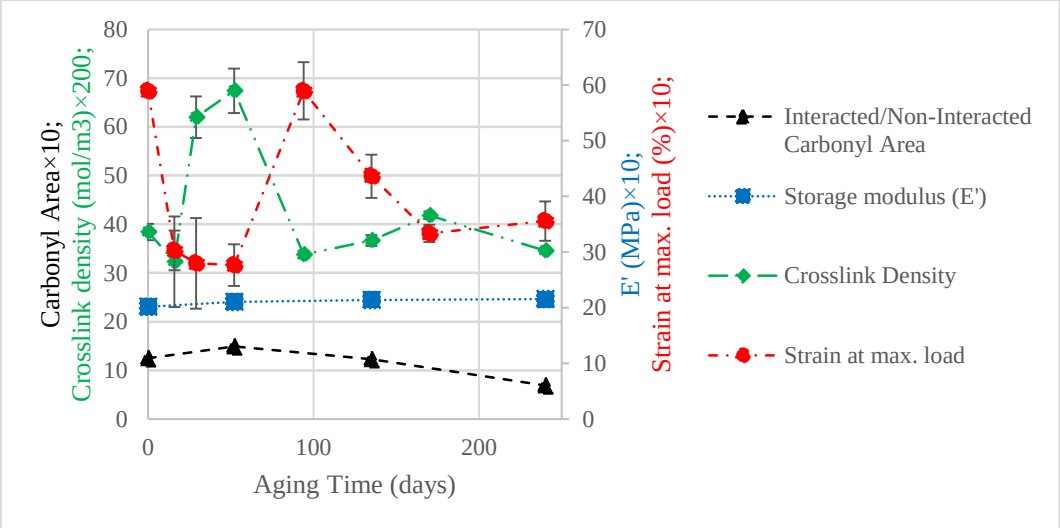


Figure 4.62. Property change of the R3 formulation as a function of time at 60°C

Despite some deviations from expected trends in the aging-related data discussed, the comparison of results from tests performed at common aging times in this section reveals largely consistent and mutually supportive findings, with a few exceptional data points. It is evaluated that results not conforming to expected behavior or contradicting other tests may stem from the material's inherent heterogeneity, measurement inaccuracies, or the inability to perform sufficient replicate tests for certain analyses.

4.9 Shelf Life Prediction

Arrhenius and Berthelot approaches, which are known to be used in the literature were used in life-time calculation (Shekhar, 2011). With the assumption of zero-order aging reaction, the time to reach a known requirement value was calculated. A lower limit elongation requirement is generally defined for explosives. For our explosive this requirement is 10% elongation. For life-time calculation with Arrhenius, it is essential to find the change behavior data of elongation at different aging temperatures. For this reason, life prediction was made only for the R1 formulation. Figure 4.63 shows the change in strain values of the R1 formulation when aged for different durations at temperatures of 30°C, 50°C, 60°C, 70°C, and

80°C. For each temperature, a linear trend line is plotted. The slopes of these trend line equations represent the rate at which the strain changes over time.

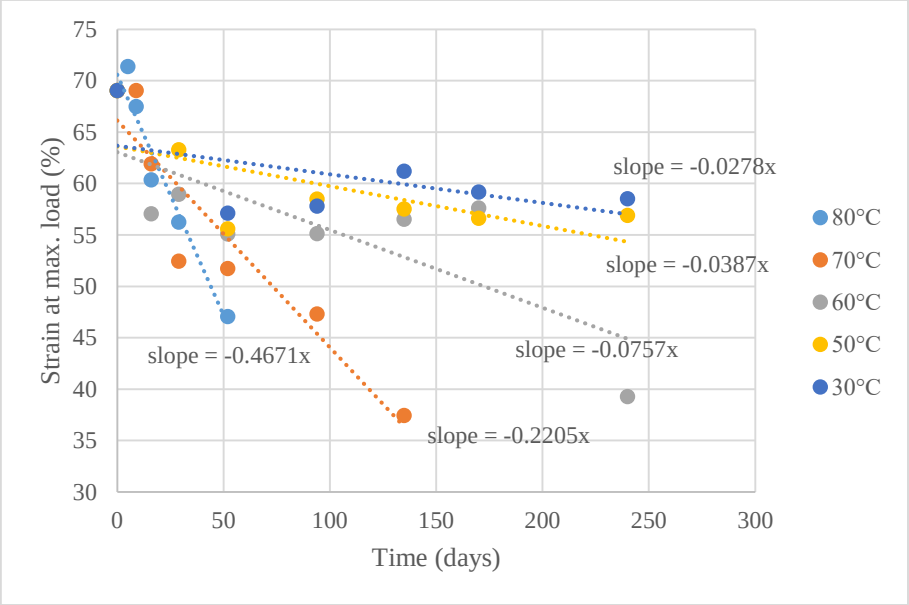


Figure 4.63. The determination of the slopes of the strain against time curves for the R1 formulation at different aging temperatures

As can be seen, the rate of strain reduction is significantly influenced by temperature. The steepest slope is observed for the 80°C curve indicating the most rapid decrease of strain at this temperature. Conversely, the slowest rate of strain decrease is observed at 30°C. These results clearly demonstrate the significant impact of temperature on the aging process of the R1 formulation, with higher temperatures accelerating the degradation of its strain properties.

The Arrhenius equation is given below, and the time-dependent slopes of the graphs are accepted as the reaction constant (k) for each temperature with the zero order rate assumption. From ln k vs. 1/T graph (Figure 4.64) activation energy (E_a) and pre-exponential factor (A) values, which assume a common reaction behavior for all these temperatures, were found.

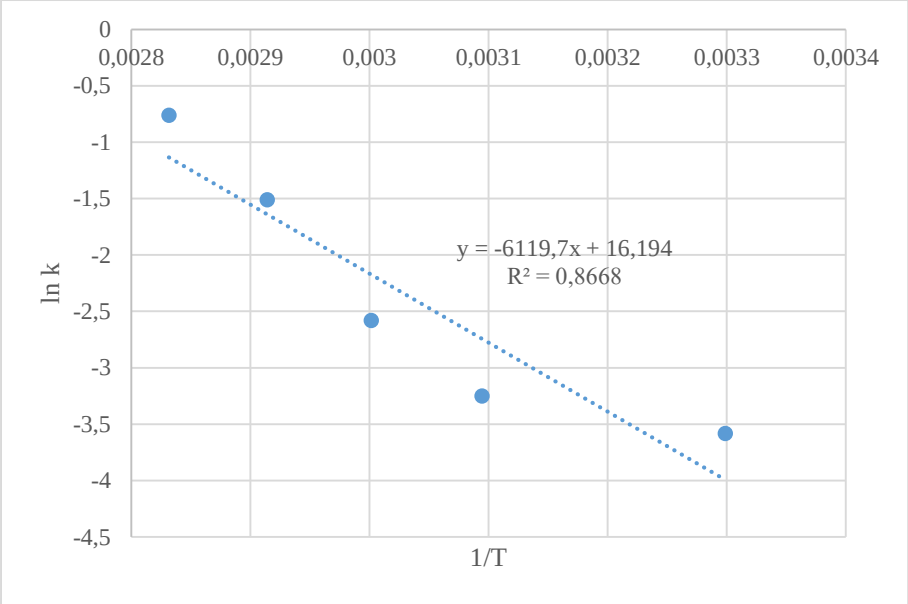


Figure 4.64. ln k vs. 1/T plot to determine Arrhenius parameters for the R1 formulation

From the figure above, E_a and A values are calculated as 50.88 kj/mol and 107.88×10^5, respectively. Using these obtained values, reaction rate constants were recalculated for each temperature. Using these rate constants, the time from the first elongation data to the required value was calculated separately for each temperature (Table 4.3). The reaction rate constant for a temperature of 80°C and the life calculation based on this rate constant are shown below as example.

$$\frac{dC}{dt} = -k,\ for\ zero\ order\ reaction\ \text{"c"}\ is\ measured\ property \qquad \text{Eqn. (5)}$$

$$k = A.e^{\frac{-E_a}{R.T}},\ Arrhenius\ expression \qquad \text{Eqn. (6)}$$

$$lnk = lnA - \frac{E_a}{R.T} \qquad \text{Eqn. (7)}$$

$$k(80℃) = (107.88 \times 10^5) \times exp^{\frac{-50.88\times10^3}{8,3145\times(80+273.15)}} = 0.3211 \qquad \text{Eqn. (8)}$$

$$t\ (T) = \frac{Strain\ (t_0) - Strain\ (requirement)}{k\ (T)} = \frac{70-10}{0.3211} = 186\ days\ \approx 0.5\ years \qquad \text{Eqn. (9)}$$

Table 4.3 Predicted life-time based on Arrhenius at different aging temperatures

T (°C)	*k(calculated)*	*Life-time based on Arrhenius (year)*
80	0.3211	0.5
70	0.1938	0.9
60	0.1135	1.5
50	0.0643	2.6
30	0.0184	9.0

The Berthelot equation is another approach to predict the shelf life of PBXs. This approach is applied to develop curves reflecting the variation in the reaction rate with temperature as follows (Shekhar, 2011).

$$logk = aT + b \qquad \text{Eqn. (10)}$$

where k is the rate constant, T is the temperature in Kelvin, and a and b are constants. The rate constant k can be calculated when the reaction order is known. For zero order reactions, the rate constant can be determined as:

$$k = \frac{c}{t} \qquad \text{Eqn. (11)}$$

where c is the chemical or physical property change of the PBX, and t is the required time to obtain a given change in PBX chemical or physical property. By substituting Eqn. (11) in Eqn. (10) it follows:

$$log\frac{c}{t} = aT + b \qquad \text{Eqn. (12)}$$

Which can be written as;

$$T = -\frac{1}{a}logt + \frac{logc-b}{a} \qquad \text{Eqn. (13)}$$

Eqn. (13) represents Berthelot's mathematical expression of the deterioration phenomena, which is a straight line function. By referring to the experimental data of Table 4.4, T vs. log t plotted (Figure 4.65) for strain change at the various

temperatures, the points t, representing the times for the 10% strain can be obtained for each aging temperature.

Table 4.4 Data for Berthelot calculations

T (°C)	*k (experimental)*	*t (from experimental k) (year)*	*log t*
80	0.4671	0.4	0.632
70	0.2205	0.8	0.958
60	0.0757	2.2	1.422
50	0.0387	4.3	1.713
30	0.0278	6.0	1.857

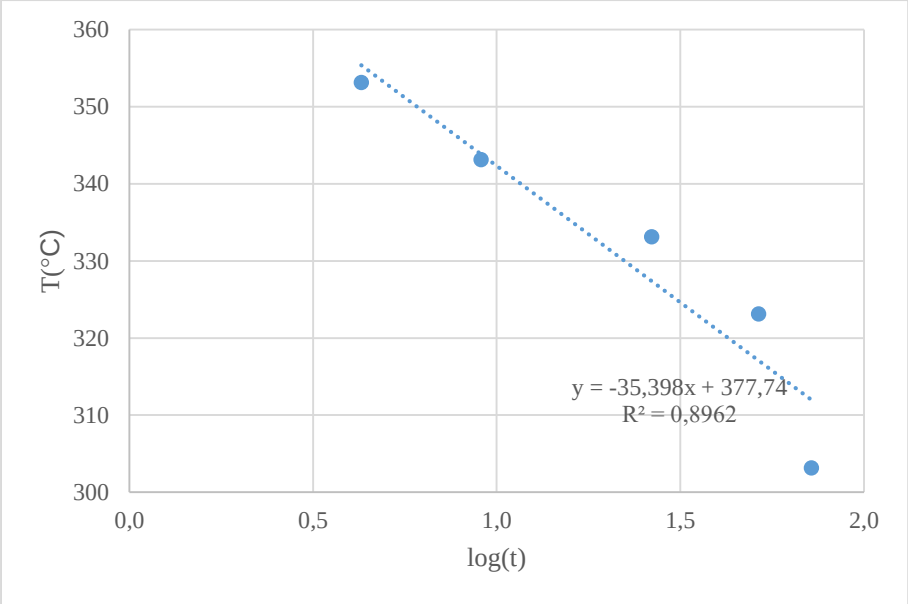


Figure 4.65. T vs. log (t) plot to determine shelf life from Berthelot

From Figure 4.65, for each temperature coresponding shelf life can be found. The predicted life values calculated with the Berthelot and Arrhenius approaches were close to each other as shown in Table 4.5 below.

Table 4.5 Predicted Shelf Life Comparison of Arrhenius and Berthelot Approaches

T (˚C)	*Shelf Life (year, Berthelot)*	*Shelf Life (year, Arrhenius)*
30	10.70	9.05
50	2.90	2.59
60	1.52	1.47
70	0.79	0.86
80	0.41	0.52

CHAPTER 5

CONCLUSION AND FUTURE WORKS

In this study, the aging behaviors of polymer bonded explosives with three different chemical formulations were investigated comprehensively in both chemical and physical dimensions. Each formulation was subjected to accelerated aging conditions at specific temperatures and evaluated with numerous analytical test methods. While the aging behavior of energetic materials has been the subject of numerous studies in the literature, only a limited number have employed such an integrative and multidimensional approach. In particular, this study attempts to elucidate aging mechanisms by concurrently examining the chemical composition, as well as both physical and chemical affects of aging phenomena. Such a comprehensive methodology offers deeper insights into the coupled degradation processes that govern the long-term stability and performance of energetic formulations. The aging behavior of an explosive frequently used (PBXN-109) for military purposes was examined in this study. In addition, the effect of antioxidant and bonding agent on aging behavior was also evaluated. On the other hand, such studies are subject to formulation specific outputs and evaluations. There is no existing literature on this scope for PBXN-109 explosive and its derivatives.

Moreover, this study examines that oxidative crosslinking and chain scission phenomena are two aging mechanisms that are in constant competition with each other. The findings indicate that an increasing tendency for the oxidative crosslinking is observed even at relatively low aging temperatures. This challenges the conventional assumption that crosslink density increases proportionally with temperature, suggesting instead that the cumulative influence of competing degradation pathways - particularly chain scission plays a significant role. To the

best of our knowledge, this is the first time such a behavior has been systematically identified and reported under these specific conditions.

The fact that the data obtained from the tensile test at different aging temperatures did not seem to coincide with the crosslink density test results revealed that the physical mechanisms of aging (i.e. dewetting, plasticizer diffusion, thermal stress) should not be ignored. Although the high antioxidant content was observed to reduce crosslink density, it didn't create a significant difference in the tensile strain curve behavior compared to the lower antioxidant content formulation. This finding supports the hypothesis that elongation behavior is the response that is more dependent on the physical effects of aging. It has been understood that physical changes due to aging can manifest themselves with the tensile test and that chemically changing the amount of antioxidants alone cannot prevent the physical effects.

It was observed that antioxidant (AO) consumption increased with increasing temperature as expected. The presence of AO also highlights chain scission reactions rather than oxidative crosslinking because of. the antioxidant's response of inhibiting crosslinking reactions. Since the formulation with higher antioxidant content was aged at a single temperature, temperature dependent crosslinking and strain properties could not be examined. However, when the elongation behavior against the physical mechanism of aging effects was examined, it was seen that it did not differ much from the lower antioxidant content formulation. It has been observed that the increased antioxidant content prevents the oxidative crosslinking and reduces crosslink density due to ongoing chain scission. However, it was also found that high antioxidant consumption occurs in the presence of higher antioxidant in the formulation. While kinetically expected, it's considered beneficial to validate this phenomenon through further studies at different temperatures, as this study only determined it for a single temperature. Yet, current findings indicate that while the antioxidant inhibits oxidative crosslinking, it does not provide evidence to suggest an effect on the physical mechanisms of aging. In this part of the thesis, which aims to slow aging by increasing antioxidant content, the reality of faster antioxidant

consumption should not be overlooked. Instead, optimum antioxidant amounts corresponding to an optimum consumption rate should be determined through formulation specific studies.

The approach to assess the efficiency of crosslinking reactions via carbonyl analysis has not been done before with FTIR. There are analyzes of some functional groups related to aging through raw spectra, but analysis with a quantitative approach through carbonyl area calculation, as examined in this study, is not available in the literature. It is obvious in the literature that aging behavior is chemically characterized more by crosslink density. Therefore, introducing a different approach to verify the crosslink density results with FTIR is another important achievement of this study.

It has been understood that the bonding agent has an important function in such formulations. Without the bonding agent, very low physical and chemical resistance to aging was observed. With the removal of bonding agent, it is aimed to keep the interaction with the solid filler material to minimum and to examine its effect on aging behavior. We have encountered a formulation with very poor mechanical properties. Filler and polymer separations are clearly visible in the SEM images for the formulation without bonding agent. The necessity of using a bonding agent in such formulations has become clear.

Finally, life estimation was made using two methods commonly used in the literature, Arrhenius and Berthelot approaches, based on elongation data for nominal formulation. The results obtained with both methods are consistent with the findings in the literature and show similar trends. However, it should be noted that such life estimations should be evaluated within the framework of the actual usage conditions considering structural and performance requirements of the relevant ammunition. The life estimation made in this study corresponds to the shelf life (storage life) and should not be confused with the service life, which depends on the variable factors (i.e. vibration, humidity, pressure, UV light etc.) in the field.

This study has the potential to be carried forward in a setup where the bonding agent is used in different proportions and subjected to aging at different temperatures. In this way it is possible to optimize the concentration of the bonding agent by considering the shelf life requirements. Similar situation also applies to antioxidant. The aging behavior of formulations with different antioxidant contents can be better understood and thus the antioxidant content can be optimized. In addition, the aging behavior of such energetic materials can be better addressed or elucidated in the future by quantitative analysis of other functional groups that will directly undergo chemical reactions spectroscopically.

As a result, this study aimed to address aging from a holistic perspective and understand the effectiveness of different aging mechanisms and response of different tests. It is considered that findings that will contribute to the literature have been obtained. It is also considered that it will be beneficial to consider the aging studies to be carried out in TUBITAK SAGE from now on in the light of the information obtained from this study. In particular, a long-term and real-time aging study could provide significant benefits in supporting or making sense of the inferences obtained here.

REFERENCES

Adel, W., & Liang, G. (2019). Service Life Prediction of AP/Al/HTPB Solid Rocket Propellants with Consideration of Softening Aging Behavior. *Chinese Journal of Aeronautics*, 361-368.

Ahmadi, S., Keshavarz, M., & Atabak, H. (2019). Correlations Between Laser Induced Breakdown Spectroscopy (LIBS) and Dynamical Mechanical Analysis (DMA) for Assessment of Aging Effect on Plastic Bonded Explosives (PBX) . *Zeitschrift für Anorganiche und Allgemeine Chemie*, 120-125.

Ali, A., & Zhang. (2008). Investigation of the Role of Aziridine Bonding Agents on the Aging of the Composite Solid Rocket Propellant. *J. Aerops. Pow.*, 2101-2106.

Bennet, S., & Carpenter, R. (1983). Migration at Interfaces. *JANNAF Propulsion Meeting*, (s. 53). California.

Biggs, G. (2009). Solid Propellant Aging Kinetics. *AIAA/ASME/SAE/ASEE Joint Propulsion Conference & Exhibit* (s. 1-13). Denver: AIAA.

Bina, C., Kannan, K., & Ninan, K. (2004). DSC Study on the Effect of Isocyanates and Catalysts on the HTPB Cure Reaction. *J. Therm. Anal. Calorim.*, 753-760.

Bohn, A., & Cerri, S. (2010). Ageing behaviour of composite rocket propellant formulations investigated by DMA, SGA and GPC. *NDIA 2010 Insensitive Munitions & Energetic Materials Technology Symposium (IMEMTS).* NDIA.

Bohn, M. (2009). Prediction of equivalent time-temperature loads for accelerated aging to simulate preset in storage aging and time-temperature profile loads. *40th International Annual Conference of ICT on Energetic Materials - Characterization, Modeling, Validation*, (s. 1-78). Karlsruhe, Germany.

Brown, D., Lowry, R., & Smith, L. (1980). Kinetics of Hydrolytic Aging of Polyester Urethane Elastomers. *Macromolecules 13 (2)*, 248-252.

Brown, R. (2006). *Physical testing of rubber.* Springer.

Bunyan, P., Cunliffe, A., Davis, A., & Kirby, F. (1993). The Degradation and Stabilization of Solid Rocket Propellants. *Polymer Degradation and Stability*, 239-250.

Cao, Z., Zhou, Q., Jie, S., & & Li, B. G. (2016). High cis-1, 4 hydroxyl-terminated polybutadiene-based polyurethanes with extremely low glass transition temperature and excellent mechanical properties. *Industrial & Engineering Chemistry Research*, 55(6), 1582-1589.

Catherine, K., Krishnan, K., & Ninan, K. (2000). A DSC Study on Cure Kinetics of HTPB-IPDI Urethane Reaction. *J. Therm. Anal. Calorim.*, 93-100.

Celina, M., J.M., S., Winters, S., Assink, R., & Minier, L. (2006). Correlation of Antioxidant Depletion and Mechanical Performance During Thermal Degradation of an HTPB Elastomer. *Polymer Degredation and Stability*, 1870-1879.

Cerri, S., Bohn, M., Menke, K., & Galfetti, L. (2009). Aging Behaviour of HTPB Based Rocket Propellant Formulations. *Central European Journal of Energetic Materials*, 149-165.

Cerri, S., Bohn, M., Menke, K., & Galfetti, L. (2013). Aging of HTPB/Al/AP Rocket Propellant Formulations Investigated by DMA Measurements. *Propellants, Explosives, Pyrotechnics*, 190-198.

Coquillat, M., Verdu, J., Colin, X., Audounin, L., & Nevie, R. (2007). Thermal Oxidation of Polybutadiene. Part 1: Effect of Temperature, Oxygen, Pressure and Sample Thickness on the Thermal Oxidation of Hydroxy-terminated Poybutadiene. *Polym. Degrad. Stab.*, 1326-1333.

Dalby, B., & Caraës, A. (2015). Lifetime Numerical Prediction of Solid Rocket Motors with HTPB Binder Based Propellants Using a Multiscale Model. *51st AIAA/SAE/ASEE Joint Propulsion Conference* , (s. 4238).

Daniel, M. (2006). *Polyurethane Binder Systems for Polymer Bonded Explosives.* Edinburgh: DSTO.

de la Fuente, J. (2009). An analysis of the thermal aging behaviour in high-performance energetic composites through the glass transition temperature. *Polymer Degradation and Stability*, 664-669.

Epure, C., Grigoriu, N., Tiganescu, T. V., Iorga, O., & Marin, A. (2022). Mechanical and Chemical Analysis of Composite Rocket Propellant Subjected to the Accelerated Ageing. *Journal of Military Technology* , Vol.5, No.2.

Eslam, E., Sherif, E., Ahmed, E., & Hosam, M. (2020). Assesment of Antioxidant Resistance to Thermal-Oxidative Degredation of Stabilized Polybutadiene Binder. *IOP Conference Series: Materials Science and Engineering.*

Flory, P., & Rehner Jr, J. (1943). Statistical mechanics of cross-linked polymer networks II. Swelling. *The journal of chemical physics*, 11(11), 521-526.

Ganivada, M., Dhara, M., Jana, S., & Jana, T. (2022). Synthetic Routes to Modify Hydroxyl Terminated Polybutadiene for Various Potential Applications. *J. Macromol. Sci.*, 167-179.

Gates, T. (2008). The Physical and Chemical Ageing of Polymeric Composites . R. Martin içinde, *Ageing of Composites* (s. 3-33). CRC Press.

Gonçalves, R. F., Iwama, E. N., Domingues, M. G., & Rocco, J. A. (2020). Shelf-life analysis of solid rocket engine using HTPB/AP based on kinetic-chemical parameters of DSC analysis and burn on a test bench. *Journal of the Brazilian Society of Mechanical Sciences and Engineering*, 42(1) 54.

Gorji, M., & Mohammadi, K. (2013). Comparison of Berthelot and Arrhenius approaches for prediction of liquid propellant shelf life. *Propellants, Explosives, Pyrotechnics*, 715-720.

Gottlieb, L., & Bar, S. (2003). Migration of Plasticizer Between Bonded Propellant Interfaces. *Propellants, Explosives, Pyrotechnics*, 12-17.

Hailu, K., Guthausen, G., Becker, W., Konig, A. B., & Geissler, E. (2010). In-situ Characterization of the Cure Reaction of HTPB and IPDI by Simultaneous NMR and IR Measurements. *Polym. Test*, 513-519.

Hasırcı, N., Akbaş, A., & Aksoy, S. (1994). Effects of Thermal Ageing on the Properties and Lifetime Prediction of Hydroxy Terminated Polybutadiene. *Polymer*, 2568-1572.

International Organization for Standardization. (2003). Plastics and ebonite — Determination of indentation hardness by means of a durometer (Shore hardness) (ISO Standard No. 868:2003).

Jaidan, M., Abou-Rachid, H., Lafleur-Lambert, X., & Brisson, J. (2011). Atomistic Studies of RDX and FOX-7 Based Plastic-Bonded Explosives. *Procedia Computer Science*, 1177-1185.

Joseph, C. (1993). *Tactical Missile Warheads* . Colorado: AIAA.

Judge, M. (2003). An Investigation of Composite Propellant Accelerated Ageing Mechanisms and Kinetics. *Propellants, Explosives, Pyrotechnics*, 114-119.

Khan, M. (1993). Simulation of Composite Propellant Aging. *Polym. Plast. Technol. Eng.*, 467.

Khanlari, T., Bayat, Y., & Bayat, M. (2022). Preparation of a novel polyurethane network based on PPG-PGN-PPG: Investigation of the effect of plasticizers on its properties. *Polym. Bull.*, 709-724.

Kishore, K., Verneker, V., & Prasad, G. (1979). Mechanism of Aging of Composite Solid Propellants . *Combustion and Flame* , 79-85.

Kumar, A., Commereuc, S., & Verney, V. (2004). Ageing of elastomers: a molecular approach based on rheological characterization. *Polymer Degredation and Stability*, 85(2), 751-757.

Kumar, B., Kumaraswamy, A., Jain, M., & Murthy, K. (2022). Assessment of Mechanical Properties of Aged Composite Propellant Using Non-Destructive Indentation Technique in Solid Propellant Rocket Motor. *Propellants, Explosives, Pyrotechnics*, 47(6).

Lai, S., Dong, K., Kong, L., Qu, Y., & Xiao, Y. (2021). Study on the Aging Performance of Propellant under Humid and Hot Conditions. *IEEE 4th International Conference on Nanoscience and Technology (ICNST)* (s. 64-68). IEEE.

Lucio, B., & De La Fuente, J. (2014). Rheokinetic Analysis on the Formation of Metallo-Polyurethanes Based on Hydroxyl-Terminated Polybutadiene. *Eur. Polym. J.*, 117-126.

Ma, H., Liu, Y., Chai, T., Yu, Y., Guo, J., Zhong, L., & Zhang, Q. (2022). The Effect of Single Curing Agents on the Curing Reactions of the HTPB-based Binder System. *Coatings*, Vol 12, No.8.

Mohamed, M., & Aggag, G. (2003). Uncertainty evaluation of shore hardness testers. *Measurement*, 33(3), 251-257.

Naseem, H., Murthy, H., & Ramakrishna, P. (2020). Accelerated Ageing of Composite Solid Propellants Under Cyclic Temperature Variations. *Journal of Energetic Materials*, 39(4), 452-478.

Naseem, H., Yerra, J., Murthy, H., & Ramakrishna, P. (2021). Ageing studies on AP/HTPB based composites solid propellants. *Energetic Materials Frontiers*, 111-124.

NATO Standardization Office. (2015, 3 30). Explosives, Assesment of Ageing of Polymer Bonded Explosives (PBXs) Cast-Cured Compositions Using Inert and Energetic Binders . Brussels, Belgium.

Ou, & Yapeng. (2018). Influence of Bismuth Complex Catalysts on the Cure Reaction of Hydroxy-terminated Polyether-based Polymer Bonded Explosives. *Journal of Energetic Materials*, 131-149.

Ou, Y., Chang, S., & Zhang, B. (2015). Effect of Bismuth-Containing Catalysts on HTPB Curing Kinetics. *Chin. J. Energ. Mater.*, 568-572.

Pan, Y., Nan, F., & Chen, P. (2022). Aging Life Prediction Model of Energetic Materials . *Proceedings of the 14th International Conference on Computer Modeling and Simulation*, (s. 14-19).

Sbegue, L., & Villar, L. (2016). Comparative Assessment of Stabilised Polybutadiene Binder Under Accelerated Ageing. *Journal of Aerospace Technology and Management*, 122-129.

Schollenberger, C., & Stewart, F. (1971). Thermoplastic Polyurethane Hydrolysis Stability. *J. Elastoplast*, 28-56.

Sciamareli, J., Takahashi, Marta, & Koshun. (2002). Solid Polyurethane Based Composite Propellant. *Quimica Nova*, 107-110.

Setyaningsih, D., Juwono, A., & Supriyatno, H. (2017). Stabilizer Effect on Thermal Decomposition of Aged Solid Propellant. *Journal of Physics Conference Series*, Vol. 909, No.1.

Shekhar, H. (2011). Prediction and comparison of shelf life of solid rocket propellants using Arrhenius and Berthelot equations. *Propellants, Explosives, Pyrotechnics*, 36(4), 356-359.

Shekhar, H. (2012). Studies on stress-strain curves of aged composite solid rocket propellants. *Defence Science Journal* , 90-94.

Standardization, I. O. (tarih yok). Plastics and ebonite — Determination of indentation hardness by means of a durometer (Shore hardness) (ISO Standard No. 868:2003).

Szala, M. (2021). Polymer-Bonded Secondary Explosives. *Materialy Wysokoenergetyczne*, 13.

Tcharkhtchi, A., Farzaneh, S., Abdallah Elhirtsi, S., Esmaeillou, B., Nony, F., & Baron, A. (2014). Thermal Aging Effect on Mechanical Properties of Polyurethane. *International Journal of Polmer Analysis and Characterization*, 571-584.

Torry, S., & Cunliffe, A. (2000). Humid Ageing of Polybutadiene Based Propellants. *31st Int. Annual Conference of ICT*, (s. p.25/1). Karlsruhe, Germany.

Vadhe, P., Pawar, R., & Sinha, R. (2008). Cast Aluminized Explosives. *Combust. Explos. Shock Waves*, 461-477.

Van Breugel, K. (2018). Urgency and Challanges of Ageing in Science and Engineering . K. Van Breugel içinde, *The Ageing of Materials and Structures* (s. 3-13). Springer International Publishing.

Villar, L. D., Cicaglioni, T., Diniz, M. F., Takahashi, M. F., & Rezende, L. C. (2011). Thermal aging of HTPB/IPDI-based polyurethane as a function of NCO/OH ratio. *Materials Research*, 14(3), 372-375.

Walid M. ADEL, G. L. (2018). Service life prediction of AP/Al/HTPB solid rocket propellant with consideration of softening aging behavior. *Chinese Journal of Aeronautics*, 361-368.

Wang, F., Chang, H., & Zhang, L. (2016). Research Progress of Crosslink Density Test Method and Its Application in Explosives and Propellants. *Chinese Journal of Explosives and Propellants*, 39:8e12.

Wang, X., Chen, Z., Qiang, H., & Fu, X. (2025). Research on Crosslink Density Testing Method of GAP Propellant Based on Swelling Method. *In Journal of Physics Conference Series* (s. Vol. 2955, No. 1, p. 012032). IOP Publishing.

Wang, Y. H., Zhang, X. R., Liu, C. C., & Hao, X. G. (2015). Characterisation of novel polymeric antioxidant and its thermo-oxidative aging resistance for natural rubber vulcanizates. *Plastics, Rubber and Composites*, 44(8), 330-338.

Wang, Z., Qiang, H., Wang, T., & Wang, G. (2019). Tensile Behaviors of Thermal Aged HTPB Propellant at Low Temperatures Under Dynamic Loading. *Mechanics of Time Dependent Materials*, 1-19.

Wojnar, C. S., Miller, T., & & Ghiassi, K. (2019). Determining the Master Curve of Aged Solid Propellant Using a Dynamic Mechanical Analyzer. *AIAA Scitech 2019 Forum.* San Diego, California.

Xie, F., Zhang, T., Bryant, P., Kurusingal, V., Colwell, J., & Laycock, B. (2019). Degradation and Stabilization of Polyurethane Elastomers. *Prog. Polym. Sci.*, 211-268.

Yaacob, I., Asli, A., Norkhairunnisa, M., Ahmad, K., Ismail, O., Salleh, N., & Shahedi, S. (2023). A review on viscoelastic behaviour of plasticizers in AP/Al/HTPB based composite solid propellant. *Materials Today: Proceedings.*

Yadav, A., Pant, C., & Das, S. (2020). Research Advances in Bonding Agents for Composite Propellants. *Propellants, Explosives, Pyrotechnics*, 695-704.

Yıldırım, H. C., & Özüpek, Ş. (2011). Structural assessment of a solid propellant rocket motor: Effects of aging and damage . *Aerospace Science and Technology*, 15(8), 635-641.

Yılmaz, G., Şen, D., & Kaya, Z. (2014). Effect of Inert Plasticizers on Mechanical, Thermal and Sensitivity Properties of Polyurethane-Bsed Plastic Bonded Explosives. *Journal of Applied Polymer Science*, 131(20).

Yongqiang, D., Jian, Z., Jianzhuang, Z., & Xin, T. (2019). Effect of Antioxidant on Storage Performance and Life Prediction of HTPB Propellant. *IOP Conference Series: Materials Science and Engineering* (s. Vol.538, No.1, p.012047). IOP Publishing.

Zhang, L., & Zheng, X. (2018). Experimental study on thermal decomposition kinetics of natural ageing AP/HTPB base bleed composite propellant. *Defence Technology*, 422-425.

Zhang, X., Zhao, F., & Tan, H. (2005). Improving Mechanical Property of CMDB Propellant Containing Nitrmaine with Bonding Agent. *Chinese J. Explos. Propell*, 28(1).

Zou, & Zi-Jie. (2023). Review on the Dewetting of the Particle-Matrix Interface in Composite Solid Propellants. *Propellants, Explosives, Pyrotechnics*, 48.3:e202200270.

CURRICULUM VITAE

Surname, Name: Yücel, Tarık

EDUCATION

Degree	Institution	Year of Graduation
MS	METU Chemical Engineering	2013
BS	METU Chemical Engineering	2010
High School	İncirlik Lisesi, Adana	2005

WORK EXPERIENCE

Research Assistant	METU Chemical Engineering	2012-2013
Researcher	TÜBİTAK SAGE	2013-Now

FOREIGN LANGUAGES

Advanced English

PUBLICATIONS/CONFERENCE PAPERS

- T. Yücel, M. S. Yavuz, D. Çetin, G. A. Yılmaz ***"Performance Evaluation of a Castable Thermobaric Explosive"*** International Annual Conference of the Fraunhofer ICT, Germany,26-29 June, 2018.

- S. Bilgen, A. Yılmaz, T. Yucel, A.F. Zeybek, D. Çetin, ***"Comparison of Performance and Insensitivity Properties of Enhanced Blast Plastic Bonded Explosives with Conventional Explosives"***, Insensitive Munition and Energetic Materials Technology Symposium, Indianapolis, October 18-20, 2022.

- A. Yılmaz, F. Zeybek, S. Bilgen, İ. E. Metin, D. Çetin, T. Yücel, ***"Comparison of Plastic Bonded Enhanced Blast Explosive with TNT and Comp-B in Terms of Thermal and Blast Properties"***, New Trends in Research of Energetic Materials University of Pardubice, Czech Republic, April 6-8, 2022.

- S. Aksu, C. Tuygun, O. Aslan, T. Yucel, D. Cetin, ***"Comparison of Castable PBXs Prepared from Different Sources of Energetic Fillers In Terms of Processability"***, New Trends in Research of Energetic Materials (NTREM), Pardubice, April 19-21, 2023.